AN ABSTRACT OF THE THESIS OF

Jinfan Duan for the degree of Doctor of Philosophy in Forest Engineering presented on May 7, 1996. Title: A Coupled Hydrologic-Geomorphic Model for Evaluating Effects of Vegetation Change on Watersheds

Abstract approved: Gordon E. Grant
Gordon E. Grant

This work describes the modeling framework and initial results for CLAWS (Coupled Landscape And Water System), a physically-based, spatially-distributed hydrologic-geomorphic model that has been coupled with a vegetation dynamics simulation. Spatial variability of topography, soil, vegetation, and climate drive a hydrology module that calculates the water budget at given time steps and with a spatial resolution defined by digital elevation data. Important hydrologic processes, including snow accumulation and melt, interception, evapotranspiration, infiltration, subsurface flow, overland flow and channel flow routing are incorporated in CLAWS. The hydrology drives hillslope and channel geomorphic processes, including probability of mass movements (landslides, debris flows). Both the hydrologic and geomorphic modules are linked to forest growth simulation so that effects of changing forest stand structure in response to cutting or other disturbances through time can be examined. Dynamic integration of CLAWS with geographic information systems enhances model parameterization and result analyses. Calibration and testing of CLAWS from three small watersheds at HJ Andrews Experimental Forest in western Oregon shows that watershed hydrologic behavior and hillslope stability can be simulated accurately. The module for snow accumulation and melt has been tested using four years of point measurements of snow water equivalent and showed that this simple energy and mass balance model accurately simulated snow accumulation and melt processes. Application of CLAWS to land use management permits long-term simulations of effects of alternative forestry practices on hydrologic and geomorphic responses of watersheds. Results from Monte Carlo simulations in small watersheds in Western Oregon, show long-term effects of forest harvesting over 100 years, which are in agreement with long-term observations. Simulations show that 40 years is needed for watershed recovery to pre-clearcutting status with respect to old growth through an exponential trend and changes in watershed responses show strong seasonal and storm variations. Models such as CLAWS, that successfully incorporate hydrologic, geomorphic and forest dynamic processes into a single model, are an

effective complement to traditional paired-watershed studies of hydrologic and geomorphic responses.

©Copyright by Jinfan Duan
May 7, 1996
All Rights Reserved

A Coupled Hydrologic-Geomorphic Model for Evaluating Effects of Vegetation Change on Watersheds

by

Jinfan Duan

A THESIS

submitted to

Oregon State University

in partial fulfillment of
the requirements for the
degree of

Doctor of Philosophy

Completed May 7, 1996
Commencement June 1996

Doctor of Philosophy thesis of Jinfan Duan presented on May 7, 1996

APPROVED:

Major Professor, representing Forest Engineering

Chair of Department of Forest Engineering

Dean of Graduate School

I understand that my thesis will become part of the permanent collection of Oregon State University libraries. My signature below authorizes release of my thesis on any reader upon request.

Jinfan Duan, Author

ACKNOWLEDGMENTS

I take this opportunity to express my appreciation to those who assisted me in this research. Many resources were contributed to the completion of this thesis. I apologize in advance for any omissions.

First and foremost, I wish to thank my major professor Gordon Grant, without his mentorship, ideas, comments and suggestions, this research would not have been possible. I owe my deepest gratitude to Fred Swanson, Bob Beschta, Gay Bradshaw, John Selker, and Ezra Tice, for their patient guidance and consistent encouragement throughout the completion of this thesis. I have also greatly benefited from discussions with David Bella, Chaur-Fong Chen, Richard Cuenca, Bill Dietrich, Mark Harmon, George Leavesley, Dennis Lettenmaier, Dave Montgomery, Michael Unsworth and Beverley Wemple.

I would like to share the completion of this thesis with Beverley Wemple and Richard Busing who read my text carefully at several stages of its evolution to get my English de-Chinesized; Don Henshaw who provided a lot of data used in this research; Hazel Hammond and George Lienkaemper for assistance with GIS analysis; Dick Janda, Kevin Scott and Rick LaHuson for their encouragements and introduction to this excellent interdisciplinary research community.

I would also like to express my deep appreciation to the faculty, staff, and fellow graduate students in the departments of Forestry Engineering and Forest Science, and researchers and staff at HJ Andrews Experimental Forest, a National Science Foundation supported Long Term Ecological Research site.

Finally, I must gratefully acknowledge the enthusiastic and unflagging encouragement and support provided to me by my wife, Jinying Zhang, and by my family and hers , and by the smile of my daughter Siqi.

CONTRIBUTION OF AUTHORS

Dr. Gordon Grant was involved in the design, analysis, and writing of each manuscript. Dr. Bob Beschta was involved in the design and result interpretation for random simulation using CLAWS.

TABLE OF CONTENTS

Page

1. GENERAL INTRODUCTION: APPROACHES TO EVALUATE EFFECTS OF FOREST LANDUSE ON HYDROLOGY 1

1.1 TRADITIONAL WATERSHED STUDIES 1

1.2 PHYSICALLY BASED SPATIALLY DISTRIBUTED MODELS 2

1.2.1 Evolution of surface hydrologic models 5

1.2.2 Spatially distributed approaches 6

1.2.3 Terrain analysis and spatial configuration 7

1.3 OBJECTIVES 9

2. STRUCTURE AND COMPONENTS OF CLAWS, A COUPLED HYDROLOGIC-GEOMORPHIC MODEL FOR LANDSCAPE AND WATERSHED STUDIES 11

2.1 ABSTRACT 11

2.2 INTRODUCTION 11

2.3 MODEL DESCRIPTION 13

2.3.1 Terrain analysis and geographical information system linkage 15

2.3.2 Hydrology 16

2.3.2.1 Meteorological data adjustment 17
2.3.2.2 Snow accumulation and melting 17
2.3.2.3 Interception 17
2.3.2.4 Evapotranspiration 18
2.3.2.5 Infiltration 21
2.3.2.6 Subsurface flow 22
2.3.2.7 Deep groundwater exchange 23
2.3.2.8 Overland and channel flow routing 24

2.3.3 Geomorphology 26

2.3.3.1 Slope stability analysis 26
2.3.3.2 Landslide runout or debris flow 27
2.3.3.3 Sediment transport 28

2.3.4 Vegetation dynamics 28

2.3.4.1 Cover density 29
2.3.4.2 Leaf area index 30

TABLE OF CONTENTS (Continued)

Page

2.3.4.3 Tree height 30
2.3.4.4 Biomass 30
2.3.4.5 Root strength 30

2.4 CONCLUSIONS 31

3. A SIMPLE ENERGY AND MASS BALANCE MODEL FOR SNOW ACCUMULATION AND MELT 33

3.1 ABSTRACT 33

3.2 INTRODUCTION 33

3.3 THEORY AND MODEL FORMULATION 35

3.3.1 Partition of precipitation 35

3.3.2 Energy budget 36

3.3.2.1 Solar radiation 36
3.3.2.1.1 Daily potential clear sky solar radiation 36
3.3.2.1.2 Daily sky cover 37
3.3.2.1.3 Daily radiation extrapolation 37
3.3.2.1.4 Forest shadowing 38
3.3.2.1.5 Snowpack reflection 38
3.3.2.2 Net longwave radiation 38
3.3.2.3 ensible and latent heat 39
3.3.2.4 Conduction 39
3.3.2.5 Advective heat of precipitation 40

3.3.3 Snowpack energy balance 40

3.3.4 Snowpack mass balance 41

3.4 MODEL PERFORMANCE TEST AND DISCUSSION 42

3.5 CONCLUSIONS 52

4. CALIBRATION AND SENSITIVITY ANALYSES FOR CLAWS, A COUPLED HYDROLOGIC-GEOMORPHIC MODEL FOR LANDSCAPE AND WATERSHED STUDIES 53

4.1 ABSTRACT 53

4.2 INTRODUCTION 53

4.3 SITE DESCRIPTION 55

TABLE OF CONTENTS (Continued)

Page

4.4 INPUT DATA AND PARAMETERIZATION 57

4.4.1 Meteorological input 57

4.4.2 Topographical attributes 58

4.4.3 Soil and vegetation distribution and characteristics 58

4.4.4 Other parameters and initial status 61

4.5 QUANTITATIVE MEASURES OF GOODNESS-OF-FIT 62

4.6 MODEL CALIBRATION AND SIMULATION RESULTS 63

4.7 SENSITIVITY ANALYSES 75

4.7.1 Maximum saturated conductivity 76

4.7.2 Saturated profile coefficient 77

4.7.3 Deep groundwater conductivity 77

4.7.4 Loss rate of deep groundwater storage 77

4.7.5 Soil depth 77

4.7.6 Soil porosity 78

4.7.7 Field capacity 78

4.7.8 Maximum biomass 78

4.7.9 Maximum root cohesion 88

4.7.10 Soil cohesion 88

4.7.11 Internal friction angle 88

4.7.12 Implications 88

4.8 CONCLUSIONS 89

5. HYDROLOGIC AND GEOMORPHIC RESPONSES OF WATERSHEDS TO LOGGING: PERSPECTIVES FROM CLAWS, A PHYSICALLY-BASED SPATIALLY-DISTRIBUTED MODEL 90

5.1 ABSTRACT 91

5.2 INTRODUCTION 91

5.3 METHODOLOGY 93

TABLE OF CONTENTS (Continued)

Page

5.3.1 Model of watershed responses 94
5.3.2 Precipitation model 95
5.3.3 Model for other meteorological variables 96
5.3.4 Initialization model 98
5.4 SIMULATION RESULTS 101
5.4.1 Runoff amount 101
5.4.2 Peakflow 102
5.4.3 Soil moisture 106
5.4.4 Landslide potential 109
5.5 DISCUSSION 109
5.5.1 Comparison with observation 109
5.5.1.1 Runoff amounts 109
5.5.1.2 Peakflows 111
5.5.1.3 Soil moisture 112
5.5.1.4 Landslides 112
5.5.3 Limitations 113
5.6 CONCLUSIONS 114
6. GENERAL SUMMARY 115
6.1 KEY ACHIEVEMENTS 115
6.2 LESSONS 117
6.3 FUTURE RESEARCH 118
6.3.1 Model improvements 119
6.3.2 Application to landuse and climate change 119
BIBLIOGRAPHY 120
APPENDIX 132
APPENDIX: CALCULATION OF SOIL PARAMETERS 133

LIST OF FIGURES

Figure		Page
2.1	General concepts of CLAWS, a coupled landscape and water system.	13
2.2	General procedure in spatial distributed hydrologic-geomorphic modeling	14
2.3	Interactions between hydrologic-geomorphic responses and forest dynamics	15
2.4	Model spatial input and output linked to Geographical Information System	16
2.5	Conceptual water movement path in an element	22
2.6	Cover density changes post cutting	29
3.1	Snow water equivalent comparison between computed and observed at Vanilla Leaf during water year 1991	45
3.2	Snow water equivalent comparison between computed and observed at Vanilla Leaf during water year 1992.	46
3.3	Snow water equivalent comparison between computed and observed at Vanilla Leaf during water year 1993	47
3.4	Snow water equivalent comparison between computed and observed at Vanilla Leaf during water year 1994	48
3.5	Spatial snow accumulation and melt pattern from CLAWS simulation for Watershed #3 during water year 1992..	49
3.6	Result from distributed simulation for WS#1 between Dec. 1, 1991 and Jan. 22, 1992.	50
3.7	Temporal changes of temperature between two meteorological gages, Primet station (430 m) and H15 station (925 m), in hourly resolution.	51
4.1	Geographical location of test sites, Watershed #1, Watershed #2 and Watershed #3 at HJ Andrews Experimental Forest, Oregon, United States.	56
4.2	Soil distribution in the three small watersheds	58
4.3	Hydrograph comparison of simulated streamflow (solid line) and observed streamflow (dotted line) of three small watersheds during three storms	64

LIST OF FIGURES (Continued)

Figure		Page
4.4	Spatial pattern of element soil moisture for watershed #3 during a 10 day simulation	66
4.5	Spatial pattern of element outflow for watershed #3 during a 10 day simulation	67
4.6	Spatial pattern of factor of safety for watershed #1, #2 and #3 during a 10 day simulation	68
4.7	Simulation results for WS#1 between Dec. 1, 1991 and Jan. 22, 1992.	71
4.8	Simulation results for WS#2 between Dec. 1, 1991 and Jan. 22, 1992.	72
4.9	Simulation results for WS#3 between Dec. 1, 1991 and Jan. 22, 1992.	73
4.10	Frequency distribution of factor of safety for three watersheds during 12/1/91-1/22/92.	74
4.11	Sensitivity analyses of maximum saturated conductivity	79
4.12	Sensitivity analyses of saturated profile coefficient	80
4.13	Sensitivity analyses of deep groundwater conductivity	81
4.14	Sensitivity analyses of loss rate of deep groundwater storage	82
4.15	Sensitivity analyses of soil depth	83
4.16	Sensitivity analyses of soil porosity	84
4.17	Sensitivity analyses of field capacity.	85
4.18	Sensitivity analyses of maximum biomass..	86
4.19	Sensitivity analyses of maximum root strength	86
4.20	Sensitivity analyses of soil cohesion	87
4.21	Sensitivity analyses of internal friction angle.	87
5.1	General procedure of Monte Carlo simulation of clearcutting on watershed responses	93
5.2	Storm characteristics at gage #2, HJ Andrews Experimental Forest:	97

LIST OF FIGURES (Continued)

Figure | Page

5.3 Observed baseflow distributions in different months for three small watersheds, WS#1, WS#2 and WS#3. 99

5.4 Relationship between outlet discharge and basin average of soil moisture for three small watersheds, WS#1, WS#2 and WS#3, simulated from CLAWS. 100

5.5 Streamflow volume changes post cutting for WS#1. 103

5.6 Monthly and storm variation of runoff/precipitation ratio after cutting. 104

5.7 Flow peak changes after cutting. 105

5.8 Peakflows postcutting. 106

5.9 Soil moisture changes after cutting. 107

5.10 Changes in the factor of safety (FS) post cutting. 108

LIST OF TABLES

Table		Page
1.1	Paired watersheds studied in Pacific Northwest	3
1.2	Forest harvesting and roading effects	4
1.3	Operational Characteristics of raster, TIN, and vector data structure	9
3.1	Point simulation statistics for different water years	43
4.1	Characteristics of three small watersheds at HJ Andrews Experimental Forest	55
4.2	Soil parameters used in model test	59
4.3	Vegetation parameters used in model test	60
4.4	Simulation results of three watersheds during three storms.	65
4.5	Simulation results for three watersheds during 12/01/91-01/22/92	70
4.6	Parameters used in sensitivity analysis	75
5.1	Observed monthly precipitation characteristics for HJ Andrews Experimental Forest, western Oregon.	95
5.2	Parameters for initial baseflow (m^3/s) at WS#1, WS#2, WS#3.	98
5.3	Parameters for discharge-soil moisture relationships of three watersheds	100

NOTATIONS

Symbol	Notation	Unit
α	albedo;	--
β	slope of element;	--
σ	Stefan-Boltzmann constant ($0.826X10^{-10}$ cal cm^{-2} min^{-1} $^0K^{-4}$);	
ψ	wetting front suction;	m
ϕ	internal frictional angle;	degree
θ	soil moisture content	m^3 m^{-3}
$\Delta\theta$	effective porosity of soil;	--
ΔC	total cohesion from root strength;	kPa
λ_f	latent heat of freezing (79.7);	cal g^{-1}
λ_i	latent heat of vaporization or latent heat of sublimation (depending on the status of the snow pack);	cal g^{-1}
γ_m	unit weight of soil at field capacity;	kN m^{-3}
θ_r	soil moisture content at field capacity	m^3 m^{-3}
θ_s	saturated soil moisture content	m^3 m^{-3}
λ_s	latent heat of fusion (sublimation, 677);	cal g^{-1}
γ_{sat}	unit weight of soil at saturation;	kN m^{-3}
λ_v	latent heat of vaporization (evaporation/condensation, 597.3);	cal g^{-1}
θ_w	soil moisture content at wilting point	m^3 m^{-3}
ρ_w	density of water (1.0);	g cm^{-3}
γ_w	unit weight of water;	kN m^{-3}
γ	psychometric constant	kPa $^0C^{-1}$
ρ_a	air density	kgm^{-3}
A	Cross sectional area of channel or overland flow;	m^2
A_i	amplitude of sine wave for any duration;	--
A_s	amplitude of sine wave in daily solar radiation;	--
a_c	constant in canopy conductance dependence calculation	--
a_c	coefficient in cover density calculation after cutting;	--
a_r	coefficient in root regrowth;	--
a_r	intercept in storage capacity calculation;	m
a_w	coefficient in biomass regrowth;	--
B	coefficient in Thompson's equation;	--
B_l	decay coefficient in leaf area index calculation;	--
B_s	shape coefficient in leaf area index calculation;	--
B_R	ratio of element solar radiation to gage solar radiation;	--
b_c	constant in canopy conductance dependence calculation	--
b_c	coefficient in cover density calculation after cutting;	--
b_r	coefficient in root regrowth;	--
b_r	slope in storage capacity calculation;	m

Symbol	Notation	Unit
b_w	coefficient in biomass regrowth;	--
C	soil cohesion;	kPa
C_D	vegetation cover density (0-1.0);	--
C_{Df}	final limit of cover density (0.7-0.8);	--
C_{Dmax}	maximum cover density (1.0);	--
C_{max}	maximum root strength of the vegetation;	kPa
C_r	root strength due to vegetation regrowth;	kPa
C_{rd}	root strength due to decay residual;	kPa
c_0	constant in tree height calculation	--
c_1	constant in tree height calculation	--
c_2	constant in tree height calculation	--
c_3	constant in tree height calculation	--
c_4	constant in tree height calculation	--
c_c	coefficient in cover density calculation after cutting;	--
c_d	vapor pressure deficit causing stomatal closure	kPa
c_p	specific heat of moist air, here used as a constant (1.013)	kJ kg^{-1} ^0C
c_s	specific heat of ice (0.5);	cal g^{-1} $^oC^{-1}$
c_w	specific heat of water (1.0);	cal g^{-1} $^oC^{-1}$
D	depth of soil;	m
d_0	zero plane displacement height in wind profile	m
d_r	coefficient in root regrowth;	--
d_w	coefficient in biomass regrowth;	--
E	evapotranspiration;	m
E_a	atmospheric emissivity	--
E_c	evaporation from tree canopy	m
E_s	evaporation from bare soil	m
E_T	transpiration from tree canopy	m
e	vapor pressure;	kPa
e_s	saturated vapor pressure;	kPa
F	cumulative infiltration;	m
FS	factor of safety for elements;	--
f	infiltration rate;	ms^{-1}
f_1	limit factor for canopy conductance from temperature	--
f_2	limit factor for canopy conductance from vapor pressure deficit	--
f_3	limit factor for canopy conductance from photosynthetically active radiation flux density(PAR)	--
f_4	limit factor for canopy conductance from soil moisture	--
G	deep groundwater storage for unit area;	m
G_0	initial groundwater storage for unit area;	m
G_t	groundwater storage of unit area at time t;	m
g_a	aerodynamic conductance	ms^{-1}
g_b	surface conductance for bare soil or non-canopy substrate	ms^{-1}
g_c	canopy conductance	ms^{-1}
g_{max}	maximum stomatal conductance for leaves in the canopy	ms^{-1}
g_s	stomatal conductance for leaves in the canopy	ms^{-1}

Symbol	Notation	Unit
H	element elevation;	m
H_h	meteorological gage elevation;	m
H_t	tree height	m
h	saturated depth of soil (count from bottom up);	m
I	Interception	m
I_{max}	storage capacity of vegetation;	m
I_T	cumulative interception;	m
K	soil saturated conductivity;	ms^{-1}
K_{max}	saturated conductivity at the near surface of the soil when it is fully saturated;	ms^{-1}
K_{mean}	average saturated conductivity for the soil profile;	ms^{-1}
K_v	von Karman's constant (0.4 in this model)	--
k_1	constant in sensible heat calculation (3.6734×10^{-5});	cm $m^{1/3}$ s min^{-1} $^oC^{-1}$ m^{-1}
k_2	constant in condensation heat calculation (2.5083×10^{-4});	cm $m^{1/3}$ s min^{-1} kPa^{-1} m^{-1}
k_d	decay coefficient in residual root strength;	--
k_I	decay coefficient in interception equation;	--
k_k	decay coefficient in variable saturated conductivity calculation;	--
k_{leak}	decay coefficient for deep ground water seep out of the element;	s^{-1}
k_{out}	decay coefficient for deep groundwater to subsurface, actually it is the saturated conductivity of deep groundwater;	s^{-1}
k_p	coefficient to adjust the element precipitation according to elevation difference;	--
k_R	Ratio of could sky radiation to clear sky potential radiation;	--
k_r	decay coefficient in root regrowth;	--
k_T	lapse rate;	$^oC/m$
k_w	decay coefficient in biomass regrowth;	--
L	day length;	T
LAI	leaf area index;	m^2m^{-2}
LAI_{max}	maximum leaf area index	$m^2 m^{-2}$
L_{cmax}	maximum liquid water holding capacity of snowpack;	--
M	month;	--
M_f	water equivalent depth frozen;	cm
M_n	water drain out of the snowpack;	L
m	soil moisture stress coefficient for surface conductance	--
m_1	coefficient in residual root strength;	--
m_s	power in Thompson's sky cover equation;	--
P	element precipitation;	m
PAR	photosynthetically active radiation flux density	Wm^{-2}
P_h	meteorological gage precipitation;	m
P_r	wetted perimeter of channel flow or overland flow;	m

Symbol	Notation	Unit
P_{rain}	rain proportion of the precipitation;	cm
P_{snow}	snow proportion of the precipitation;	cm
P_T	cumulative precipitation;	m
p_0	sea level atmospheric pressure;	kPa
p_a	surface atmospheric pressure;	kPa
p_c	percolation from unsaturated layer to saturated layer;	m
Q	discharge of channel flow or overland flow;	m^3s^{-1}
Q_e	latent heat exchange;	ly
Q_m	heat for melting or freezing;	ly
Q_{out}	total deep groundwater flow to next element;	m
Q_n	advection heat of precipitation;	ly
Q_s	sensible heat exchange;	ly
q_{in}	flow rate from subsurface to deep groundwater;	ms^{-1}
q_l	lateral flow for overland or channel;	m^2s^{-1}
q_{leak}	deep ground seepage rate out of the element;	ms^{-1}
q_{out}	flow rate from deep ground to next element;	ms^{-1}
q_s	saturated subsurface flow of unit width;	m^2s^{-1}
q_{upper}	deep groundwater flow from upper elements;	m
R_c	solar radiation after forest shadowing	ly
RDC	intercept of sky cover-daily air temperature range relationship;	--
RDM	slope of sky cover-daily air temperature range relationship;	--
Rh	relative humidity;	--
R_i	total solar radiation for a period	ly
R_l	net longwave radiation;	ly
R_n	net radiation;	ly
R_o	potential solar radiation;	ly
R_{oh}	potential solar radiation at gage;	ly
R_r	solar radiation after ground reflection;	ly
R_s	short wave radiation after cloud reduction;	ly
R_{sh}	solar radiation at gage site;	ly
R_{t1-t2}	solar radiation between t_1 and t_2;	ly
S	channel or overland flow plane slope;	--
S_i	site index of tree height (tree height at 100 year at a site)	m
S_k	daily sky cover;	--
S_y	yield strength of debris flow	Pa
s_e	slope of the relation between saturated vapor pressure and temperature	--
T	element air temperature;	°C
T_h	gage station temperature;	°C
T_{max}	daily maximum temperature;	°C
T_{min}	daily minimum temperature;	°C
T_s	ground surface or snow pack temperature;	°C
T_{smax}	threshold temperature above which precipitation is rain;	°C
T_{smin}	threshold temperature below which precipitation is snow;	°C
t	time;	T

Symbol	Notation	Unit
t_1	time;	T
t_2	time;	T
t_n	days after the last snow event	T
t_{Dmax}	time after cutting at which the maximum cover density located;	year
t_{end}	time;	T
t_f	time after cutting at which the final limit of cover density approached;	year
t_{rise}	sunrise time of the day;	T
t_{set}	sunset time of the day;	T
t_{start}	time;	T
u	wind speed;	ms^{-1}
W_{ice}	solid water phase in snowpack (water equivalent depth);	cm
W_{liquid}	liquid water phase in snowpack;	cm
W_{max}	maximum biomass of the vegetation	kPa
W_r	weight surcharge of vegetation (biomass);	kPa
W_s	water equivalent depth in the snowpack;	cm
x	distance between elements;	m
Z	element elevation;	m
Z_0	roughness length in wind profile	m
Z_a	elevation where the air temperature T is measured;	m
Z_b	elevation where the wind speed is measured;	m

To my wife Jinying and daughter Noel

獻給妻子晉英和女兒思齊

A COUPLED HYDROLOGIC-GEOMORPHIC MODEL FOR EVALUATING EFFECTS OF VEGETATION CHANGE ON WATERSHEDS

1. GENERAL INTRODUCTION: APPROACHES TO EVALUATE EFFECTS OF FOREST LANDUSE ON HYDROLOGY

Land use activities that alter the type and extent of vegetation cover on a watershed can change the hydrologic and geomorphic responses of the watershed. The potential for forest harvesting to alter watershed processes is increasingly a focus of research, as forested watersheds become more intensively managed and attempts are made to minimize possible adverse impacts and maintain the biodiversity and sustainability of forested systems.

Logging not only removes biomass and changes the vegetation cover of a watershed, but also modifies water and sediment production, transport and storage processes and affects streamflow quantity, quality and timing (Brown and Beschta, 1985). Understanding the effects of forest harvesting on watersheds has relied on various approaches, including field studies of paired experimental/manipulated watersheds, and lumped and distributed modeling of watershed processes. More recent emphasis has shifted to predicting spatially-varying hydrologic and geomorphic responses to landuse at fine spatial resolutions (Storck et al., 1995; Duan and Grant, 1996b).

1.1 Traditional Watershed Studies

The paired-watershed method is often used to evaluate effects of timber harvesting on watershed processes. Watersheds in close proximity to one another are selected on the basis of similar soil, vegetative cover, geology, topography, and size (Brooks et al., 1991). After several years of calibration, one watershed is typically maintained as a control while others receive various treatments. Subsequent analyses of streamflow and sediment production are used to quantify the effects of the treatments.

In the Pacific Northwest, U.S.A., for example, at least 23 watersheds in seven locations have been monitored in paired-watershed studies over the past several decades (Table 1.1). These watersheds are located in the Coast Range and Cascade Mountains and range from 10 hectares to 500 hectares in size. These watersheds also have various topographic settings, geologic substrates, vegetation covers, elevations, slopes and aspects. Effects of forest treatments, typically observed as change in annual water yield and peakflow responses, are analyzed to see different management effects (Table 1.2). Annual water yields have increased for initial years after cutting in most of the treated watersheds. Peakflows, on the other hand, are controversial due to the complex responses from differences in disturbances, variation in biotic and geomorphic controls, and lack of adequate data.

One major problem of paired-watershed studies is that relating cause and effect of harvesting to watershed processes requires many years of data collection and analysis before conclusions can be drawn (Hewlett and Doss, 1984). Another problem is the difficulty in generalizing from a specific site to a region. Even though decades of data may be available, there are still problems in dealing with low frequency phenomena, such as the major peakflow. Recently, studies that centered on observation, theory, and experimentation have been augmented by numerical simulation using computer models. In particular, physically-based, spatially-distributed models may provide new approaches for studying watershed behavior.

1.2 Physically Based Spatially Distributed Models

The construction and application of watershed models has been a prime focus of hydrologic research for many decades. Various models have provided frameworks in which to conceptualize and investigate hydrologic systems and the relationship between climate, landuse and water resources (Leavesley, 1994). These models perform the system transformations which link hydrologic input, such as precipitation, to catchment output, such as streamflow (Chow et al., 1988). Hence models can be structured according to the

Table 1.1 Paired watersheds studied in Pacific Northwest

No	Study Location	Watershed	Area (ha)	Aspect	Elevation (m)	Precipitation		Mean Annual Flow At Control (cm)	Mean Slope (%)	Parent Material	Vegetation		Study Begin-End
						Mean Annual (cm)	Type				Type	Age (yr)	
1	HJ Andrews 1	HJA-1	96.0	NW	400-1080	233	rain snow	141	53-63	altered volcaniclastic	Douglas-fir W.Hemlock	100 - 500	1953 1946-continue
2		HJA-2*	60.3										
3		HJA-3	101										
4	HJ Andrews 2	HJA-6	13.0	S	830-1100	215	rain snow	129	27-31	relatively unaltered volcaniclastic	Douglas-fir	120 - 140	1964-continue
5		HJA-7	15.4										
6		HJA-8*	21.4										
7	HJ Andrews 3	HJA-9*	8.5	SW	425-715	233	rain snow	165	65-70	altered volcaniclastic	Douglas-fir W.Hemlock	300-500	1967-continue
8		HJA-10	10.2										
9	Coyote Creek	CC-1	69.2	N-NE	730-1065	133	rain	58	23-36	altered volcaniclastic	Douglas-fir Mixed Conifer	100 - 300	1964-1981
10		CC-2	68.4										
11		CC-3	49.8										
12		CC-4*	48.6										
13	Alsea	FB*	203	S	135-485	243	rain	196	34-40	sandstone	Alder Douglas-fir	120	1957-1973
14		NB	70										
15		DC	303										
16		DC-2	56										
17		DC-3	40										
18		DC-4	16										
19	Casper Creek	SF	424		37-320	119	rain		20	sandstone shale	Redwood Douglas-fir	85	1963-continue
20		NF*	508										
21	Fox Creek	FC-1	59	W-NW	840-1070	272	rain snow	175	5-9	igneous, glacial till	Douglas-fir W.Hemlock	300 - 500	1957-1980
22		FC-2*	253										
23		FC-3	71										

** Control watershed*

Table 1.2 Forest harvesting and roading effects (adapted after Wright et al., 1990)

Watershed	Logging System	Silvicuture* Treatment (%)	Area Compacted (%)	Water Yield Increase				Low Flow (%)	Peakflow		Timing
				Max (cm)	Initial (cm)	Mean cm	Mean %		Road	Logging(L/S ha-%	
HJ-1	cable	CC-100,BB-100		56	53	38	34	NS		fall peaks increased up to 7(200%);large winter peaks,ns	
HJ-3	cable	CC-25,BB-25	10	27	15	18	17	NS	-	mean increase .33(10%);data on larger peaks lost	
HJ-6	10%tracter 90%cable	CC-100.BB-100		42	42	38	30	135		no significant changes	NS
HJ-7	60%tracter 40%cable	SC-60,BB-100		24	19	20	22	133		NS	NS
HJ-10	cable	CC-100,YUM-100	19							annual rain-on-snow peaks decreased 4.4(36%);annual rain fall peaks ns	
CC-1	tractor	SC-50,UT	13	NS	1 NS	6 NS	8			mean peaks increased.85(30%);larger peaks(9 year return) increased 3.2(48%)	
CC-2	14%tractor 16%cable	CC-30,TP14 YUM-16	5	9	7	9	14			NS	
CC-3	23%tractor 77%cable	CC-100,TP-23 YUM-77	12	37	33	29	43			mean peaks increased 1.5(44%);larger peaks(9 year return) increased 3.0(35%)	
NB	10%tractor 72%cable	CC-82,BB-82	5	62		49	27		ns	large peaks >5.5 ns;peaks >.03:fall increased 1.7(50%) and winter increased 1.1(19%)	
DC	cable	CC-26,UT	4	15		7	5		ns	NS	
DC-2	cable	CC-30,YUM30									
DC-3	cable	CC-65,UT	12						+.55	fall increase .33(50%) and winter 1.3(30%)	
DC-4	cable	CC-90,UT								fall increased 3.0(51%) and winter 1.1(20%)	
SF	tractor	SC-60,UT	16					43	NS	peaks .19-.78 increased .52(107%);larger peaks>4.7,ns	
FC-1	cable	CC-25,BB-25				-		-		NS	
FC-3	cable	CC-25,YUM-25				-		-		NS	

ns = No significant change detected.

* CC, clearcut; SC, sheltwood harvest; BB, broadcast burn; TP, tractor piled; YUM, slash was cable yarded; UT, slash nontreated.

treatment of randomness, spatial heterogeneity, and temporal variations in natural hydrologic processes (Chow et al., 1988).

The principal purpose of utilizing models, as discussed by Linsley (1982) and Beven (1989), is to understand processes and predict future outputs. Process investigations include understanding the sensitivities of various factors influencing hydrologic responses and testing theoretical concepts of certain hydrologic mechanisms. Future prediction involves forecasting the change in hydrologic and geomorphic responses after climatic and/or landuse change. Engineering applications include accelerating engineering tasks and improving data accuracy, such as record extension, data fill-in and revision, and operational simulation.

1.2.1 Evolution of surface hydrologic models

Hydrologic models have evolved from simple linear models of precipitation-runoff relationships (Perreault, 1674, cited from Linsley, 1982) to spatially distributed complex models (Beven and Kirkby, 1979). Linsley (1982) and O'Connell (1991) review the history of hydrologic modeling in detail. Quantitative hydrology, immature at the beginning of the twentieth century, gradually evolved as rational analysis has replaced empiricism (Chow et al., 1988). The rational method developed by Mulvaney (1851) represented the first formal and longest-used relationship for predicting discharge from rainfall. Research on catchment hydrology has greatly advanced through unit response studies, based on time variations (e.g. Nash, 1958; O'Donnell, 1960; Dooge, 1965), following the introduction of the unit hydrograph by Sherman (1932). The publication of Box and Jenkin's (1970) text on time series analysis, forecasting, and control, led to a "new flurry" (O'Connel, 1991) of algebraic activity in the domain of conceptual modeling. The topic of spatial variation received some attention, although progress was limited by computational power. In recent years, the natural evolution of modeling and increasingly powerful computers have driven progress in physically-based and spatially-distributed models. Two events in 1979 provided more momentum to spatially-varied catchment hydrology studies. One was the development of TOPMODEL in Europe (Beven and Kirkby, 1979) and the other was the introduction of the Geomorphic Instantaneous Unit

Hydrograph (GIUH) developed in America (Rodriguez-Iturbe and Valdes, 1979). Both models incorporated spatial variation into catchment response but with different emphases. TOPMODEL focused on the upland or hillslope and the "contributing area", whereas GIUH emphasized the stream network itself with greatly simplified hillslopes.

1.2.2 Spatially distributed approaches

The last decade has seen an increasing emphasis on the need to predict spatially variable hydrologic and geomorphic processes at quite fine resolutions. Many spatially-distributed hydrologic and geomorphic watershed models have been developed in recent decades, including TOPMODEL (Beven and Kirkby, 1979), PRMS (Leavesley et al., 1983), SHE (Abbott et al., 1986), THALES (Grayson et al., 1992), and dSLAM (Wu, 1993).

Unlike lumped models that treat watersheds as homogeneous with respect to topography, soil, vegetation and land use and calculate hydrologic response as a dependent variable of meteorological input, physically-distributed models divide the catchment into homogenous elements within which all the characteristics are assumed uniform, with differences among elements. The hydrologic response of each element are computed within a proper time and spatial sequence.

The aims of developing a physically-based model are laudable, given the problems presented by spatial heterogeneity. While lumped models are simple, objective and often provide good predictability, they provide limited understanding of basic hydrologic processes. Lumped models describe all basin variations and temporal differences by altering coefficients.

Several limitations exist for lumped parameter models (Abbott et al., 1986). Sufficiently-long paired data for calibrations are needed and may not always be available. Calibration involves curve fitting, making physical interpretation of the fitted parameter values very difficult. Therefore, predicting effects of land use change by changing parameter values may not be done with confidence; and such models have not generally made use of data such as topography, soil type, and patterns and changes of vegetation. On the other hand, physically-based distributed models "can in principle overcome many

of these deficiencies through their use of parameters which have a physical interpretation and through their representation of spatial variability in the parameter values" (Abbott et al, 1986). Another benefit of physically-based models is the potential to understand some of the processes controlling hydrologic response. Although recently developed, physically-distributed models have not provided much more predictability than simple models (Beven, 1989; Grayson et al., 1992b).

This recent trend toward spatially-distributed modeling is largely due to recognition of the disadvantages of lumped watershed models and the development of technology, especially GIS, remote sensing, and digital terrain analysis (Abbott et al., 1986). All of these factors make it feasible to consider smaller scale heterogeneity.

Distributed models are essentially lumped at finer scales, which implies that the hydrologic response of a watershed is sensitive to the resolution of the elements. Wood et al. (1988; 1990) investigated the existence of a representative elementary area (REA) in the context of hydrologic modeling at the catchment scale and defined it as the minimum area within which "implicit continuum assumptions can be used without knowledge of the patterns of parameter values, although some knowledge of the underlying distributions may still be necessary" (Wood et al., 1988). Their investigation of a 13 km^2 watershed resulted in 1 km^2 REAs (Wood et al., 1988). This area is larger than the element sizes utilized in most spatially-distributed hydrologic models (e.g. Bathurst, 1986; Grayson et al., 1992a).

1.2.3 Terrain analysis and spatial configuration

The basic prerequisite for distributed hydrologic modeling is data preparation and estimation of model parameters. The time and expertise required for this can be prohibitive, especially if large areas are involved. Recent advances in GIS and increasing availability of commercial and freely distributed data sets can reduce the time involved in parameter estimation and in performing scenario change analyses for a number of watershed conditions. Physically-distributed hydrologic models are inherently map-based and provide a productive area for application of GIS techniques and associated terrain analysis.

Spatial heterogeneity plays a central role in runoff and related sediment yield issues as well as in other landscape ecological issues. Hydrologic processes, such as streamflow generation, are controlled by storm throughflow and the generation of overland and subsurface flow within a basin. The frequency and magnitude of these processes are controlled by local soil hydraulic properties and topographic factors, along with a variety of other factors, such as micro-climate, and vegetation type and cover density. Simulation of these processes over large spatial scales requires both a model structure and a parameterization strategy that can capture and identify the variability of system behavior over space and time, in addition to maintaining simplicity in model applications (Band and Wood, 1988). There is a trade-off between accuracy and process representation for operational convenience. Accordingly, the structure and size of the hydrological response units or elements can be somewhat subjective.

In distributed hydrologic models, the geometry (i.e., size, shape and aspect) and connectivity (i.e., spatial relations among elements) of distributed elements are handled in several ways. For fine resolution models, the geometry and spatial connectivity are both considered in most cases. For some coarse grain models, such as PRMS (Leavesley et al., 1983), the connectivity is ignored and spatial connections between elements are abstracted especially when the model is run in daily mode.

Terrain analysis is one of the important tools used to partition a watershed into elements and extract attributes. Topographic attributes of primary and secondary or compound attributes (Moore et al., 1991) can all be obtained directly or calculated from spatial layers or coverages. As shown in Moore et al. (1991), primary attributes are calculated directly from elevation data, such as slope and aspect; compound attributes involve combinations of the primary topographic attributes and are physically-based or empirically derived indices, such as wetness index (O'Loughlin, 1986). There are three principle ways of structuring digital elevation data of a watershed for use in hydrologic-geomorphic models, as reviewed by Moore et al. (1991). The three data structures possess different operational advantages and drawbacks (Jones et al., 1990; Moore et al., 1991) (Table 1.3). Also shown are examples of hydrologic and geomorphic models using different data structures built around RASTER-, TIN- and contour-based DEM networks.

1.3 Objectives

Models that couple landuse (e.g., forestry) to watershed hillslope and channel processes (e.g. streamflow, sediment transport, water chemistry) and account for spatial heterogeneity will improve watershed analyses and provide quantitative assessments of different management scenarios. In principle, these models can be used to predict the effects of watershed changes (e.g., landuse, fire), and climate change (e.g., global warming), to predict the output of ungaged watersheds, or to assess the spatial variability of watershed input and output (Abbott et al., 1986). These advantages are due to the physical interpretations of parameters which can be evaluated for the changed watershed conditions. Coupled models will also give us an opportunity to examine hydrologic and

Table 1.3 Operational Characteristics of raster, TIN, and vector data structure

Data Structure	Advantages	Disadvantages	Model
Raster	Most common structure and widely used; easy transferring for pixel-based remote sensed data; less data storage; implementational and computational efficiency.	Flow paths are not necessarily down the greatest slope line; difficult to handle abrupt changes in elevation; size or scale of grid mesh affects the results and efficiency; zig-zag flow paths; lack of precision in defining catchment area.	TOPMODEL (Beven & Kirkby, 1979); ANSWERS (Beasley & Huggins, 1982); SHE (Abbott et al., 1986); AGNPS (Young et al., 1989)
TIN	More accurate representation of the original grid data; Boundaries of triangulation can conform to any desired shape; Piecewise linear nature.	Priori knowledge required to orient the outflow edge; non-trivial modeling because variable boundary conditions; difficulties in determining the upslope connection of a facet; the irregularity of the TIN makes the computation of attributes difficult	
Vector	Based on the stream path analogy; flow is more realistic than the above two.	Larger (order of magnitude) data storage; computational slower.	THALES (Grayson et al., 1992); dSLAM (Wu, 1993);
Abstracted	Irregular shape with flexible boundary.	The spatial connections between elements are not explicitly described.	PRMS (Leavesley, 1983)

geomorphic responses simultaneously over a broader range of climatic conditions than what might actually have been realized. Models linking with forest dynamics will also let us to investigate the relationship between forest growth patterns and watershed responses. Research to develop, validate, and apply these models in different physiographic and climatic settings is a key area of interaction between biological and physical disciplines.

The objectives of this research are:

1. Develop a physically-based, spatially-distributed and coupled hydrologic-geomorphic model with vegetation dynamics. The interactions between important hydrological, geomorphic and vegetation processes should all be included in this model.

2. Test and validate the coupled model and identify the influence of parameter uncertainties to model performance.

3. Explore the effects of landuse and management practices on geomorphic and hydrologic processes of forest watersheds using the model.

2. STRUCTURE AND COMPONENTS OF CLAWS, A COUPLED HYDROLOGIC-GEOMORPHIC MODEL FOR LANDSCAPE AND WATERSHED STUDIES

2.1 Abstract

Interest in effects of forest management and other disturbances on watershed processes has prompted the need to develop models that are sensitive to landuse changes. Models are needed to allow researchers and resource managers to investigate the effects of alternative cutting patterns on stream flows and geomorphic processes in small and large watersheds and thereby provide tools for planning harvest activities across landscapes. While hydrologic, geomorphic and forest dynamics are closely coupled, most models treat them independently. Here we describe the modeling framework for a physically based, spatially distributed hydrologic-geomorphic model that has been coupled with vegetation-dynamics simulation. The spatial variability of topography, soil, vegetation, and climate drive a hydrology module that calculates the water budget at given time steps with a user-specified spatial resolution; hydrologic processes incorporated in the model include snow hydrology, interception, evapotranspiration, infiltration, subsurface flow, deep ground water exchange, overland flow and channel flow. The hydrology drives hillslope and channel geomorphic processes including probability of mass movements (landslides, debris flows) and fluvial sediment transport. Both the hydrologic and geomorphic modules are linked to the forest growth simulation so that effects of changing forest stand structure in response to clear cutting or other disturbances through time can be examined.

2.2 Introduction

With increasing awareness and concern for the environment, considerable research effort has focused on evaluating the effect of landuse changes, especially those associated with human activities, such as forest management, on watershed hydrology and erosion.

Commonly, this research has been based on paired watershed studies of similar small drainages with controls and treatments (e.g. Harr, 1976, 1979, 1983; Grant and Wolff, 1991). Recently, a new land management paradigm called watershed analysis (WA), essentially ecosystem analysis at the watershed scale, seeks to systematically understand and organize ecosystem information including biological, hydrologic and geomorphic features, conditions, processes and interactions (RIEC, 1995). Watershed analysis can provide a practical analytical framework for spatially-explicit, process-oriented scientific assessment to guide management decisions to meet specific management and social objectives (Montgomery et al., 1995). Watershed models linking physical and ecological processes at basin scales are some of the tools needed to achieve these objectives. Hydrology, geomorphology and forest dynamics are systematically linked, but most researchers study them independently. Models which couple landuse (e.g., forestry) to watershed hillslope and channel processes (e.g. streamflow, sediment transport, water chemistry) will improve watershed analyses and provide quantitative assessments of different management scenarios. Research to develop, validate, and apply these models in different physiographic and climatic settings is a key area of interaction between biological and physical disciplines.

Because of the spatial heterogeneity of topography, soil, vegetation and climatic conditions, landuse activities must also be explored on a finer scale to investigate their influence on hydrologic and geomorphic processes of a watershed. Recently, physically-based, spatially-distributed models have been developed to study the interaction between hydrology, geomorphology and vegetation dynamics with the increasing power of computer hardware and extensive data availability to understand the underlying hydrologic-geomorphic processes. Wu (1993) advanced a conceptual model linking forest management and slope stability based on the infinite slope approach developed by Sidle (1991, 1992) and incorporated it into a distributed model using contour-based data structure (Moore et al., 1988; Moore and Grayson, 1991) to investigate the possible influences of forest cutting on mass movement. Wigmosta et al. (1994) developed a distributed hydrology-vegetation model that explicitly describes the soil-vegetation-

atmosphere interactions for complex terrain. No attempts have been made to combine the hydrologic-geomorphic processes together with forest dynamics.

We describe here the structure and components of a physically-based, spatially-distributed hydrologic-geomorphic model with vegetation dynamics. Note that the objective of being "physically based" is not adhered to in the strictest sense, since some of our processes, primarily vegetation dynamics, are modeled using characteristic functions. The spatial variability of topography, soil, vegetation and climate have been handled to the extent that it is incorporated in the important processes within the hydrology-geomorphology-vegetation system.

2.3 Model Description

The model is designed to integrate hydrologic and geomorphic processes with forest dynamics in complex terrain described by digital elevation data (Figure 2.1). The general approach of this model is detailed in Figure 2.2. These three parts of hydrology, geomorphology and forest dynamics, are linked together using physically based process equations or characteristic functions (Figure 2.3).

A watershed is partitioned into elements or hydrologic response units (HRUs) and topographic attributes of each element are obtained, based on terrain analysis. Input data such as precipitation, temperature and solar radiation are adjusted in terms of elevation. Spatial soil and vegetation distribution and logging history are also read in from a GIS database and assigned to each element.

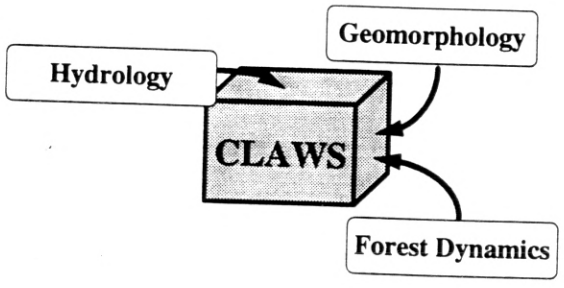


Figure 2.1 General concepts of CLAWS, a coupled landscape and water system.

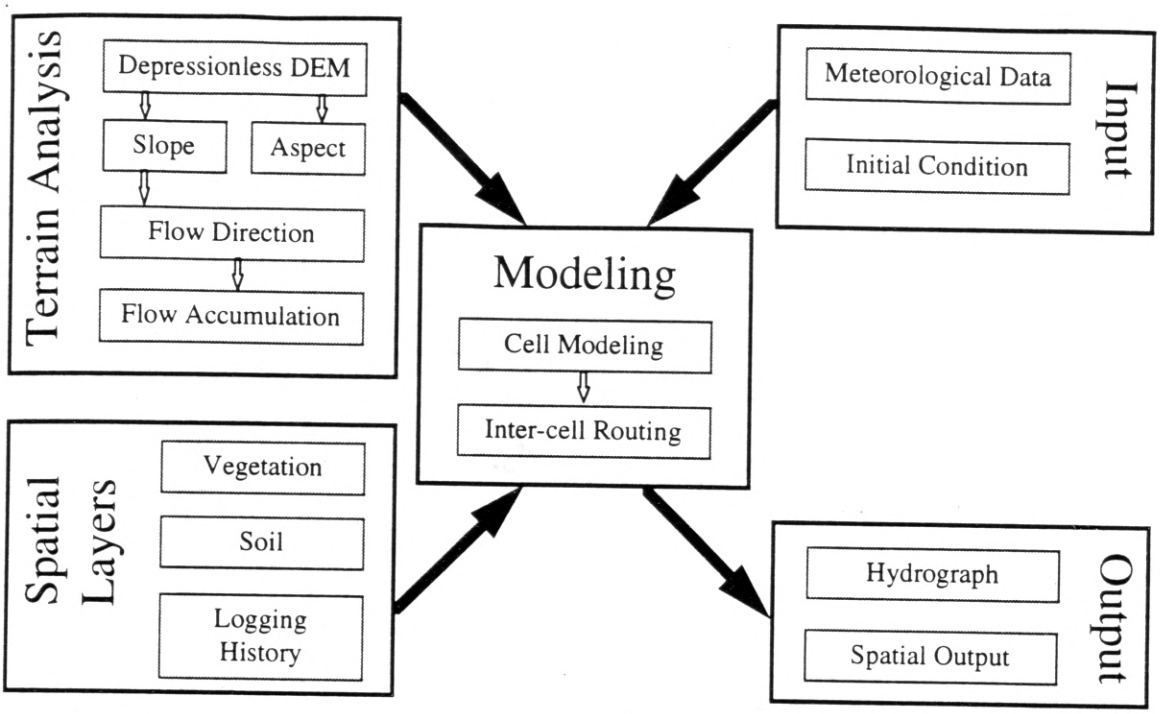


Figure 2.2 General procedure in spatial distributed hydrologic-geomorphic modeling

Vegetation characteristics such as biomass, tree height, cover density, leaf area index, and root strength are calculated based on the logging history to simulate the vegetation dynamics after cutting or in non-cutting conditions. In the present version of this model, only clearcutting and partial cutting can be handled and we assume a single layer canopy structure.

Precipitation, after accounting for interception and evapotranspiration, is routed from each element with a combined subsurface and overland flow equations.

Landslide occurrence is simulated with an infinite-slope model using the hydrologic results and vegetation conditions. Following any slope instability, the possible runout path of a debris flow is simulated using the local slope, channel geometry and a mass decay function. Sediment transport out of the watershed by streamflow is based on an empirical rating curve relating discharge to sediment transport.

The following sections describe the hydrologic and geomorphic processes, and vegetation dynamics incorporated in CLAWS, as well as the dynamic integration between CLAWS and GIS.

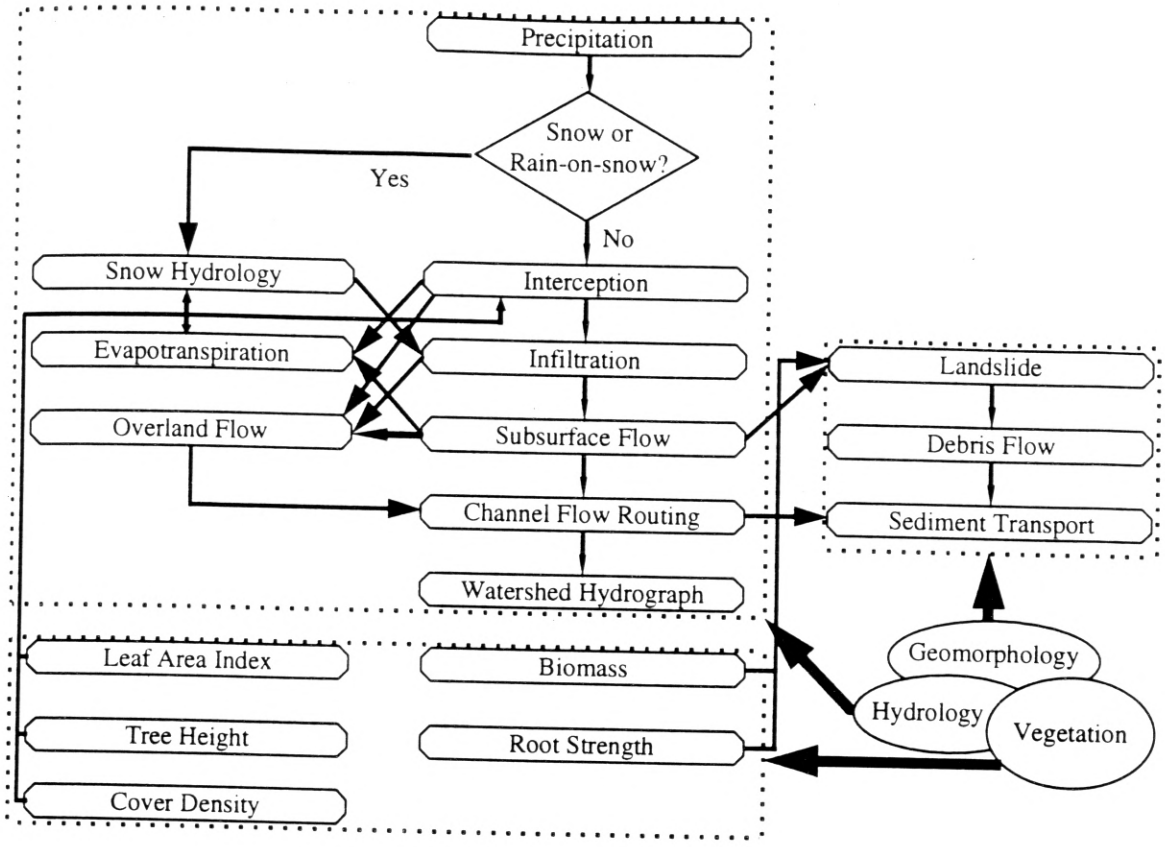


Figure 2.3 Interactions between hydrologic-geomorphic responses and forest dynamics

2.3.1 Terrain analysis and geographical information system linkage

The relative magnitude of many hydrologic processes operating in natural landscapes are sensitive to topographic position. Indices of these processes can be developed as functions of distributed soil, vegetation and topographic attributes. Terrain analysis is one of the basic and pre-requisite steps for further distributed hydrologic modeling using various data structures. Those different data structures (grid, TIN, vector or contour based) have different advantages and disadvantages that may impose limitations according to research goals, computer hardware and the problem itself (Moore et al., 1991).

Although the hydrologic and geomorphic process modules in CLAWS are independent of the topographic data structure, the grid based data structure is used because of its simplicity and the ease of obtaining spatial data (e.g., remotely sensed

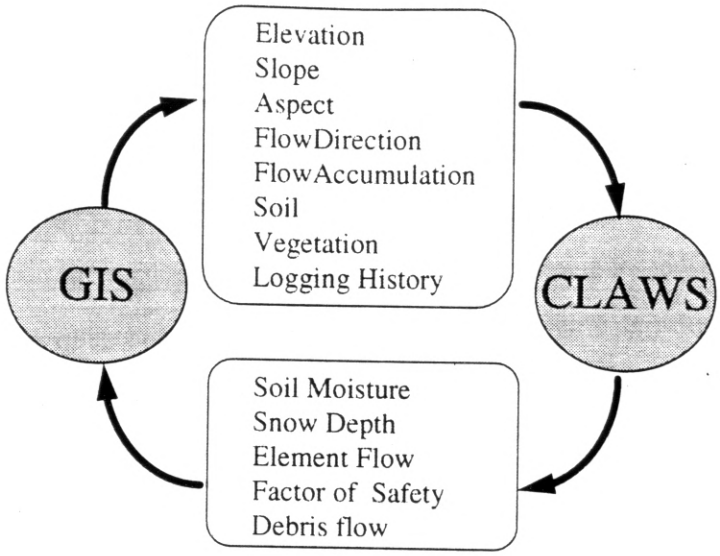


Figure 2.4 Model spatial input and output linked to Geographical Information System

imagery). A commercial Geographical Information System software, ARC/INFO®[1], is used to accomplish the terrain analysis of the watershed based on the topographic Digital Elevation Model data and other spatial layers of soil and vegetation characteristics.

CLAWS produces temporal output including hydrographs at any user indicated locations, several basin averages such as basin mean soil moisture and mean snow depth, while spatially distributed results are dynamically linked to ARC/INFO®. The model writes a series of ASCII files such as element flow, soil moisture content, factor of safety, debris flow and snow depth distribution at any time of the simulation as well as Arc Macro Language (AML) files that let users directly display their spatial results in the Arc environment (Figure 2.4).

2.3.2 Hydrology

Incoming precipitation is differentiated as rain and/or snow. Snow accumulation and melt are computed when the incoming precipitation includes snow or there is snow on the ground. Interception is described as a linear function with leaf area index. Total evapotranspiration from each element is based on the Penman-Monteith equation

[1] ARC/INFO is a trademark of Environmental Systems Research Institute, Inc. This is only for information purposes and is not to be considered a product endorsement by the authors, the Oregon State University or the USDA.

(Monteith, 1965) and subdivided into three components of evaporation from bare soil and non-canopy substrate, evaporation from canopy, and transpiration from the canopy.

Subsurface water movement is based on the Dupuit assumptions (Dupuit, 1863) of slope-parallel saturated flow through a limited depth of soil over a relatively impermeable layer of parent material or bedrock. Overland flow is assumed only to occur when the ground is saturated. Some exchange between deep groundwater and the subsurface layer is incorporated. Intercell water movement is modeled with a kinematic continuity equation, and a combined subsurface and overland flow equation are solved to route water from one element to another.

2.3.2.1 Meteorological data adjustment

Description of topographic influences on precipitation amounts have been greatly simplified by a linear relationship between precipitation amount and the elevation difference between the base gage and distributed elements. Hence

$$P = \left[1 + k_p(H - H_b)\right]P_b \tag{2.1}$$

where P, P_b are element precipitation and base gage precipitation respectively at elevations H and H_b; k_P is a constant.

Temperature is also linearly adjusted as

$$T = k_T(H - H_b) + T_b \tag{2.2}$$

where T, T_T are element and gage temperatures; k_T is the lapse rate.

2.3.2.2 Snow accumulation and melting

Two point linear temperature partitioning is used to differentiate the incoming precipitation into rain and snow. A single layer snowpack energy and mass-balance model is utilized with a finite difference solution to simulate snow accumulation and melt when the incoming precipitation has a snow component or there is snow on the ground. This is described in detail in the next chapter.

2.3.2.3 Interception

Interception refers to the amount of water retained by a vegetation canopy during a storm. As an important water-balance component of precipitation, it is incorporated in

the storm mode of the distributed model, but ignored in daily mode since interception is accounted for by evapotranspiration as a whole (Zinke, 1965). Usually it is a function of storm character (i.e. type, intensity and duration), plant species and density, and season (Zinke, 1965; Brooks et al., 1991). In heavily forested lands, it may account for up to 25% of annual precipitation (Bras, 1990). Interception is modeled as a decay function

$$I_T = I_{\max}(1 - e^{-\frac{k_I P_T}{I_{\max}}}) \tag{2.3}$$

where I_T is cumulative interception; P_T is accumulated precipitation of a given storm; I_{max} is the storage capacity of vegetation for the projected area of canopy and k_I is a constant (Aston, 1979). The water balance in the vegetation is accounted for as follows

$$I_t = \begin{cases} \min\{I_{t-1} + P - E_c, I_{\max}\} & I_{t-1} + P - E_c > 0 \\ 0 & I_{t-1} + P - E_c < 0 \end{cases} \tag{2.4}$$

where I_t and I_{t-1} are water stored in vegetation at time t and t-1 respectively; E_c is the evaporation from canopy which is discussed in the next section. The precipitation after interception P_s is adjusted with the cover density C_D of the distributed element as

$$P_s = \begin{cases} P - C_D(E_c + I_t - I_{t-1}) & I_t = I_{\max} \\ (1 - C_D)P & I_t < I_{\max} \end{cases} \tag{2.5}$$

The storage capacity is a linear function of leaf area index LAI (Herwitz, 1985):

$$I_{\max} = a_I + b_I LAI \tag{2.6}$$

Herwitz (1985) observed constant a_I ranges from $0.5\text{x}10^{-3}$ to $1.5\text{x}10^{-3}$ and b_I from $2.2\text{x}10^{-4}$ to $3.3\text{x}10^{-4}$. The resulting value of I_{max} in this equation has units of meters. Dickinson's approach (1984) using a_I as zero and b_I as $2\text{x}10^{-4}$ is utilized here in determining interception for this model.

2.3.2.4 Evapotranspiration

Three types of evapotranspiration are considered in this model. They are evaporation and transpiration from the vegetation canopy and evaporation from bare soil or non-canopy substrate. The total evapotranspiration for the grid element is the summation of the three based on the weights of canopy cover density in this element.

Evapotranspiration from the tree canopy is calculated using the Penman-Monteith equation (Monteith, 1965). Assuming the similarity of the tree canopy conductance for

sensible heat and water vapor, maximum canopy evaporation E_c and transpiration E_T are calculated based on Hancock et al. (1983) and Whitehead and Kelliher (1991) as:

$$E_c = \frac{s_e R_n + \rho_a c_p (e_s - e) g_a \Delta t}{\lambda_v} \left[\frac{I_T / I_{\max}}{s_e + \gamma} \right] \tag{2.7}$$

$$E_T = \frac{s_e R_n + \rho_a c_p (e_s - e) g_a \Delta t}{\lambda_v} \left[\frac{1 - I_T / I_{\max}}{s_e + \gamma (1 + g_a / g_c)} \right] \tag{2.8}$$

where R_n is the net radiation available to the canopy during time Δt in units of Wm^{-2}; λ_v is latent heat of vaporization in J kg^{-1} $^oC^{-1}$; s_e is the slope of the relation between saturated vapor pressure and temperature calculated as follows (Tetens, 1930):

$$s_e = \frac{4098 e_s}{(T + 237.3)^2} \tag{2.9}$$

c_p is the specific heat of moist air, here used as a constant (1.013 kJ kg^{-1} ^oC); ρ_a is air density as

$$\rho_a = 1.23 - 0.112Z \tag{2.10}$$

where Z is the element elevation above sea level. The psychometric constant, γ, represents a balance between the sensible heat gained from air flowing past a wet bulb thermometer and the sensible heat transformed into latent heat (Brunt, 1952), and is calculated as

$$\gamma = \frac{c_p p_a}{0.622 \lambda_v} \tag{2.11}$$

where p_a is the air pressure; g_a and g_c are the aerodynamic conductance and canopy conductance, respectively.

Assuming neutral atmospheric stability, the aerodynamic conductance to the transfer of water is calculated as (Monteith and Unsworth, 1990; Louis, 1979)

$$g_a = \frac{1.351 K_v^2 u}{\left[\ln \left(\frac{Z_b - d_0}{Z_0} \right) \right]^2} \tag{2.12}$$

where K_v is von Karman's constant, which we take as 0.4, d_0 is the zero plane displacement height and Z_0 is the roughness length; Z_b is the elevation where the wind

speed is measured; u is the windspeed. It has been found that a reasonable approximations to d_0 and Z_0 for coniferous forest are (Jarvis et al., 1976)

$$d_0 = 0.78H_t \tag{2.13}$$

$$Z_0 = 0.075H_t \tag{2.14}$$

where H_t is the tree height.

Canopy conductance g_c is represented as a summation of stomatal conductance, g_s, of individual leaves. Leaves are assumed to contribute in parallel, so conductance g_s is averaged (Dickinson et al., 1991; Whitehead and Kelliher, 1991):

$$g_c = g_s LAI \tag{2.15}$$

Following Dickinson et al (1991), we represent the dependence of g_s on model variables and for different ecosystems by a maximum value g_{max} and a product of limiting factors of temperature (T), vapor pressure deficit (e_s-e), photosynthetically active radiation flux density (PAR) and soil moisture (θ):

$$g_s = g_{\max} f_1(T) f_2(e_s - e) f_3(PAR) f_4(\theta) \tag{2.16}$$

where f values represent the dependence, and each has a maximum value of one. These are described as (Dickinson et al., 1991; Sellers et al., 1986):

$$f_1 = 0.08T - 0.0016T^2 \tag{2.17}$$

$$f_2 = 1 - \frac{e_s - e}{c_d} \tag{2.18}$$

$$f_3^{-1} = 1 + \frac{a_2 g_{\max}}{b_2 + PAR} \tag{2.19}$$

$$f_4 = \begin{cases} 0 & \theta \le \theta_w \\ \dfrac{\theta - \theta_w}{\theta_r - \theta_w} & \theta_r > \theta > \theta_w \\ 1 & \theta \ge \theta_r \end{cases} \tag{2.20}$$

where c_d is the vapor pressure deficit causing stomatal closure and taken as 4 kPa (Wigmosta et al., 1994). a_2 and b_2 are adjustable constants; θ, θ_w, θ_r are current soil moisture, soil moisture at wilting point and field capacity respectively.

Maximum evaporation from bare soil or non-canopy substrate is also based on the Penman-Monteith equation (Monteith, 1965) by substituting canopy conductance with the surface conductance of the substrate g_b following Shuttleworth and Wallace (1985), or

$$E_s = \frac{s_e R_n + \rho_a c_p (e_s - e) g_a \Delta t}{(s_e + \gamma(1 + {}^{g_a}\!/_{g_b}))\lambda_v} \tag{2.21}$$

In the study by Shuttleworth and Wallace (1985), the substrate resistance, g_b^{-1} ranged between 0 and 2000 sm^{-1}, for soil at two extreme situations of fully saturated and fairly dry conditions. Here we present a equation to estimate the resistance for different moisture levels based on Shuttleworth and Wallace (1985):

$$g_b^{-1} = 2000\left[\frac{\theta_s - \theta}{\theta_s - \theta_w}\right]^m \tag{2.22}$$

where m is a coefficient we arbitrarily took as 3.0 in this model and θ_s is the saturated moisture content.

So the total evapotranspiration from the element is

$$E = C_D(E_c + E_T) + (1 - C_D)E_s \tag{2.23}$$

2.3.2.5 Infiltration

Runoff is calculated for each element only when the rain intensity is greater than the saturated conductivity, at which point Horton overland flows occur. Green-Ampt infiltration (1911) is used, due to its strength as a physically-derived equation, its widespread use, and its simple form. Many techniques have been developed to estimate the parameters of this equation. The algorithm, described by Chow et al (1988), is adopted here along with the Newton-Raphson method to obtain a numerical solution of infiltration. The rate of infiltration, f, and cumulative infiltration, F, are as follows:

$$f = K(\frac{\psi\Delta\theta}{F} + 1) \tag{2.24}$$

$$F - \psi\Delta\theta \ln(1 + \frac{F}{\psi\Delta\theta}) = Kt \tag{2.25}$$

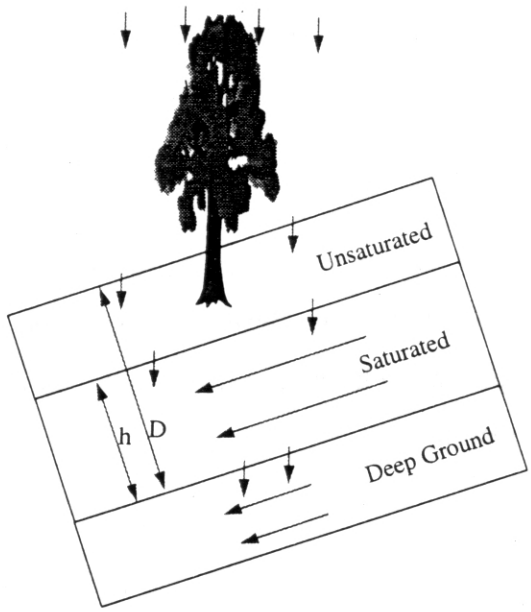


Figure 2.5 Conceptual water movement path in an element

where K is the saturated conductivity of soil. For variable saturated conductivity, a depth average saturated conductivity is used in the above equation; ψ is wetting front suction; and $\Delta\theta$ is effective porosity of soil.

2.3.2.6 Subsurface flow

Subsurface flow is an important quick flow mechanism in forested areas. The scheme used here divides the soil into two layers: a lower saturated layer and an upper unsaturated layer (Figure 2.5). Conceptually, the upper layer comprises mainly vertical movement, and the lower layer transports water parallel to the slope. This is essentially an extended Dupuit assumption (Dupuit, 1863; Beven, 1981, 1982). The assumption is that infiltrated water flows downslope in a saturated layer overlaying a base of much slower water movement of impermeable base. The governing equation for saturated flow is

$$\frac{\partial q_s}{\partial x} + \Delta\theta \frac{\partial h}{\partial t} = p_c - q_{in} \tag{2.26}$$

with

$$q_s = Kh\sin\beta \tag{2.27}$$

where h is the saturation level, q_s is the subsurface flow, x is the length of the hillslope and p_c is the percolation from the upper layer to the lower layer; $\Delta\theta$ is the effective storage of porosity; β is the slope, and q_{in} is the exchange between subsurface and deep groundwater reservoir.

Saturated conductivities for soils have been treated as varying with the saturated depth, following Beven et al. (1982). Several functions (linear, power function, exponential) have been tested and the following exponential function has been found to be superior:

$$K = K_{\max} e^{k_k(\frac{h}{D}-1)} \tag{2.28}$$

Here h is saturation depth and D soil depth. K_{max} is the saturated conductivity when the soil profile is fully saturated and k_k is a decay coefficient.

As should be noted, the hydraulic conductivities in forested watersheds are quite high and small response times are needed. This may be due to water flowing through interconnected macropores created by roots, or other organic matter, and cracks between aggregates and rocks rather than through the soil matrix (e.g. Beven and Germann, 1982; Sloan and Moore, 1984). Hence the hydraulic conductivity used to characterize subsurface flow may be different from that measured from small soil cores (Moore and Grayson, 1991). For field applications of this model, this parameter should be considered as an "effective" hydraulic conductivity of the soil rather than the measured value of hydraulic conductivity for the soil matrix (Moore and Grayson, 1991).

The subsurface moisture change due to evapotranspiration is treated in accordance with the excess of precipitation and the saturated depth in the element. If the saturated depth is not zero, the transpiration from canopy and evaporation from bare soil are treated as negative flux to the above continuity equation; when the saturated depth is zero, the whole soil profile is assumed to uniformly contribute to evapotranspiration.

2.3.2.7 Deep groundwater exchange

Exchanges between the subsurface layer and deep ground water (Figure 2.5) have been simulated based on two decay functions. Deep groundwater is described as a

reservoir in this model. The flow from subsurface to deep groundwater, q_{in}, is simulated as a function of saturated depth of the soil profile,

$$q_{in} = k_{out} h \tag{2.29}$$

The flow rate from deep groundwater to deep groundwater storage of the next element, q_{out}, is a function of deep groundwater storage, G, such that

$$q_{out} = k_{out} G \tan\beta \tag{2.30}$$

Here Dupuit's assumption (1863) is used and k_{out} is deep groundwater saturated conductivity.

Deep groundwater may also leak out of the element to outside the system. The sink term, q_{leak}, is also defined a function of storage,

$$q_{leak} = k_{leak} G \tag{2.31}$$

So the continuity equation for deep groundwater storage is

$$\frac{dG}{dt} = q_{in} + q_{upper} - k_{out} G \tan\beta - k_{leak} G \tag{2.32}$$

where q_{upper} is the deep groundwater flow from deep groundwater storage of upper elements. To simplify the solution, q_{in} and q_{upper} are taken as constant over each time period. Integrating the above gives the storage at the end of each time interval:

$$G_t = \frac{q_{in} + q_{upper}}{k_{out} \tan\beta + k_{leak}} + (G_0 - \frac{q_{in} + q_{upper}}{k_{out} \tan\beta + k_{leak}}) e^{-(k_{out} \tan\beta + k_{leak})t} \tag{2.33}$$

Therefore total deep groundwater flow to the next element for the period is

$$Q_{out} = \int_0^t q_{out} dt = \frac{k_{out} \tan\beta}{k_{leak} + k_{out} \tan\beta} \left[(q_{in} + q_{upper})t + G_0 - G_t \right] \tag{2.34}$$

When a channel is located in the element, deep groundwater will be intercepted by the channel.

2.3.2.8 Overland and channel flow routing

For possible saturated overland flow in the variable source areas and channel flow, the kinematic wave model (e.g. Chow et al., 1988) is applied:

$$\frac{\partial Q}{\partial x} + \frac{\partial A}{\partial t} = q_l \tag{2.35}$$

where Q is the discharge, A is the cross-section area and q_l is the lateral flow. It has been used extensively for the calculation of overland flow and channel flow hydrographs because of its relative simplicity and agreement with observed hydrographs. Considering the high infiltration capacity in forest soils, saturation overland flow is the most likely case for any possible overland flow in forest areas. We follow Moore and Grayson (1991) and adapt the combined surface and subsurface approach described by Takasao and Shiiba (1988), which does not require the explicit calculation of exfiltration. Manning's equation is used to characterize the relation between A and Q for overland flow and channel flow as:

$$A = (nP_r^{\frac{2}{3}} S^{\frac{1}{2}})^{\frac{3}{5}} Q^{\frac{3}{5}} \tag{2.36}$$

where P_r is the wetted perimeters of overland flow or channel flow, S the slope of element, and n the Manning's roughness.

The four point finite difference solution presented by Brakensiek (1967) is used here. It is unconditionally stable, and the dispersion of the numerical scheme overcomes the problems of kinematic shocks that can occur on cascading planes when solving the kinematic equations using the method of characteristics. However, the numerical dispersion, which causes an under-prediction and delay in the magnitude and timing of the peak runoff with this method is a recognized limitation (Kibler and Woolhiser, 1970). The finite difference form of the equation then is

$$A_4 + 2Q_4 \frac{\Delta t}{\Delta x} = A_1 - A_2 + A_3 + 2Q_2 \frac{\Delta t}{\Delta x} + 2q_l \Delta t \tag{2.37}$$

where the Q and the A variables are the discharges and "apparent" flow cross-sectional areas including surface and subsurface flow (Moore and Grayson, 1991), respectively, Δt is the time interval, subscripts 1 and 3 refer to time t at positions x and $x+\Delta x$, respectively, and subscripts 2 and 4 refer to time $t+\Delta t$ at positions x and $x+\Delta x$, respectively. At any time and any element, the terms on the right hand side are known quantities and the Q_4 can be solved according to the discharge-area relationships.

2.3.3 Geomorphology

The geomorphic processes considered in this model include three types of material displacement mechanisms: shallow landslides, debris flows and stream sediment transport. The three processes involve hillslope and channel interactions and are driven by watershed hydrologic processes. Sheet erosion is not incorporated in the model at present since it is not a major concern in forested regions due to the scarcity of overland flow.

2.3.3.1 Slope stability analysis

Following Wu's (1993) model dSLAM, this model adopts the algorithm and concept from Sidle (1991, 1992) relating forest management to land stability. The Infinite Slope model is used here to characterize the stability of each element with a factor of safety (FS):

$$FS = \frac{C + \Delta C + \{[(D-h)\gamma_m + h(\gamma_{sat} - \gamma_w)] + W_r\}\cos\beta\tan\phi}{[(D-h)\gamma_m + h\gamma_{sat} + W_r]\sin\beta} \qquad (2.38)$$

where C is soil cohesion; ΔC root strength; W_r is the surcharge weight of vegetation; γ_m and γ_{sat} are the unit weight of soil at field moisture content and saturation, respectively; D the soil depth; β slope; and ϕ the internal frictional angle.

The Infinite-Slope method is a popular slope stability analysis tool owing to its simplicity and applicability to shallow landslides. Generally, the infinite slope model does not adequately analyze deep-seated rotational failures, but is adequate for failures of a soil mantle that overlie a sloping drainage barrier, which may be bedrock or denser soil mass (Hammond, 1992). The infinite slope model relies on several simplifying assumptions (Hammond, 1992):

- The failure plane and the groundwater (phreatic) surface are assumed to be parallel to the ground surface. The drainage barrier and ground surface often are found to be nearly parallel on colluvial slopes. Also, a large hydraulic conductivity contrast between the soil and drainage barrier can cause groundwater flow to be nearly parallel to the drainage barrier. Therefore, the conditions of parallelism often are approximately met. If their criterion is not met, the factor of safety calculated from the above setting may be in significant error (Iverson and Major, 1986, 1987).

- The failure plane is assumed to extend infinitely. Because in nature the failure plane does extend to the ground surface, the values for root strength and soil cohesion along the true failure plane, not just along the drainage barrier, are used.
- Only a single soil layer is considered. In the CLAWS model, failures are assumed to occur along the upper boundary of the deep groundwater layer.
- The infinite slope equation is based on a two-dimensional analysis, and is most appropriate for wide blocks where resistance along failure sides is not significant relative to resistance along the base. If failures are narrower, the infinite slope mode is conservative in that it over predicts failures (Burroughs, 1984).

  Theoretically, failure will occur unconditionally when the slope is so steep that

$$\frac{C + \Delta C + (D\gamma_m + W_r)\cos\beta\tan\phi}{(D\gamma_m + W_r)\sin\beta} \leq 1.0 \qquad (2.39)$$

and land with sufficiently low gradient will be stable even when saturated if

$$\frac{C + \Delta C + \{D(\gamma_{sat} - \gamma_w) + W_r\}\cos\beta\tan\phi}{(D\gamma_{sat} + W_r)\sin\beta} \geq 1.0 \qquad (2.40)$$

2.3.3.2 Landslide runout or debris flow

Upon the calculation of the factor of safety, an unstable mass may be moving as landslide runout or in liquefied state as a debris flow. Several researchers have suggested some theoretical methods to calculate the run-out distance of sliding mass (e.g. Hungr et al., 1984; Cannon and Savage, 1988), but the practical applicability of these methods is limited because the initial velocity of a sliding mass is impossible to simulate. Benda (1985) summarizing field observation in the Oregon Coast Range, indicated that channel floor slopes less than 3.5° or stream junction angles greater than 70° are the stopping sites for debris flows. In this study, the debris flow paths are estimated based on three criteria:

- The channel slope must be greater than 3.5° for debris flow to continue moving.
- We assume the mass in the debris flow is changing because of local depositions. The total moving mass is simulated using a decay function based on how many spatial elements have been traversed. In actual calculation, we used a constant 0.1 meter as the decay rate for runout material.

- Stream geometry (here width) is another limiting factor. As Johnson (1970) indicated, debris flows stop because they become too thin to sustain continued flow. Cannon and Savage (1988) suggested that thinning is a combined result of the loss of material from the flowing mass through deposition and the spreading of debris on relatively planar slopes. Based on the geometry, if the spreading depth of the flow is less than a critical depth, the debris flow will also stop. The critical depth D_T is calculated as (Johnson, 1976)

$$D_T = \frac{S_k}{\gamma_{sat} \sin \beta} \tag{2.41}$$

if yield strength S_k is known. But the applicability of this equation is limited by the unknown yield strength. So in this paper, we arbitrarily defined a coefficient so that if the volume of flowing debris spreading on the channel in an element is less than 0.1 meter, the flow is assumed to have stopped.

We did not include the stream junction angle because, in the topographic raster data structure of the watershed used here, the stream junction angle is not well defined.

2.3.3.3 Sediment transport

Suspended and bedload sediment transport out of the watershed is simulated based on the empirical relationship of the sediment rating curve with discharge in the form of

$$Q_s = a_s Q^{b_s} \tag{2.42}$$

where a_s and b_s are constants.

2.3.4 Vegetation dynamics

The role of vegetation is very important in hydrologic and geomorphic processes. Precipitation is intercepted and soil moisture is depleted by transpiration from vegetation. Vegetation also creates ground roughness, impeding overland flow. Subsurface water paths may be changed by macropores produced by vegetation roots (Beven and Germann, 1982). Geomorphically, vegetation generally prevents sheet erosion, although root throw produces some sediment (Swanson 1979; Swanson et al., 1986). Root strength of vegetation increases soil cohesion and slope stability (Sidle 1991, 1992). In this model, vegetation regrowth is modeled over time since harvest or other disturbance (e.g., fires).

Leaf area, cover density, biomass, tree height and root cohesion and the dynamic changes with time are simulated on a yearly basis.

2.3.4.1 Cover density

The pattern of cover density after cutting is a complex process that involves plant succession and competition. The early dominance of Douglas-fir will increase the cover density to maximum, and after silver fir invades the cover density gradually decreases to a final limit (Figure 2.6). So here we approach this pattern using a three parameter model as

$$C_D = \begin{cases} \dfrac{c_c t}{a_c^2 + (t + b_c)^2} & t \le t_f \\ C_{Df} & t > t_f \end{cases} \tag{2.43}$$

where C_D is cover density and a_c, b_c, c_c are constants depending on the maximum cover density C_{Dmax} and the time required to reach maximum cover density, t_{Dmax}, the final cover density and the time, C_{Df} and t_f.

$$b_c = \frac{t_f t_{D\max} C_{D\max} - \dfrac{C_{Df}}{2}(t_f^2 + t_{D\max}^2)}{t_f (C_{Df} - C_{D\max})} \tag{2.44}$$

$$a_c = \sqrt{t_{D\max}^2 - b_c^2} \tag{2.45}$$

$$c_c = 2C_{D\max}(t_{D\max} + b_c) \tag{2.46}$$

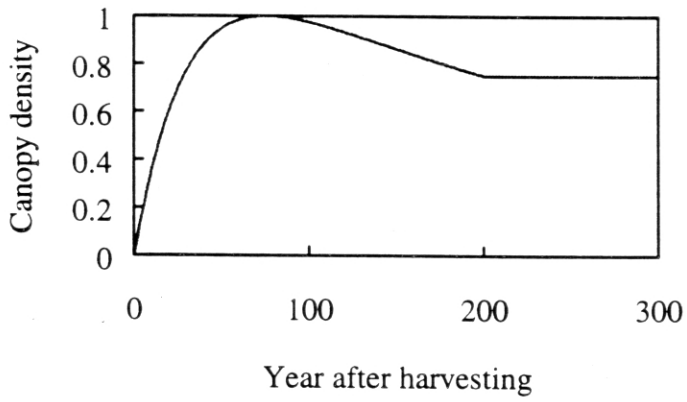


Figure 2.6 Cover density changes post cutting

For HJ Andrews Experimental Forest, C_{Dmax}, t_{Dmax}, C_{Df} and t_f are respectively 1.0, 75 year, 0.75 and 200 years (Personal communication, Dr. Mark Harmon, OSU, 1994), which results in $a_c = 42.19$, $b_c = 62.01$ and $c_c = 234.38$.

2.3.4.2 Leaf area index

Leaf area index is modeled using Chapman-Richards' function (Richards, 1959)

$$LAI = LAI_{\max}(1 - e^{-B_1 t})^{B_2} \tag{2.47}$$

where the maximum leaf area index for this region is about 10 and B_1 about 0.075, and B_2 about 1.0 (Personal communication, Dr. Mark Harmon, OSU, 1994).

2.3.4.3 Tree height

Tree height growth curves for different regions may differ significantly and environmental variation within that area may cause differences in height growth curve form (Means and Sabin, 1989). For this study, we use Richards' equation (Richards, 1959) on a 5-parameter base as

$$H_t = (c_0 + c_1 S_i)(1 - e^{-c_2 S_i t})^{c_3 + c_4 S_i} \tag{2.48}$$

where c's are parameters and S_i is the site index defined as tree height at 100 years age.

2.3.4.4 Biomass

Different functions have been used for calculating biomass after harvesting. The sigmoid function described by Sidle (1987) is used here:

$$W_r = W_{\max}[(a_w + b_w e^{-k_w t})^{-1} + d_w] \tag{2.49}$$

where W_t is the biomass over the element at t years after cutting; W_{max} is the maximum weight trees can grow in unit area, usually using the weight average of trees of certain age; a_w, b_w, c_w and d_w are constants. As indicated by Sidle (1992), the model assumes that tree surcharge is uniformly distributed across each element.

2.3.4.5 Root strength

A similar regrowth curve is used to model root cohesion from regrowth C_r as used in modeling biomass (Sidle, 1992). An exponential curve is used to model the decay of old

root strength C_{rd} (Sidle, 1992). Mathematically, the general shape of conceptual root strength regeneration is

$$C_r = C_{\max}[(a_r + b_r e^{-k_r t})^{-1} + d_r] \tag{2.50}$$

and old root deterioration as:

$$C_{rd} = C_{\max} e^{-k_d t^{m_1}} \tag{2.51}$$

Then the total root strength is given as

$$\Delta C = C_r + C_{rd} \tag{2.52}$$

where a, b, d, m, k's are all parameters and C_{max} is the maximum root strength (Sidle, 1991, 1992).

Sidle (1992) discussed partial cutting and shelterwood cutting management options with rotations in relation to root strength and biomass in each element. These options were also incorporated in this model.

2.4 Conclusions

Interest in effects of forest management and other disturbances on watershed processes has prompted the need to develop models that are sensitive to landuse changes. Models are needed to allow researchers and resource managers to identify areas of the landscape and components of the ecosystem sensitive to future changes and potential responses to land management. Because hydrologic, geomorphic and forest dynamics are coupled, it is desirable to have models that link hydrologic processes, geomorphic processes and vegetation dynamics.

CLAWS, a physically-based, spatially-distributed hydrologic-geomorphic model that has been coupled with vegetation dynamics has been presented here. The spatial variability of topography, soil, vegetation, and climate drive hydrology modules that calculate the water budget at given time steps with a user specified spatial resolution, based on the important hydrologic processes incorporated including snow hydrology, interception and evapotranspiration, infiltration, subsurface flow, deep ground water exchange, overland flow and channel flow. The hydrology drives hillslope and channel

geomorphic processes including probability of mass movements (landslides, debris flows) and fluvial sediment transport. Both the hydrologic and geomorphic modules are linked to forest growth simulation so that effects of changing forest stand structure in response to clear cutting or other disturbances through time can be examined.

Coupled hydrologic-geomorphic models, such as CLAWS, give us the opportunity to examine watershed response from changed scenarios (e.g., landuse), climatic change (e.g., global warming) and ungaged drainages, with accounting for the spatial variability. These models also provide the opportunity to examine hydrologic and geomorphic responses simultaneously over a broader range of climatic conditions than what might actually have been realized. They present tools for watershed analysis to investigate the relationship between forest regrowth pattern and watershed responses.

3. A SIMPLE ENERGY AND MASS BALANCE MODEL FOR SNOW ACCUMULATION AND MELT

3.1 Abstract

Snow accumulation and melt processes play an important role in the hydrologic and geomorphic responses of montane watersheds. It is necessary to model snow accumulation and melt from limited input data and parameters, particularly for spatially-distributed hydrologic models (such as CLAWS). Previous approaches to modeling snow processes have included empirical degree-day methods, These have the advantage of limited data requirements and the drawback of disregarding snow accumulation processes. Physically-based numerical models were constructed to account for the energy and mass exchange in snowpack. In this paper, we present a single layer, energy and mass balance model for snow accumulation and melt. The incoming precipitation is separated into rainfall and snow. The state of the snowpack is simulated based upon energy and mass exchange between atmosphere and subsurface soil using a finite difference numerical scheme. This energy and mass balance procedure is used for each element or hydrologic response unit in a distributed watershed subdivided into facets. Water is assumed to flow out of the snowpack and into the subsurface soil layer when the maximum liquid water holding capacity of the snowpack is exceeded. This algorithm has been tested using temporal observations and incorporated into a physically-based, spatially-distributed hydrologic and geomorphic model, CLAWS, that simulates the hydrologic and geomorphic responses of watersheds.

3.2 Introduction

In general, precipitation can include rain, snow, or rain-on-snow. The hydrologic and geomorphic responses of montane watersheds are strongly affected by snow accumulation and melt processes. Peakflows enhanced by rain-on-snow events are

responsible for most of the major flood events in western Oregon (Harr, 1981). Such floods commonly include mass movements triggered by the deep saturation zone created by rainfall combined with melting of warm, wet shallow snowpacks (Swanston, 1974; Swanson, 1976). Recent investigations also found that forest management can affect snow accumulation and melt processes (Berris and Harr, 1987). For hydrologic modeling, it is often desirable to model snow accumulation and melt from limited input data and parameters. Such models need to account for the spatial variability of landscapes and temporal variability of meteorological input. Two major modeling practices have been used in snow hydrology. The first calculates snow accumulation and melt from meteorological data (usually air temperature) by simple linear empirical equations; the other calculates all components of the energy input to the snow surface, the energy losses from the surface, and hence the residual energy available to melt the snow (Morris, 1991). The simplest empirical approaches using degree-day methods have been in use for almost 60 years (e.g. Collins,, 1934). These have the advantage of limited data requirements but the drawback that processes governing both snow accumulation and melt are ignored; the latter include solar radiation, albedo, topography, and the turbulent energy exchange (Anderson, 1976; Kustas et al., 1994). A recent study showed that combining a radiation component with the temperature-based approach improved the snowmelt estimation (Kustas, et al., 1994).

With the advent of digital computers physically based conceptual models were constructed to account for the energy and mass exchange in snowpacks (Anderson, 1968, 1976). More sophisticated approaches to model the energy balance of internal and boundary processes, and flow in porous media snow have been written for "unpolluted" snow which is only a mixture of ice, water, water vapor and air without impurities (Kelly, 1987; Morris, 1991).

Accounting for the spatial heterogeneity of snow accumulation and melt processes has been a major focus in hydrologic models (Leavesley, 1989; Ranzi and Rosso, 1991; Wigmosta et al., 1994). The primary difficulty in trying to incorporate point process knowledge into a watershed system with spatial heterogeneity has been further complicated because of incomplete knowledge of the physical and hydrologic parameters

of the watershed, and the meteorological data that influence the melt and runoff processes (Donald et al., 1995). Leavesley (1989) gave a detailed review of the problems involving snowmelt-runoff modeling and concluded that "developing snowmelt process algorithms which have parameters that are closely related to measurable basin and climatic characteristics" is the approach which is most likely to yield useful results.

In this paper, we first present the theory and model structure of a single layer, energy and mass balance model for snow accumulation and melt. Then we provide the test results using temporal observations from western Oregon mountains. Results from the incorporation into a physically-based, spatially-distributed hydrologic and geomorphic model, CLAWS, that simulates the hydrologic and geomorphic responses of watershed, is also shown using runoff production and spatial snowpack patterns.

3.3 Theory and Model Formulation

The incoming precipitation is separated into rainfall and snow based on a two point linear scheme. A single layer snowpack is simulated based on the energy and mass exchange between atmosphere and subsurface soil. This energy and mass balance procedure is used for each element or hydrologic response unit in a distributed subdivided watershed. Water is assumed to flow out of the snowpack and into the subsurface soil layer when maximum liquid water holding capacity is exceeded.

3.3.1 Partition of precipitation

There are several ways to determine if precipitation is rain or snow (Osborn et al., 1982). The simplest is to assume that all precipitation is either rain or snow based on a fixed temperature (0 °C or some similar value). For example, in the SCS Model TR-20, 1.7 °C serves as the dividing line between rain and snow (SCS, 1965). It is reasonable to employ an air temperature greater than 0 °C at the ground level since the snow is formed at considerable heights in the atmosphere (Osborn et al., 1982). Based on work by the U.S. Army Corps of Engineers (ACE, 1956; Wigmosta et al., 1994), a two point separation of the precipitation events is used in our model.

$$P_{snow} = \begin{cases} P & T \le T_{s\min} \\ \dfrac{T_{s\max} - T}{T_{s\max} - T_{s\min}} P & T_{s\min} < T < T_{s\max} \\ 0 & T \ge T_{s\max} \end{cases} \quad (3.1)$$

$$P = P_{rain} + P_{snow} \quad (3.2)$$

where P_{snow} and P_{rain} are the water equivalent depths of snow and rain respectively; T_{smin} is a threshold temperature below which all precipitation is in the form of snow, and T_{smax} is a threshold temperature above which all precipitation is rain. When the air temperature falls within the range of T_{smin} and T_{smax} (typically, -1.1°C and 3.3°C), a rain and snow mixture results.

The temperature and precipitation in distributed elements are adjusted from a linear relationship with elevation, which interpolate the gage measurements to each element based on a lapse rate and precipitation gradient.

3.3.2 Energy budget

3.3.2.1 Solar radiation

The potential solar radiation is attenuated by three factors, sky cloud cover, forest shadowing and snow reflection. Incoming daily short-wave solar radiation of each element is computed with the equations of Swift (1976), Thompson (1976), and Leavesley et al. (1983). Using information about slope, aspect, latitude, and daily maximum and minimum air temperature as input, solar radiation is estimated if the observed data is not available. First, potential clear sky solar radiation for the given slope, aspect, and latitude is computed. Sky cover is estimated as a function of daily range in air temperature. A ratio of "cloud sky" radiation to potential "clear sky" radiation (k_R) is then computed to estimate actual radiation as a fraction of potential solar radiation.

3.3.2.1.1 Daily potential clear sky solar radiation

Daily potential solar radiation (R_p) is computed as a function of Julian day, latitude, slope, and aspect of the site (Swift 1976). The declination and radius vector of the sun are computed as a function of Julian date to avoid the need for the solar tables

used by some algorithms (e.g., Frank and Lee, 1966). A detailed algorithm has been presented by Swift (1976).

3.3.2.1.2 Daily sky cover

If observed solar radiation data are not available, daily sky cover (S_k) is computed by the following relationship (cf. Leavesley et al., 1983):

$$S_k = RDC(M) + RDM(M)(T_{max} - T_{min}) \tag{3.3}$$

where RDC and RDM are the intercept and slope of the sky cover and daily air temperature range relationship for month M; T_{max} and T_{min} are observed maximum and minimum daily air temperatures. This appears to be more applicable to humid regions where extensive periods of cloud cover occur with or without precipitation such as the Pacific Northwest.

The sky cover value obtained above is used to compute the ratio (k_R) of cloud sky radiation to potential clear sky radiation (Thompson, 1976) by the parabolic function:

$$k_R = B + (1 - B)\ (1 - S_k)^{m_s} \tag{3.4}$$

where B is the y-axis intercept. Thompson (1976) produced a map of values of the intercept for different locations in the United States; m_s is a variable parameter less than 1.0 and suggested to be 0.61. The above equations are inverted to obtain parameters RDM and RDC when some observed solar radiation data from or near the site is available.

3.3.2.1.3 Daily radiation extrapolation

Computed daily potential solar radiation (R_p) for the slope-aspect combination is then adjusted to estimate shortwave radiation (R_s) for the site as:

$$R_s = k_R R_p \tag{3.5}$$

For days when observations are available, a ratio between potential solar radiation of the element and observation station is computed as:

$$B_R = \frac{R_p}{R_{pb}} \tag{3.6}$$

where B_R is dependent on the slope-aspect combination. Using the observed solar radiation R_{sb} at the station, the solar radiation for any element can be calculated by

$$R_s = B_R R_{sb} \tag{3.7}$$

This is based on the assumption that cloud condition is the same for the whole watershed during the interval of calculations.

3.3.2.1.4 Forest shadowing

Solar radiation below forest stands R_c is computed as (WMO, 1974):

$$R_c = k_c R_s \tag{3.8}$$

with

$$k_c = 1 - A_c\left[1 - (1 - C_D)^2\right]^{0.5} \tag{3.9}$$

where A_c is the transmission coefficient with 100% canopy density (about 0.9), dependent on forest type; C_D is the cover density of forest canopy.

3.3.2.1.5 Snowpack reflection

Solar radiation reduced from reflection R_r is computed:

$$R_r = R_c(1 - \alpha) \tag{3.10}$$

where the albedo α is a function of time. Albedo is calculated using equations (Laramie and Schaake, 1972) from Anderson's (1968) data:

$$\alpha = \begin{cases} 0.85(0.94)^{t_D^{0.58}} & \text{snow accumulation season} \\ 0.85(0.82)^{t_D^{0.46}} & \text{snow melt season} \end{cases} \tag{3.11}$$

where t_D is the days after the last snow event.

3.3.2.2 Net longwave radiation

The effect of forest cover on longwave radiation at the ground surface is treated like that of the overcast sky situation; black-body radiation and ground surface emissivity are unified (Eagleson, 1970). Therefore,

$$R_l = \sigma \Delta t\left\{\left[C_D + (1 - C_D)E_a\right]T^4 - T_s^4\right\} \tag{3.12}$$

where T and T_s are air temperature and ground surface (or snowpack) temperature respectively; σ is the Stefan-Boltzmann constant. Atmospheric emissivity, E_a, is calculated using (Idso, 1981):

$$E_a = \begin{cases} 0.740 + 0.049e & \text{No snow} \\ 0.757 & \text{Snow on the ground} \end{cases} \tag{3.13}$$

where e is vapor pressure in units of kPa.

3.3.2.3 Sensible and latent heat

Both latent and sensible heat transfer are turbulent transfer processes (Anderson, 1973). Latent heat involves the turbulent flux of energy exchanged at the surface due to vapor movement determined by vapor pressure difference between the snow surface and the overlying air. The transfer rate depends on turbulence, which is controlled by wind speed. Sensible heat, on the other hand, describes the energy exchange at the surface due to a difference in temperature between the snow surface and overlying air and is determined by the temperature gradient.

Here empirical relationships are used to describe latent heat exchanges Q_e, and sensible heat Q_s as (US Army Corps of Engineers, 1956):

$$Q_e = k_2 \lambda_i \rho_w (Z_a Z_b)^{-\frac{1}{6}} [e(T) - e_s(T_s)] u \Delta t \tag{3.14}$$

$$Q_s = k_1 \lambda_v \rho_w (Z_a Z_b)^{-\frac{1}{6}} [T - T_s] u \Delta t \tag{3.15}$$

$$p_a = 101.3 - 0.01055Z \tag{3.16}$$

$$\lambda_v = 597.3 - 0.57T_s \tag{3.17}$$

$$\lambda_s = 677 - 0.07T_s \tag{3.18}$$

$$\lambda_f = 79.7 \tag{3.19}$$

where ρ_w is the density of water, p_a is the surface atmospheric pressure, p_0 is the sea level atmospheric pressure, Z is the element elevation, Z_a is the elevation at which air temperature T is measured, u is wind speed at elevation Z_b, λ_v is latent heat of vaporization, λ_s is latent heat of sublimation and λ_f is latent heat of freezing; λ_i depends on the status of the snow pack (Anderson, 1968). If the snowpack is ripe and melting, λ_i is equal to λ_v; if snowpack is not melting, λ_i is equal to λ_s; k_1 and k_2 are constants that calculated from US Army Corps of Engineers (1956) as $k_1 = 3.6734 \times 10^{-5}$cm $m^{1/3}$second $minute^{-1}$ $^oC^{-1}$ m^{-1} and $k_2 = 2.5083 \times 10^{-4}$cm $m^{1/3}$ second $minute^{-1}$ kPa^{-1} m^{-1}.

3.3.2.4 Conduction

Heat conducted from the ground into snowpack is difficult to estimate. Usually it is important for long duration simulations (e.g., month) and negligible for short duration calculations (e.g., daily or finer). Brooks et al. (1991) estimate a constant snowmelt of

about 0.05 mm/day due to conduction. In this model, a constant heat transfer of 2 Langley/day is used and evenly distributed within the time interval of computation.

3.3.2.5 Advective heat of precipitation

Heat from rainfall is one of the major energy sources for snowmelt, especially in the Cascades Mountains of the Pacific Northwestern United States. The energy delivered via precipitation is given by:

$$Q_P = \rho_w T(c_w P_{rain} + c_s P_{snow}) \tag{3.20}$$

where c_w and c_s are respectively specific heat of water and ice.

3.3.3 Snowpack energy balance

Consequently the energy budget of the snowpack is (Anderson, 1976; Duan and Grant, 1996):

$$\frac{d(c_s W_s T_s)}{dt} = \sum q \tag{3.21}$$

where W_s is the water equivalent depth in the snowpack and Σq is rate of the energy delivery to the snowpack from various sources. The above equation can also be written as

$$c_s W_s \frac{d(T_s)}{dt} + c_s T_s \frac{d(W_s)}{dt} + W_s T_s \frac{d(c_s)}{dt} = \sum q \tag{3.22}$$

The specific heat of ice c_s is a function of temperature and can be expressed as (Anderson, 1976):

$$c_s = 0.503 + 0.00176 T_s \tag{3.23}$$

So we have

$$(c_s W_s + 0.00176 W_s T_s)\frac{d(T_s)}{dt} + c_s T_s \frac{d(W_s)}{dt} = \sum q \tag{3.24}$$

By using a finite difference scheme then:

$$T_s^{t+\Delta t} = \frac{R_r + Q_P + Q_m + Q_s + Q_e + R_l + (c_s + 0.00176 T_s^t) W_s T_s^t}{c_s(W_s + \Delta W_s) + 0.00176 W_s T_s^t} \tag{3.25}$$

where Q_m is the internal energy for melting or refreezing in the snowpack. If we ignore the mass change caused by latent heat transfer in the above equation (this is reasonable

because the amount is relatively small compared to precipitation) and considering the mass change is solely produced by any precipitation, then ΔW_s=P and

$$T_s^{t+\Delta t} = \frac{R_r + Q_P + Q_m + Q_s + Q_e + R_l + (c_s + 0.00176T_s^t)W_s T_s^t}{c_s(W_s + P) + 0.00176W_s T_s^t} \tag{3.26}$$

During periods of melt, the pack is isothermal at 0 °C (i.e., $T_s^{t+\Delta t} = 0$) and the heat available for snowmelt is:

$$Q_m = -\left[R_r + Q_P + Q_s + Q_e + R_l + (c_s + 0.00176T_s^t)W_s T_s^t\right] \tag{3.27}$$

During freezing periods, heat stored depends on the equivalent water depth frozen M_f with:

$$Q_m = \rho_w \lambda_f M_f \tag{3.28}$$

3.3.4 Snowpack mass balance

The snowpack is composed of two water phases, liquid and ice (Wigmosta et al., 1994):

$$W_s = W_{liquid} + W_{ice} \tag{3.29}$$

The dynamics of the two components are:

$$\Delta W_{liquid} = \begin{cases} P_{rain} - \dfrac{Q_m}{\rho_w \lambda_f} & T_s < 0.0 \\ P_{rain} + \dfrac{Q_e}{\rho_w \lambda_v} - \dfrac{Q_m}{\rho_w \lambda_f} & T_s = 0.0 \end{cases} \tag{3.30}$$

$$\Delta W_{ice} = \begin{cases} P_{snow} + \dfrac{Q_e}{\rho_w \lambda_s} + \dfrac{Q_m}{\rho_w \lambda_f} & T_s < 0.0 \\ P_{snow} + \dfrac{Q_m}{\rho_w \lambda_f} & T_s = 0.0 \end{cases} \tag{3.31}$$

A maximum liquid-water holding capacity is defined, L_{cmax}, that if the liquid-water content in the snowpack is greater than L_{cmax}, excess water will be drained from the snow pack and infiltrate to the soil subsurface. Or mathematically, the amount will be:

$$M_P = \begin{cases} W_{liquid} - \dfrac{W_{ice} L_{c\max}}{1 - L_{c\max}} & \text{if } \dfrac{W_{liquid}}{W_{liquid} + W_{ice}} > L_{c\max} \\ 0 & \text{if } \dfrac{W_{liquid}}{W_{liquid} + W_{ice}} \le L_{c\max} \end{cases} \tag{3.32}$$

and the liquid content of the snowpack is adjusted as:

$$W_{liquid} = W_{liquid} - M_p \tag{3.33}$$

3.4 Model Performance Test and Discussion

To evaluate model performance on simulating snow accumulation and melting, two kinds of tests, point simulation and distributed simulation, were utilized in the comparison of observed snow measurements and streamflow hydrographs.

Point simulations were constructed based on detailed snow moisture measurements at Vanilla Leaf gage, a high elevation meteorological station at H. J. Andrews Experimental Forest, located in the Cascade mountains of Oregon. The gage is located in an open canopy at an elevation of 1250 meters. Snow moisture (water equivalent) has been recorded from a snow pillow at hourly intervals since water year 1991, using a Campbell Scientific CR21X data logger. Additional observations of precipitation, temperature, relative humidity, solar radiation and wind speed were also automatically logged using appropriate equipment. Data have covered one high snow year (1993), one low snow year (1992), and two intermediate years (1991 and 1994), representative of the general snow pattern in the Cascades mountains.

The point simulation results compare observed and computed snowpack water equivalent for four sequential water years at Vanilla Leaf gage (Figure 3.1 to Figure 3.4). The root mean square errors for different water years were computed and expressed as a percentage of the measured mean (Kustas et al., 1994). The coefficients of determination (correlation) and the maximum accumulation were also assessed (Table 3.1)

Results show that this model described the general shape of the snow moisture accumulation and depletion curves for three of the four water years we simulated (Figure 3.1, Figure 3.2, Figure 3.3 and Figure 3.4), with an R^2 correlation between 0.83 to 0.94 for the overall data. The computed maximum water equivalent in the snowpacks are close to the observed data with a small range of errors between -11.3% to 3.5%. The simulated water equivalents do appear to smooth the small perturbations apparent in the observed

data, although these small perturbations could be noise from the electronic data logger as occurred in spring of 1992 (Figure 3.2). The error is a fluctuation pattern of 3-4 day periodicity with an amplitude of less than 2 cm (Figure 3.2).

The model results are more consistent with observed data in the rising part of the water equivalent curve than the falling part, as the correlation coefficients are much better for the snow accumulation season with smaller mean errors than that of the snow melt season (Table 3.1). This suggests that this model describes the snow accumulation season better than the melting season, although the exact cause of this discrepancy is unknown.

A detailed examination showed that temperature data acted as an important error source causing a large discrepancy between observed and simulated snow water equivalent in spring of 1993 (Figure 3.3). A large mean square error (109% larger than the observed mean of this water year) was produced by this disagreement. This is checked out by comparing the temperature readings with that of other neighboring stations, which shows the temperature readings between March 10th to April 22nd are unreasonably low. The lower error temperature readings delayed the melting from snowpack during our simulation. Another error source might be the limitation of single layer assumption of the snowpack, which will give poor representation of a thick snowpack.

Distributed simulation is based on the comparison of observed streamflow with simulated hydrologic responses resulting from the incorporation of this algorithm into a physically based, spatially distributed hydrologic and geomorphic model, CLAWS (Duan et al., in preparation). Interception is described as a linear function with leaf area index

Table 3.1 Point simulation statistics for different water years

Year	Peak Snow Accumulation			Correlation between observed and computed			Root Mean Square of Error (normalized with observed mean)		
	Observed (cm)	Computed (cm)	Error (%)	Accumulation	Melt	Total	Accumulation	Melt	Total
1991	27.10	28.05	3.5	0.93	0.72	0.83	0.34	0.85	0.57
1992	8.70	8.86	1.8	0.91	0.91	0.91	0.56	0.52	0.54
1993	78.00	75.12	-3.6	1.00	0.78	0.84	0.10	1.09	0.66
1994	24.50	21.74	-11.3	0.96	0.92	0.94	0.35	0.49	0.42

through the storage capacity. Total evapotranspiration from each element is calculated with the Penman-Monteith (Monteith, 1965) equation and subdivided into three components of evaporation from bare soil and non-canopy substrate, evaporation from canopy and transpiration from canopy. Subsurface water movement is based on Dupuit (1863) assumption of slope-parallel saturated flow through a limited depth of soil over a relative impermeable layer of parent material or bedrock. Overland flow is assumed only to occur when the ground is saturated. Some exchange between deep groundwater and the subsurface layer is incorporated. Intercell water movement is modeled with the kinematic continuity equation, and the combined subsurface and overland flow equation is solved to route water from one element to another. CLAWS also possesses modules to simulate landslide and sediment transport and vegetation regrowth, which are beyond scope of this paper.

The input data of temperature and precipitation at each spatial element were adjusted based on linear relationships with elevation. Solar radiation was adjusted based on slope-aspect combination described in chapter 2. WS#1, a 100-ha watershed at HJ Andrews Experimental Forest, is used as the test site for distributed simulations. WS#1 is located between elevation 440-1010 meters above sea level.

Figure 3.5 gives the spatial distribution of snow during 1992 from the distributed simulation. The dynamic change of snowpack is dominated by the elevation zones that largely control the precipitation and temperature patterns. The snow accumulation is a down-hill process (from Dec. 25, 1992 to March 8, 1993) and the melt is an up-hill process (from March 8, 1993 to April 19, 1993). Small variations from the elevation control are influenced by aspect and slope of the distributed elements.

Figure 3.6 shows the simulated and observed streamflow for the watershed outlet and basin average snow water equivalent for WS#1 between Dec. 1, 1991 and Jan. 22, 1992. The simulated hydrograph is reasonably consistent with the observed.

The model presented here is parsimonious. The few existing parameters may be changed including two point temperatures that partition the precipitation into rain or snow; the ground conduction constant; and the two coefficients in the equations for sensible and latent heat exchanges. The values we used for these mentioned parameters are

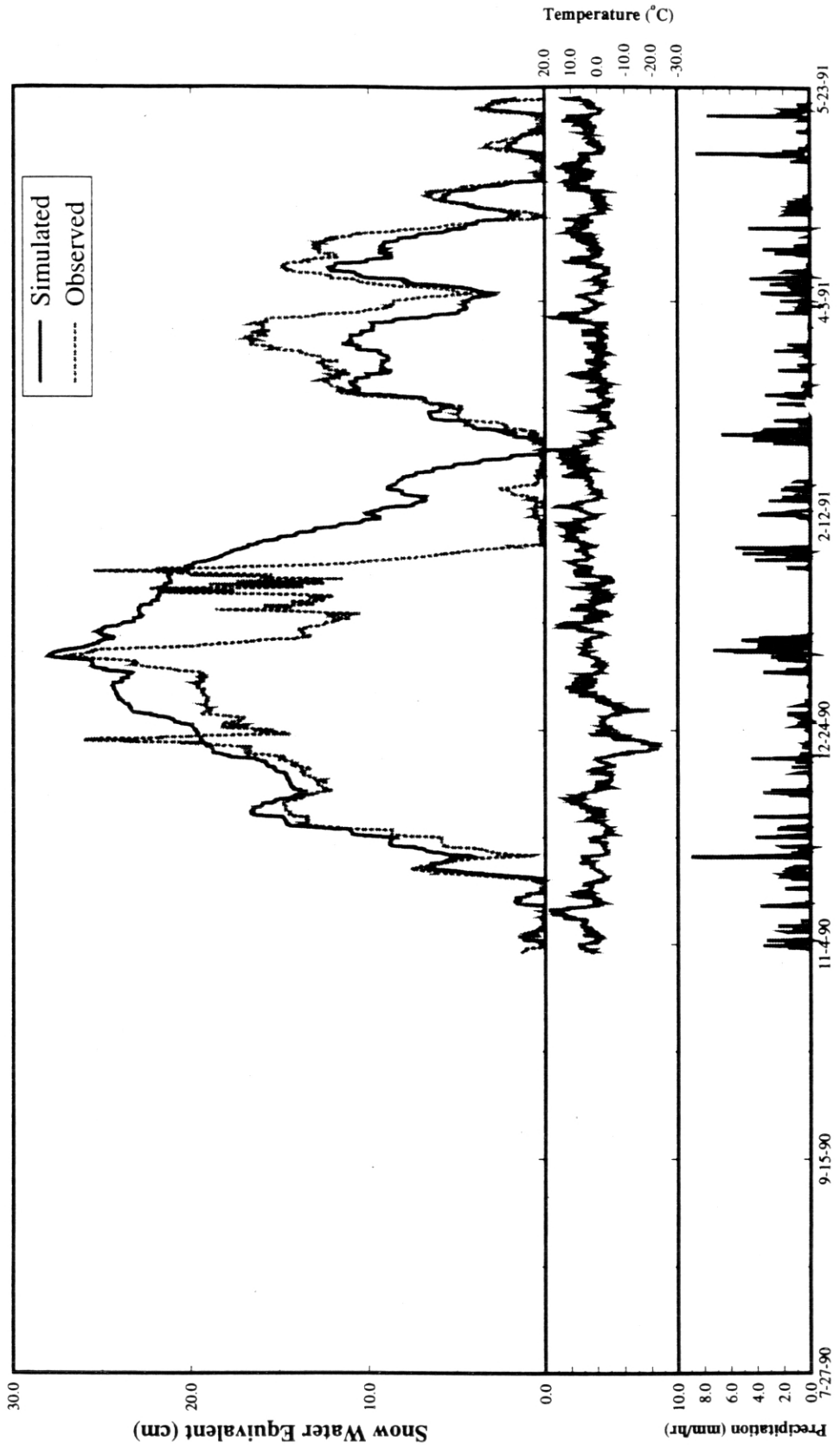


Figure 3.1 Snow water equivalent comparison between computed and observed at Vanilla Leaf during water year 1991 (medium snow).

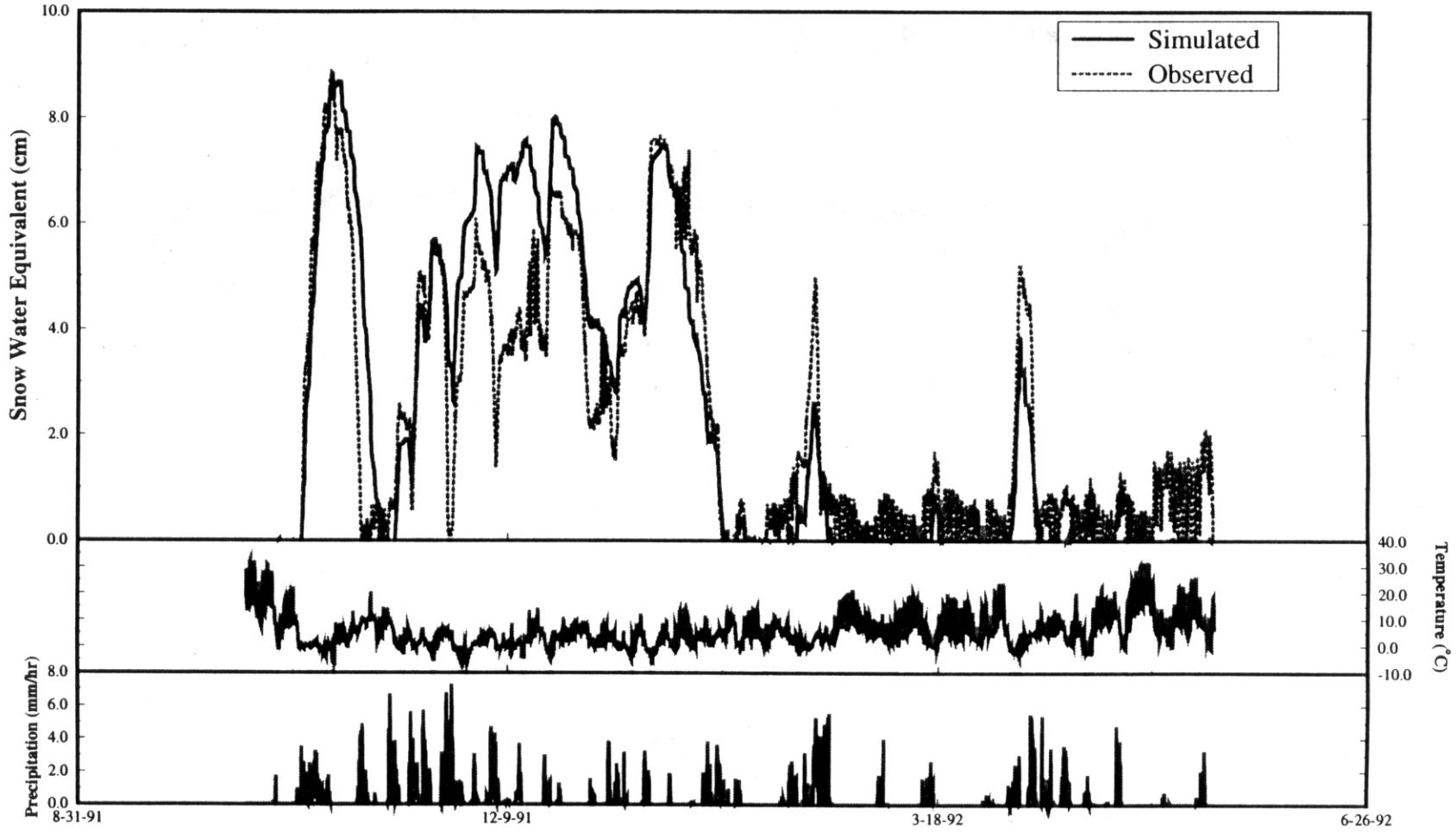


Figure 3.2 Snow water equivalent comparison between computed and observed at Vanilla Leaf during water year 1992 (low snow). Note the observed snow water data error of 2-3 days periodicity of low value from the data logger noise.

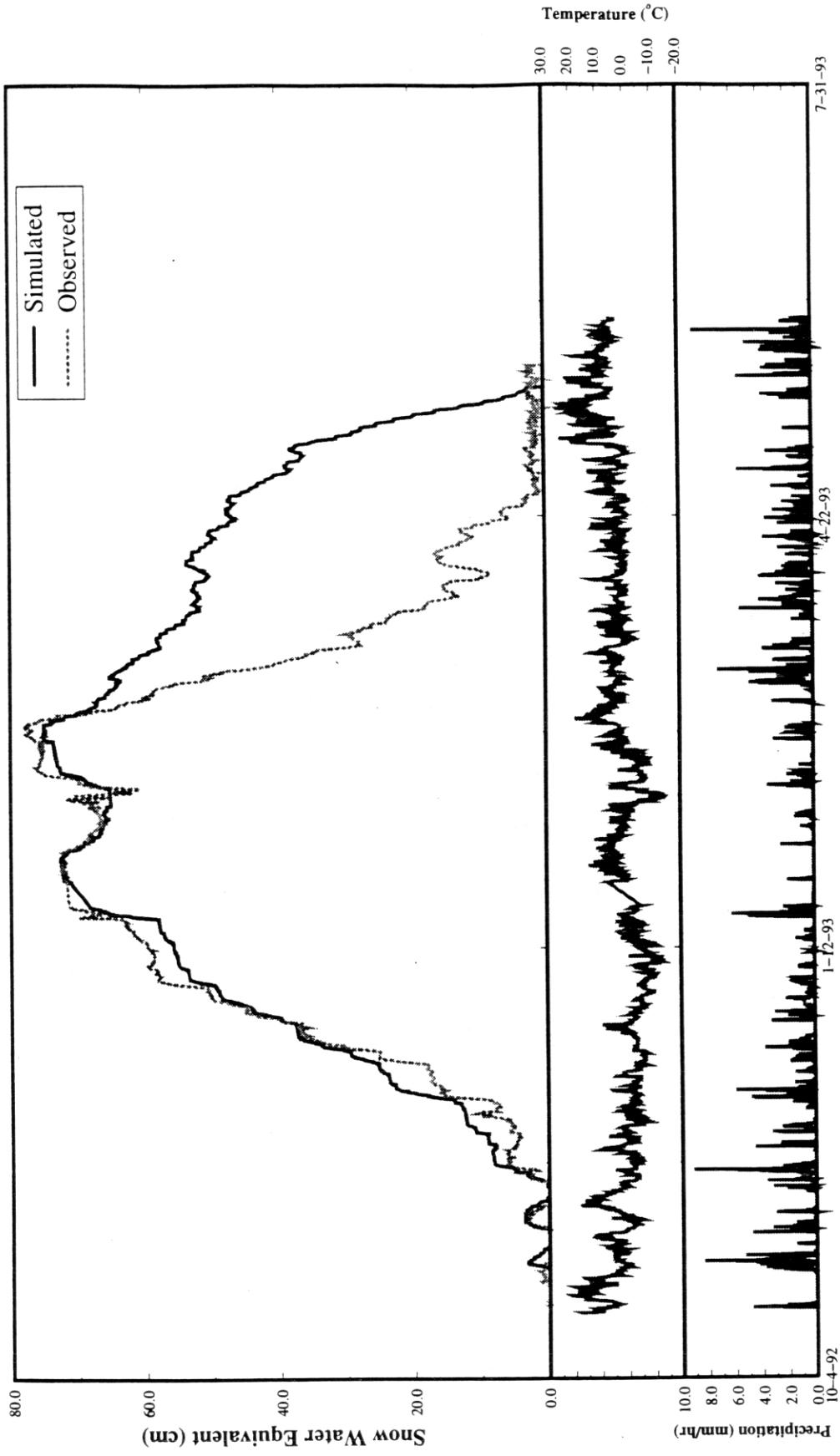


Figure 3.3 Snow water equivalent comparison between computed and observed at Vanilla Leaf during water year 1993 (high snow).

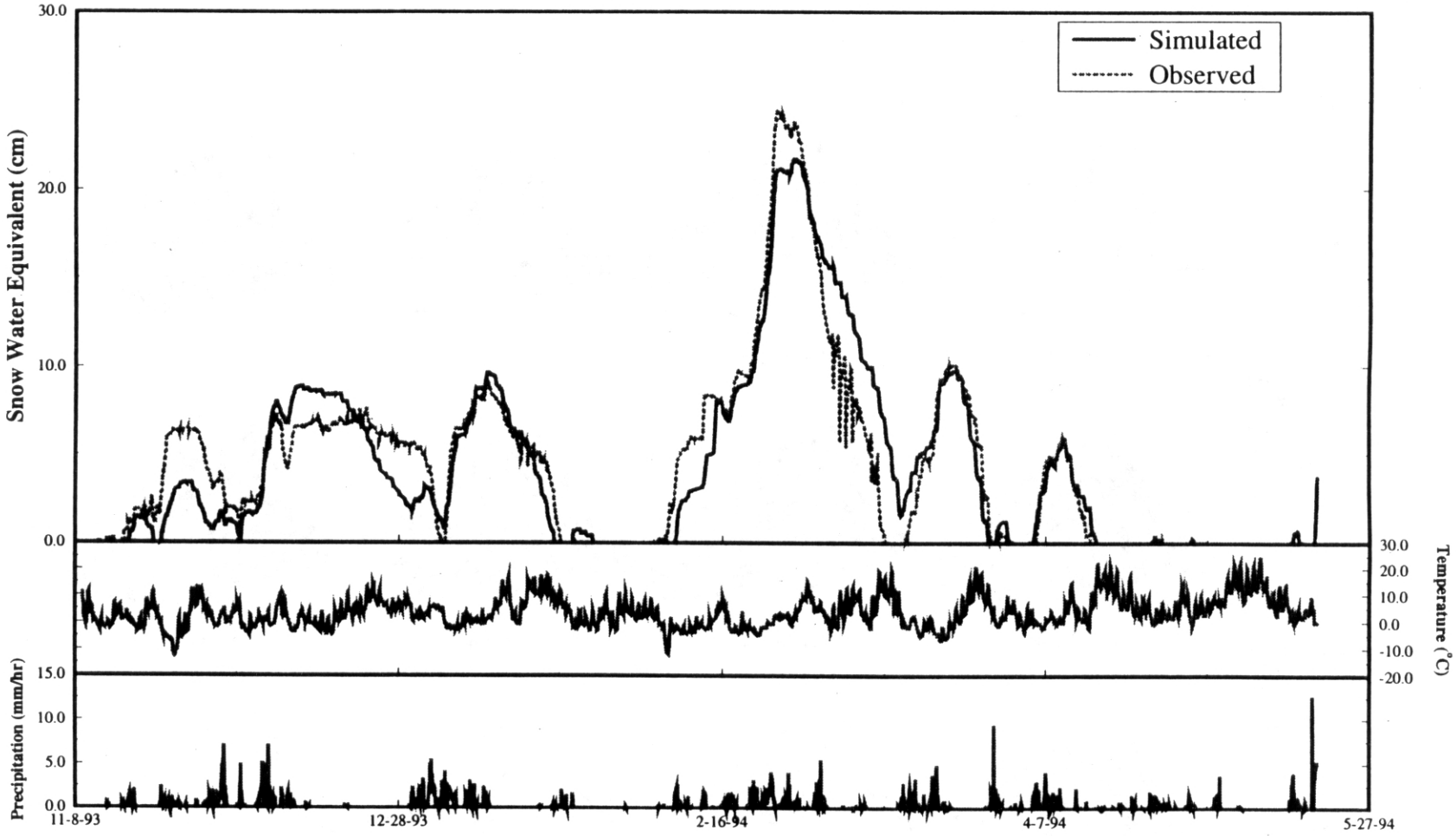


Figure 3.4 Snow water equivalent comparison between computed and observed at Vanilla Leaf during water year 1994 (medium snow).

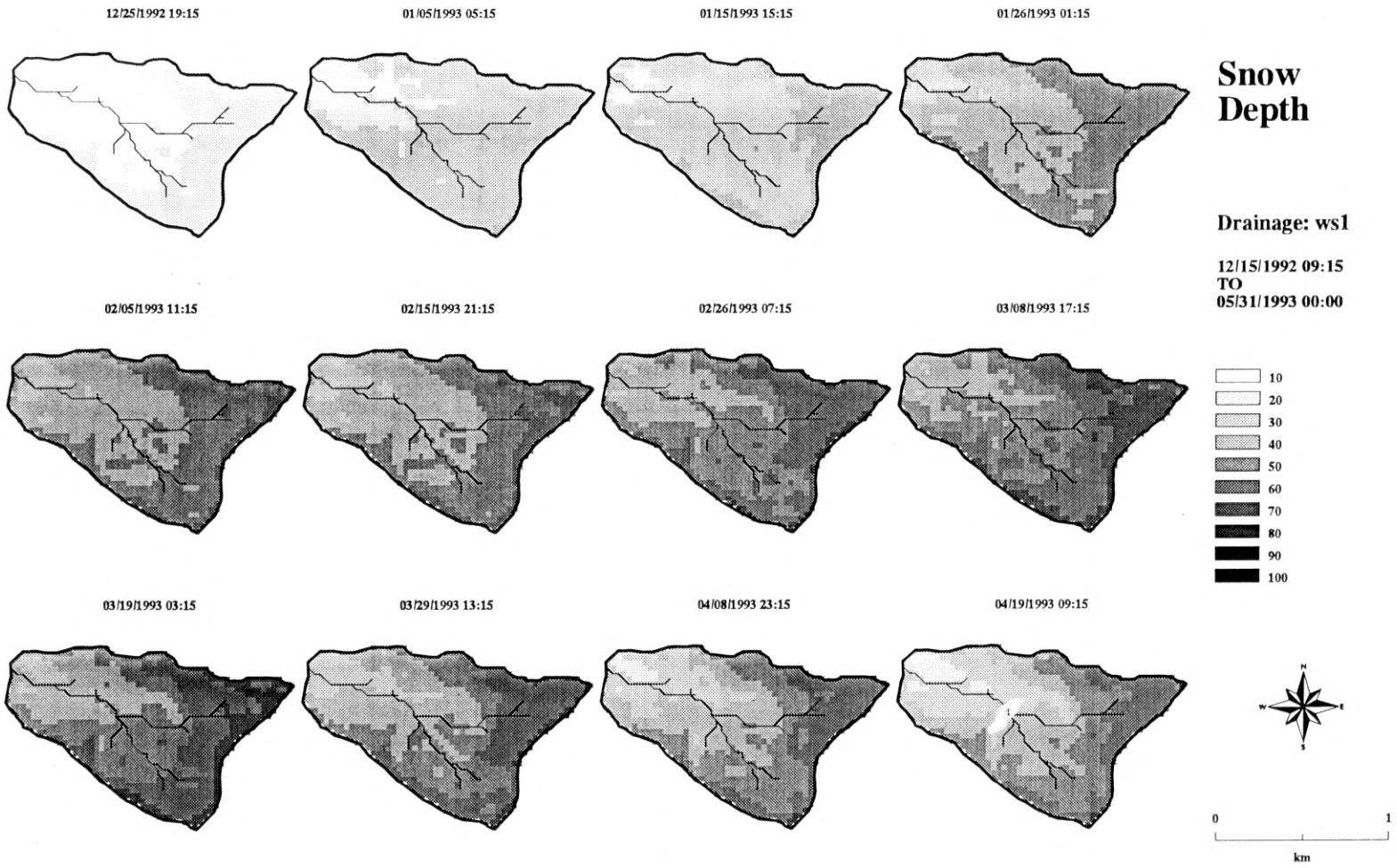


Figure 3.5 Spatial snow accumulation and melt pattern from CLAWS simulation for Watershed #3 during water year 1992. Snow water equivalents are in units of centimeters.

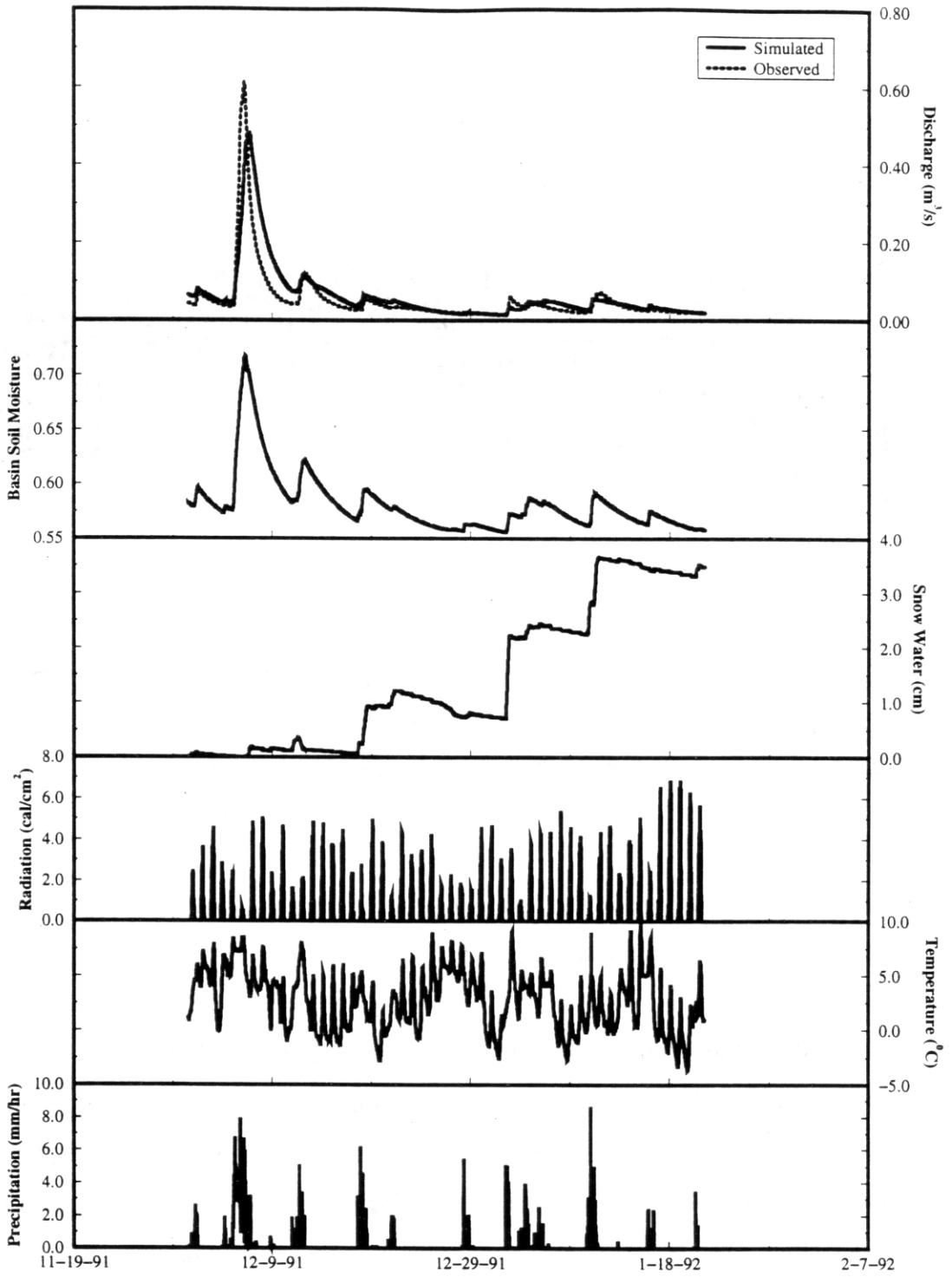


Figure 3.6 Result from distributed simulation for WS#1 between Dec. 1, 1991 and Jan. 22, 1992. Observed and simulated hydrographs, simulated basin mean soil moisture, computed basin average snow water equivalent, the input solar radiation, temperature and precipitation are plotted from top down.

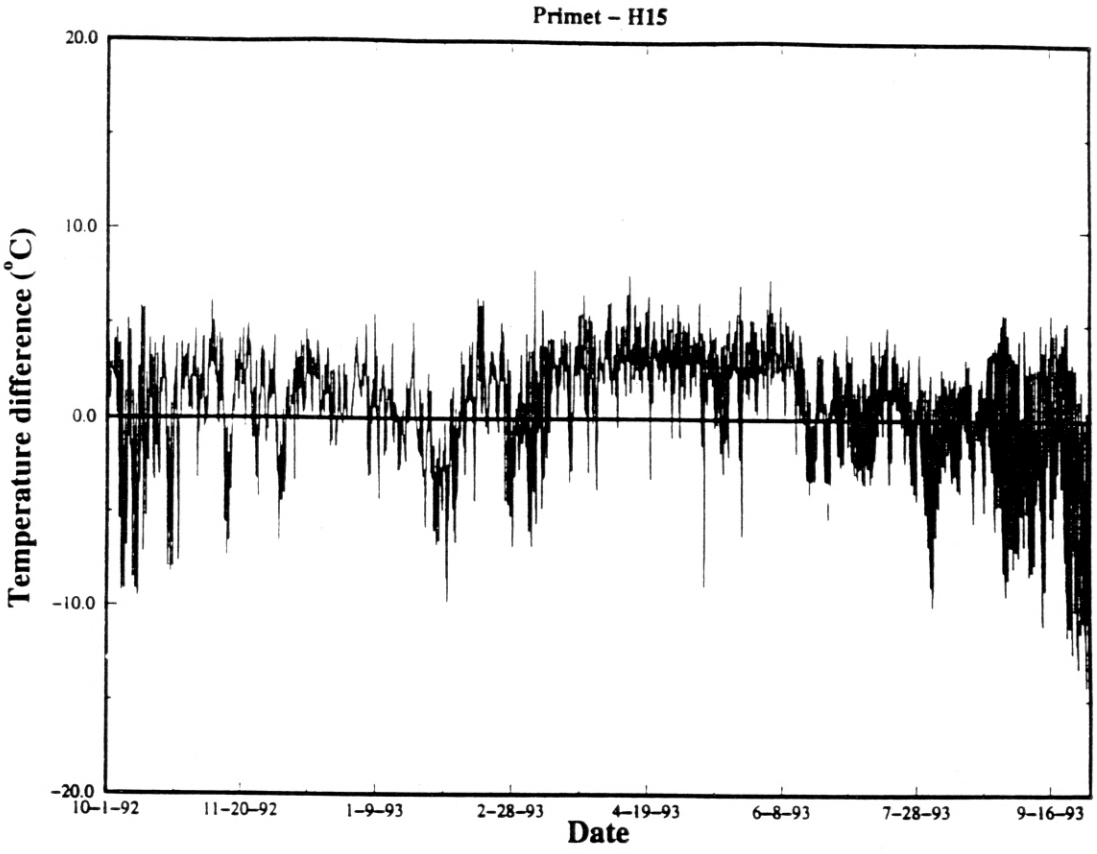


Figure 3.7 Temporal changes of temperature between two meteorological gages, Primet station (430 m) and H15 station (925 m), in hourly resolution.

from observations made by the US Army Corps of Engineers (1956) and are used for various regions. The almost parameter-free characteristics of this model enhance its versatility.

As in other models, the input data are crucial to the accuracy of the simulation of snowpack accumulation and melting. Temperature is the most critical input. It not only controls how much of the precipitation is rain or snow, but also influences the energy exchange in the snowpack. This is especially important in distributed modeling. We use a linear lapse rate to adjust the gage temperature to distributed elements. Detailed examinations of observed temperature readings among tens of gage stations and reference stands in HJ Andrews Experimental Forest found that lapse rate differs with time (day and night pattern, seasonal changes), elevation, and aspect (personal communication, Lynn Rosentrater of University of Oregon, 1995). Figure 3.7 presents a picture of the complex

temperature variation across the terrain. Two gage stations of 500 meter elevation difference at HJ Andrews Experimental Forest show a strong diurnal pattern, although there is a general trend of about 0.006 ^{0}C/meter. This suggests that the temperature interpolation we use poorly estimates the real temperature of distributed elements in the watershed. This is one of the error sources of distributed modeling in general.

Some other factors that not well represented in the CLAWS but may influence the accuracy of snow accumulation and melt from the distributed model include wind conditions, snow drifting, and differential interception on canopies of different densities.

3.5 Conclusions

An energy and mass balance model for single layer snowpack has been presented to model snow accumulation and melt. This simple energy and mass balance model accurately simulated snow accumulation and melt processes based on our point snow pillow measurement of four water years in western Oregon. Distributed small watershed application also shows simulated streamflow hydrographs compared well with observed streamflow. Extrapolating distributed parameters or data is one of the major limitations to the performance of distributed models. Because of its simplicity and few parameters, this algorithm can easily be incorporated into other hydrologic models given reasonable estimates of precipitation, temperature, solar radiation, relative humidity and wind speed.

4. CALIBRATION AND SENSITIVITY ANALYSES FOR CLAWS, A COUPLED HYDROLOGIC-GEOMORPHIC MODEL FOR LANDSCAPE AND WATERSHED STUDIES

4.1 Abstract

Calibration and testing of physically-based models are difficult tasks because of the large number of model parameters involved and the computational requirements of making multiple runs of such models. This paper investigates the sensitivities and uncertainties of watershed hydrologic and geomorphic responses from a coupled hydrologic-geomorphic model (CLAWS) to selected soil and vegetation parameters using observed data from three small watersheds at H. J. Andrews Experimental Forest, western Oregon. Simulated hydrographs from CLAWS agreed well with recorded observations. They matched measured hydrographic patterns such as peak size, timing, and decay coefficient, with the overall consistency represented by high correlations and low mean square errors. Sensitivity analyses on eleven soil and vegetation parameters not only identified their significance in the model, but also represented different watershed behavior under different watershed conditions.

4.2 Introduction

A physically-based, spatially-distributed hydrologic model, no matter how complex, will have uncertainties and errors from many sources. These sources of error may be inherent in the model or associated with problems such as input data quality, unknown parameter values, poorly known boundary conditions, unknown effects of spatial heterogeneity, scale problems, and oversimplification of processes (Stephenson and Freeze, 1974; Binley et al., 1991; Beven, 1993).

Calibration and testing of physically-based models are not straightforward, due to the large number of model parameters involved and the computational requirements of

making multiple runs of such models (Binley et al., 1991). Different methods may be derived for different objectives. When simulating stream peakflows is of interest, for example, lowflows and even the shape of the hydrograph can reasonably be ignored. Comparison of predicted and observed hydrographs is often used to test model prediction, although such a comparison has been criticized as insufficient due to uncertainties produced by non-linearities inherent in the watershed responses (Beven, 1989). Methods of assessing the goodness-of-fit of hydrographs are widely used to make such comparisons. These techniques may range from subjective visualizations to purely objective, statistical functions (Green and Stephenson, 1986).

Visual comparison of simulated and observed hydrographs provides a quick and often comprehensive means of assessing the accuracy of model output (Green and Stephenson, 1986). Discrepancies between modeled and observed peakflows or total flow volumes are evident immediately, and qualitative assessment can readily be made. However, visualization tends to be subjective when similar but not identical outputs are compared to observed data and the "best" fit is sought. To overcome this difficulty, as well as to highlight certain model particularities, one or more statistical goodness-of-fit tests can be employed.

Several goodness-of-fit criteria for assessing the accuracy of model output have been proposed. Any one particular method may give more weight to certain aspects of disagreements between simulated and observed data than another, due to the choice of objective functions (Gorgens, 1983). Different model outputs may use different techniques and objective functions for model evaluation. For storm-event simulations the comparison between hydrographs is more important. For long-term simulations, the variation and budget between observed and simulated streamflows are significant statistics (e.g., Liang et al., 1994).

In most numerical techniques available for comparing the goodness-of-fit of two sets of data, the objective functions for comparisons are based on analysis of the errors or residuals (Green and Stephenson, 1986) as

$$\text{residual} = \text{simulated value} - \text{observed value} \qquad (4.1)$$

This type of analysis is purely objective although semi-objective analysis of residuals has been proposed. Green and Stephenson (1986) summarized some of the widely-used objective functions.

This paper investigates the sensitivities and uncertainties of watershed hydrologic and geomorphic responses of a coupled hydrologic-geomorphic model CLAWS to selected soil and vegetation parameters using observed data from three small watersheds at H. J. Andrews Experimental Forest, western Oregon, United States.

4.3 Site Description

The study site we have chosen for model testing and sensitivity analysis is the H. J. Andrews Experimental Forest (HJA) (Figure 4.1), a basin in the western Cascades of Oregon. Bedrock of the site is a mixture of volcaniclastic rocks and lava flows cut by scattered dikes (Sherrod and Smith, 1989). Landforms have been sculpted by fluvial and various soil mass-wasting processes (Swanson and James, 1975). Mass movements include shallow, rapid movements of soil on hillslopes (debris slides), rapid movements of alluvium, colluvium, and organic matter down stream channels (debris flows), and large, slow-moving landslides (slumps and earthflows) (Grant and Wolff, 1991). Annual precipitation averages 2300 mm, much of it between October and March. Rain-on-snow events within the transient snow zone (400 to 1200 m elevation) are a major factor in generating most floods. Conifer forest dominated by 400 to 500 year old Douglas-fir (*Pseudotsuga menziesii*) blankets hillslopes and undisturbed valley floors.

Table 4.1 Characteristics of three small watersheds at HJ Andrews Experimental Forest

Watershed	Area (km^2)	Elevation (m)	Average hillslope gradient (%)	Average mainstem channel gradient (%)	Cut area (%)	Road area (%)
1	0.96	440-1010	63.2	27.8	100	0
2	0.60	525-1065	61.1	36.4	0	0
3	1.01	480-1080	52.6	27.2	25	6

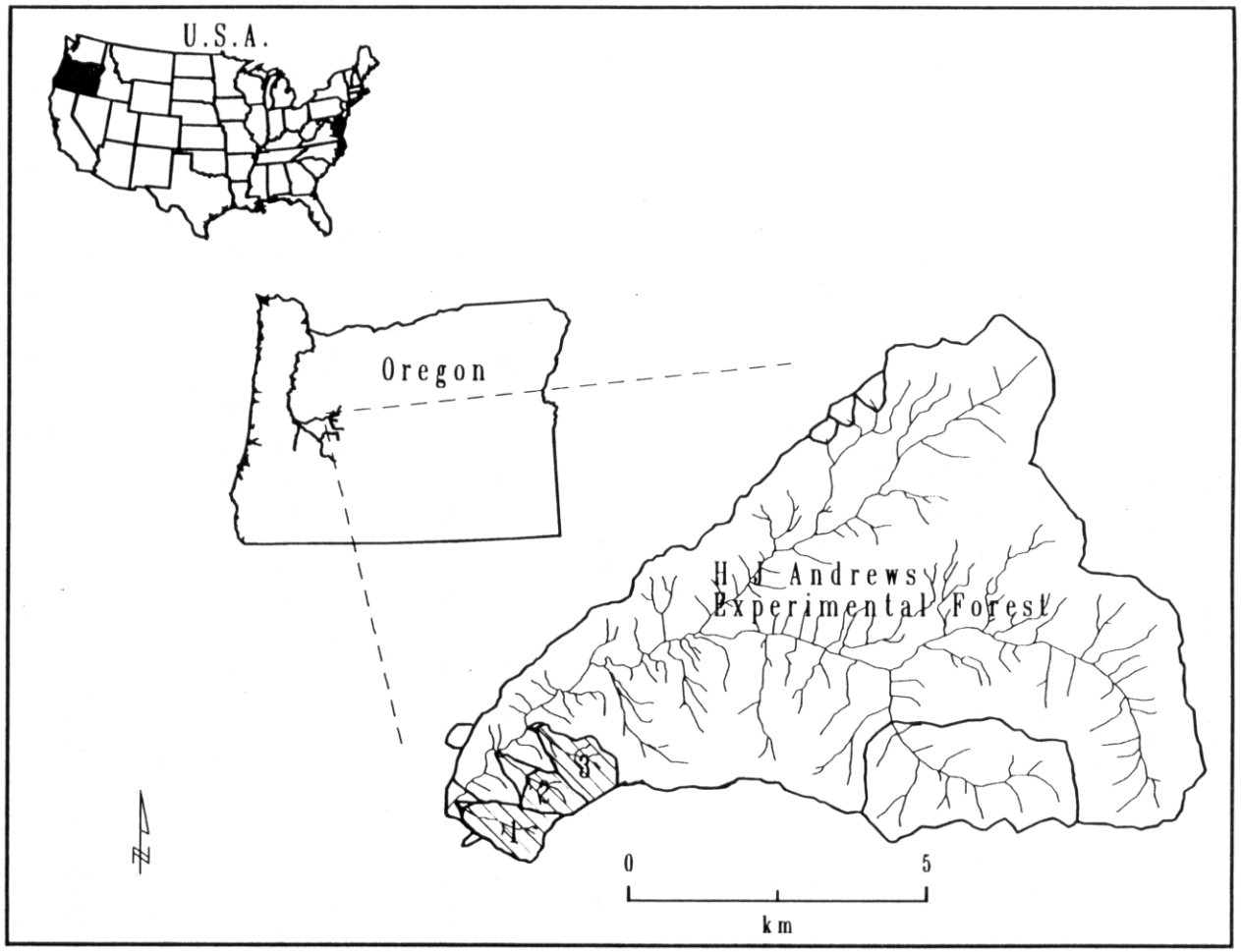


Figure 4.1 Geographical location of test sites, Watershed #1, Watershed #2 and Watershed #3 at HJ Andrews Experimental Forest, Oregon, United States.

Three small adjoining watersheds in the HJ Andrews Experimental Forest, hereafter referred to as WS#1, WS#2 and WS#3, were selected for testing CLAWS (Table 4.1). Originally established as paired-watersheds for studying the effects of forest management on streamflow, these three watersheds have been studied in detail for more than four decades. Cutting, which began in WS#1 in Fall 1962 and ended in Summer 1966, used a skyline suspension system to minimize surface soil disturbance. Residual logging debris was burned in October 1966. On WS#3, roads covering 2.64 km (6% of the drainage) were completed in 1959. Three discontinuous clearcuts of 0.05, 0.08, and 0.11 km^2 (25% of the watershed area) were logged in winter 1962-1963 by a high-lead cable logging system. This method resulted in twice the area of deep soil disturbance (10%) and nearly three times the area of compacted soil (9%) compared to WS#1 (Dyrness, 1967b). Logging debris was burned in September 1963. WS#2 served as a forested control.

4.4 Input Data And Parameterization

The CLAWS model was designed to be implemented independent of pixel size and time step. Temporal and spatial resolution of input data are therefore fully adjustable. The input data consist of meteorological data, topographic attributes, and soil and vegetation distribution. Initial conditions for atmospheric, vegetation and soil characteristics are set prior to model runs. All input or initialization files are written in a fixed-formatted control file for CLAWS to read. The input data are obtained from Forest Science Data Bank (FSDB) at Oregon State University.

4.4.1 Meteorological input

Meteorological input variables include observed precipitation, temperature, relative humidity (or dew point temperature), wind speed and solar radiation at any time. Precipitation data at WS#2 were used, because of the length of record (since 1957) and proximity to the test sites. Existing digitized precipitation records of 5-minute resolution were reconstructed into 15-minute resolution for CLAWS. Temperature, relative

humidity, wind speed and solar radiation have only been observed, at an hourly resolution, since 1972 at the nearby Primary Met Station. These data were reconstructed to 15-minute resolution using linear interpolation or a theoretical algorithm.

4.4.2 Topographical attributes

Drainage basin characteristics and networks were described by digital elevation data (DEM) at 30-meter resolution. GRID operations of SLOPE, ASPECT, FLOWDIRECTION and FLOWACCUMULATION in a commercial geographical information system (ARC/INFO) were used to get the attributes of slope, aspect, flow direction and flow accumulation for each element. The results of the terrain analysis files were then output using GRIDASCII to ASCII format for input into CLAWS.

4.4.3 Soil and vegetation distribution and characteristics

Soil types were surveyed at HJA in 1964 by the Soil Conservation Service (SCS, 1964). Eight soil series are present on the watersheds, and seven of them are plotted in Figure 4.2. One unnamed soil is ignored because of its minor areal extent within WS #3. Shallow soils predominate the steep terrain. WS #1 is dominated by Budworm soils

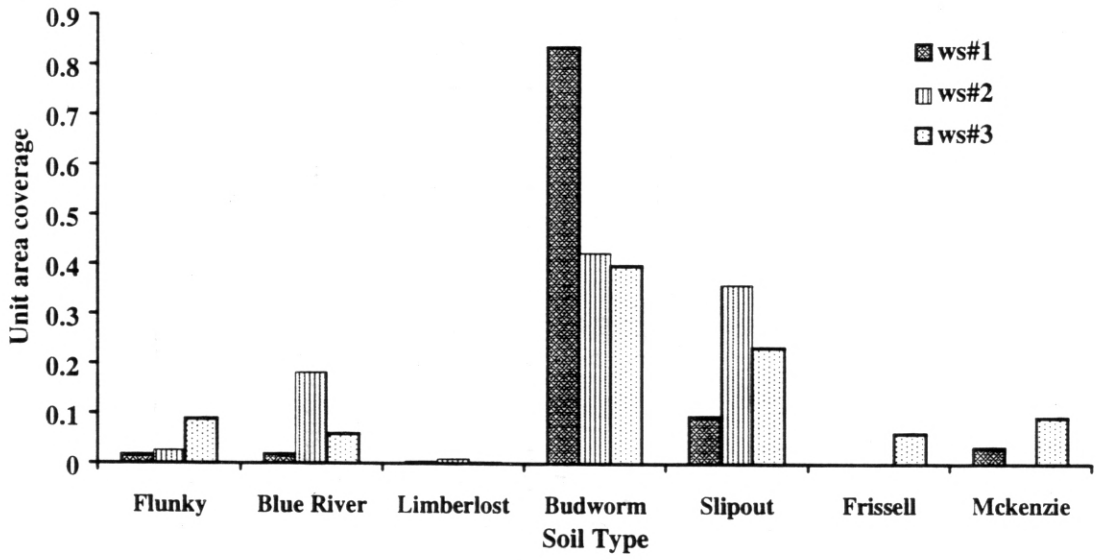


Figure 4.2 Soil distribution in the three small watersheds (data generated from FSDB GIS coverage).

Table 4.2 Soil parameters used in model test

Soil Parameters	**Soil Type**								**Reference**
	Flunky	Blue River	Limberlost	Budworm	Slipout	Frissell	Mckenzie	Others	
Bulk Density (g/cm^3)	2.317	1.034	1.421	1.564	1.477	1.954	1.585	1.6002	Rothacher et al., 1967
Porosity (vol/vol)	0.29	0.63	0.52	0.5	0.48	0.4	0.53	0.486	Rothacher et al., 1967
Wilting point (vol/vol)	0.05	0.25	0.187	0.195	0.17	0.14	0.186	0.1756	Rothacher et al., 1967
Field Capacity (vol/vol)	0.102	0.285	0.277	0.324	0.343	0.217	0.265	0.2852	Rothacher et al., 1967
Channel roughness	0.03	0.03	0.03	0.03	0.03	0.03	0.03	0.03	Chow et al., 1959
Overland sheet roughness	0.06	0.06	0.06	0.06	0.06	0.06	0.06	0.06	Chow et al., 1959
Cohesion (kpa)	2.5	2.5	2.5	2.5	2.5	2.5	2.5	2.5	Hammond et al., 1992
Frictional angle (^{o})	38	38	38	38	38	38	38	38	Hammond et al., 1992
Soil depth (m)	0.584	1.78	1.27	1.83	1.7	0.787	1.09	1.3354	Rothacher et al., 1967
Ground water conductivity (m/s)	4E-08	4E-08	4E-08	4E-08	4E-08	4E-08	4E-08	4E-08	Calibrated
Saturated conductivity (m/s)	0.004178	0.001567	0.002089	0.001567	0.000627	0.000627	0.000418	0.001044	Calibrated
Coefficient for conductivity profile	3	3	3	3	3	3	3	3	Calibrated

Table 4.3 Vegetation parameters used in model test

Parameters	Value used	Reference
Root strength		*Sidle, 1991*
C_{max}: maximum (kPa)	12.5	
k_d: coefficient in residual	0.402	
m_1: coefficient in residual	0.647	
a_f: coefficient in regrowth	0.952	
b_f: coefficient in regrowth	19.05	
d_r: coefficient in regrowth	-0.05	
k_r: coefficient in regrowth	0.12	
Biomass		*personal communication with Harmon, 1995; Sidle, 1992*
W_{max}: maximum (kPa)	3	
a_w: coefficient	0.952	
b_w: coefficient	19.05	
c_w: coefficient	-0.05	
k_w: coefficient	0.12	
Leaf Area Index (LAI)		*personal communication with Harmon, 1995*
LAI_{max}: maximum	10	
B_1: coefficient	0.075	
B_2: coefficient	1	
Cover density		*personal communication with Harmon, 1995*
t_{Dmax}: year after cutting at which the cover density is maximum	75	
C_{Dmax}: maximum	1	
t_f: year after cutting at which the cover density is steady	200	
C_{Df}: steady cover density	0.75	
Tree height		*Means, 1989*
S_i: Site Index (m)	40	
g_{max}: Max Canopy Conductance (ms^{-1})	0.004	

(84% of the area). A large portion of WS#2 and WS#3 are covered by Budworm and Slipout. Only small areas are covered by other soil types.

Previous investigation (Rothacher et al., 1967) indicated that soils in WS#1, WS#2 and WS#3 have moderately-high moisture holding capacities, coupled with high saturated conductivity. Stoniness plays an important role in influencing the soil hydrologic characteristics. Observed soil characteristics (Rothacher et al., 1967) were used, including

bulk density, porosity, soil depth, and soil moisture at wilting point and field capacity (Table 4.2). The Manning's roughnesses for channel and overland flow were referenced from Chow et al. (1959). Since there are no measurements for soil cohesion and internal frictional angle, average values were taken from Hammond et al. (1992). Other parameters, such as apparent saturated conductivity, were calibrated based on the outlet hydrograph, as discussed later.

Vegetation is dominated by Douglas-fir with varying amounts of western hemlock. Douglas-fir ages range from about 100 to 500 years except in clearcut areas. In practice, we did not distinguish between different species, and one vegetation parameter set was used (Table 4.3).

The distribution of soils and vegetation cover of the HJ Andrews Experimental Forest were stored in vector-based ARC/INFO polygon maps and were reconstructed into grid-based pixel values of soil and vegetation indexes.

4.4.4 Other parameters and initial status

Temperature lapse rates and precipitation gradients with elevation were developed and used to interpolate the temperature and precipitation for each element distributed over the watershed. The precipitation gradient, calculated from ten gagging stations over the HJ Andrews Experimental Forest, is 0.000159 unit/m based on the annual precipitation. The average temperature lapse rate of -0.006 °C/m is used. Lapse rates in HJA vary with aspect, elevation and time (Personal communication, Lynn Rosentrater, University of Oregon, 1995), but we did not consider such variation.

Initial state variables such as initial snow depth and temperature, initial watershed outlet discharge, initial soil moisture, and deep groundwater storage were also interpolated using the ratio of elemental topographic convergence index (TCI) to the basin mean TCI (Beven, 1979).

4.5 Quantitative Measures of Goodness-of-Fit

Comparison of model results and sensitivity analyses were based on three groups of characteristics, (1) water balance and size (runoff precipitation ratio, peakflow and lowflow discharges); (2) timing (peakflow time and decay coefficient); and (3) statistical measures (mean square error, correlation coefficient). Initial validation included visual checks of simulated hydrographs.

The runoff precipitation ratio

$$RP \text{ ratio} = \frac{\text{Total runoff during the simulation}}{\text{Total precipitation during the simulation}} \tag{4.2}$$

only calculates the runoff and precipitation during the simulation period and discounts the delayed runoff after the simulation. This index describes the runoff volume.

Peakflow size and timing were simply compared between the observed and simulated hydrographs.

We considered a decay coefficient k of the form

$$Q_t = Q_0 k^{-t} \tag{4.3}$$

where time t is arbitrarily chosen in units of hours, Q_0 and Q_t are discharge at peak and time t respectively. By regression based on hourly intervals, k is solved for each storm. This equation is a variant of equation

$$Q_t = Q_0 e^{-k't} \tag{4.4}$$

and one can easily show that

$$k = e^{k'} \tag{4.6}$$

Peakflow size and time, decay coefficient are important characteristics in hydrograph. they describe the general pattern of the hydrograph.

The objective function we utilized is the sum of square error averaged over the total points (MSE) as

$$MSE = \frac{1}{n}\sum_{t=1}^{n}\left[Q_{obs}(t) - Q_{sim}(t)\right]^2 \tag{4.7}$$

where Q's are observed and simulated discharges at time t and n is the total number of data points. In spite of its alleged short comings (e.g. Clarke, 1973; Green and

Stephenson, 1986), this function has been used by many workers in other model comparisons, model calibrations and parameter optimizations (Green and Stephenson, 1986).

The linear correlation coefficient between observed and simulated hydrographs is also computed as

$$R = \frac{\sum_{t=1}^{n}\left[Q_{obs}(t) - \overline{Q_{obs}}\right]\left[Q_{sim}(t) - \overline{Q_{sim}}\right]}{\sqrt{\sum_{t=1}^{n}\left[Q_{obs}(t) - \overline{Q_{obs}}\right]^2}\sqrt{\sum_{t=1}^{n}\left[Q_{sim}(t) - \overline{Q_{sim}}\right]^2}} \tag{4.8}$$

4.6 Model Calibration and Simulation Results

Two schools of thought have emerged on model calibration, one advocates the use of subjective judgment and operator experience with a trial-and-error framework for parameter estimation, while the second pursues an optimization approach (O'Connell, 1988). With the former approach, parameter estimation is a subjective art in which the original model developer is the most skilled. The optimization approach however remains somewhat intractable for complex models. A study by the World Meteorological Organization (WMO, 1975) suggested a combination of manual and optimization techniques, based on their conclusions that manual calibration, while expensive and time consuming, could produce a good calibration, while optimization, which was cheap and fast, could produce unrealistic parameter values that in turn, could lead to poor predictions.

Since the only parameters lacking measured data are saturated conductivity and the accompanying shape coefficients, we required a reasonable set of values for each soil, based on visualization and quantitative assessment, that could be used for three watersheds. Three storms from 1984, 1991 and 1992 were chosen to complete this task. These storms are single-peak events in the observed hydrograph. The 1991 and 1992 storms created the peakflows for that water year, and the 1984 storm is the first large storm for that water year.

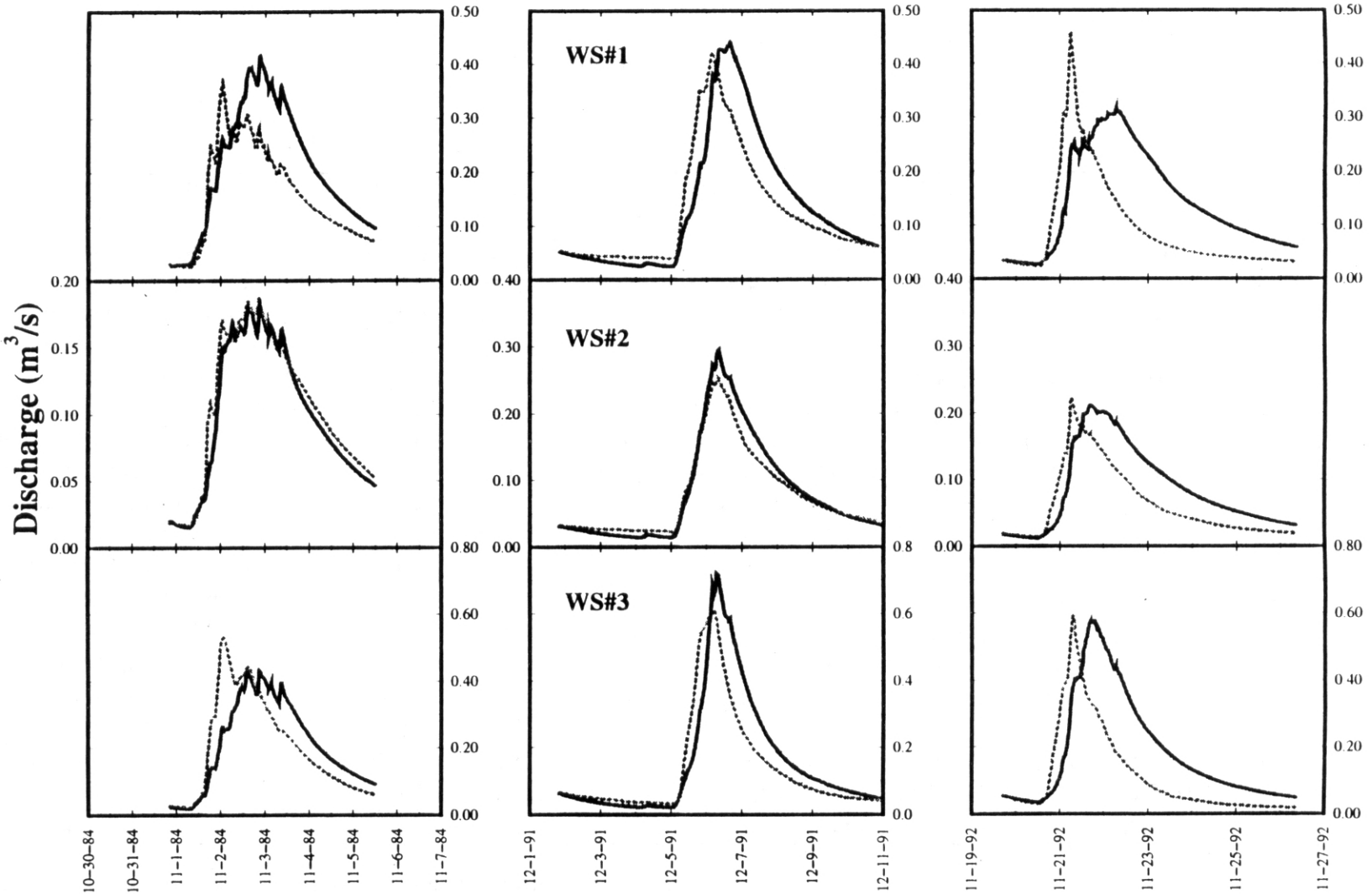


Figure 4.3 Hydrograph comparison of simulated streamflow (solid line) and observed streamflow (dotted line) of three small watersheds during three storms. Note each row shows a watershed response and each column a storm.

Table 4.4 Simulation results of three watersheds during three storms.

Watershed	WS#1			WS#2			WS#3		
Storm Date	11/1/84	12/2/91	11/20/92	11/1/84	12/2/91	11/20/92	11/1/84	12/2/91	11/20/92
Total Precipitation(m):	0.146	0.131	0.127	0.146	0.131	0.127	0.146	0.131	0.127
Rain start time (hr):	0	51	10.5	0	51	10.5	0	51	10.5
half rain time (hr):	27.1	92.4	33.8	27.1	92.4	33.8	27.1	92.4	33.8
Rain end time (hr):	60.8	176.5	65.3	60.8	176.5	65.3	60.8	176.5	65.3
Initial flow (m^3/s)	0.027	0.066	0.056	0.019	0.033	0.019	0.03	0.054	0.035
Observed runoff/precipitation	0.546	0.807	0.507	0.461	0.759	0.456	0.449	0.769	0.435
Simulated runoff/precipitation	0.477	0.879	0.757	0.447	0.797	0.615	0.612	0.84	0.661
Observed Peak time(hr):	29.3	103.5	38.5	48.3	108	37.5	28.3	103.8	37
Simulated Peak time(hr):	60.5	116.3	57.5	48.8	108.3	48	48.5	116	61.5
Observed Peak size(m^3/s):	0.53	0.61	0.59	0.19	0.25	0.22	0.37	0.42	0.46
Simulated Peak size(m^3/s):	0.31	0.44	0.36	0.19	0.3	0.21	0.45	0.44	0.32
Observed rising slope(m^3/s hr):	0.029	0.021	0.029	0.005	0.008	0.011	0.017	0.012	0.024
Simulated rising slope(m^3/s hr):	0.006	0.01	0.008	0.005	0.005	0.007	0.009	0.01	0.007
Observed decay coefficient (1/hr):	1.0064	1.007	1.0087	1.0049	1.0048	1.0058	1.005	1.0049	1.007
Observed decay correlation:	0.995	0.977	0.969	0.998	0.99	0.984	0.991	0.982	0.945
Simulated decay coefficient (1/hr):	1.0044	1.0044	1.0039	1.0055	1.0053	1.0044	1.0059	1.0052	1.0046
Simulated decay correlation:	0.999	0.999	0.998	0.998	0.997	0.998	0.998	0.995	0.997
Mean sum square error	0.015	0.012	0.018	<0.001	<0.001	0.002	0.008	0.003	0.009
R Square (obs. vs. Sim.)	0.326	0.493	0.254	0.966	0.989	0.698	0.693	0.786	0.358

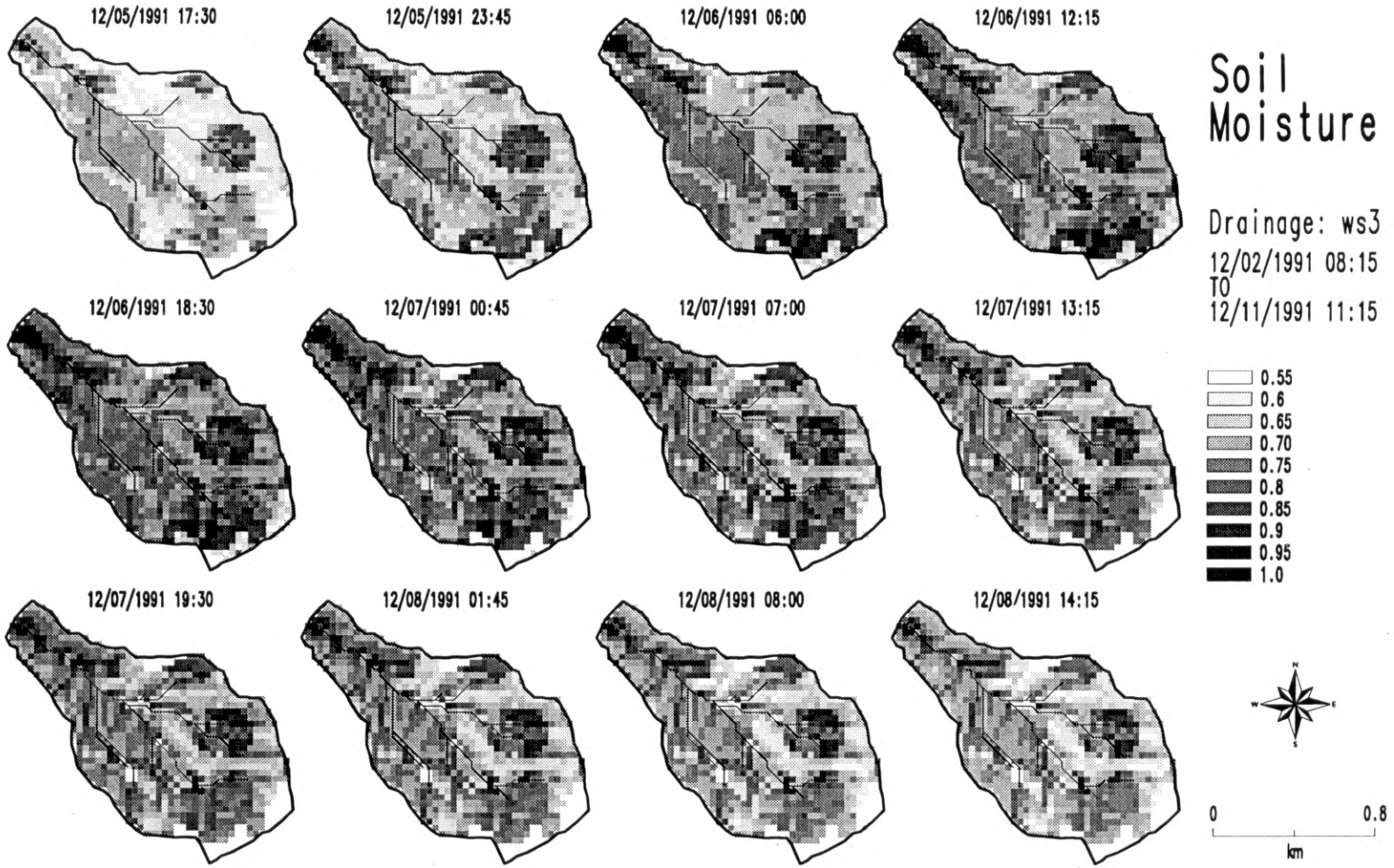


Figure 4.4 Spatial pattern of element soil moisture for watershed #3 during a 10 day simulation

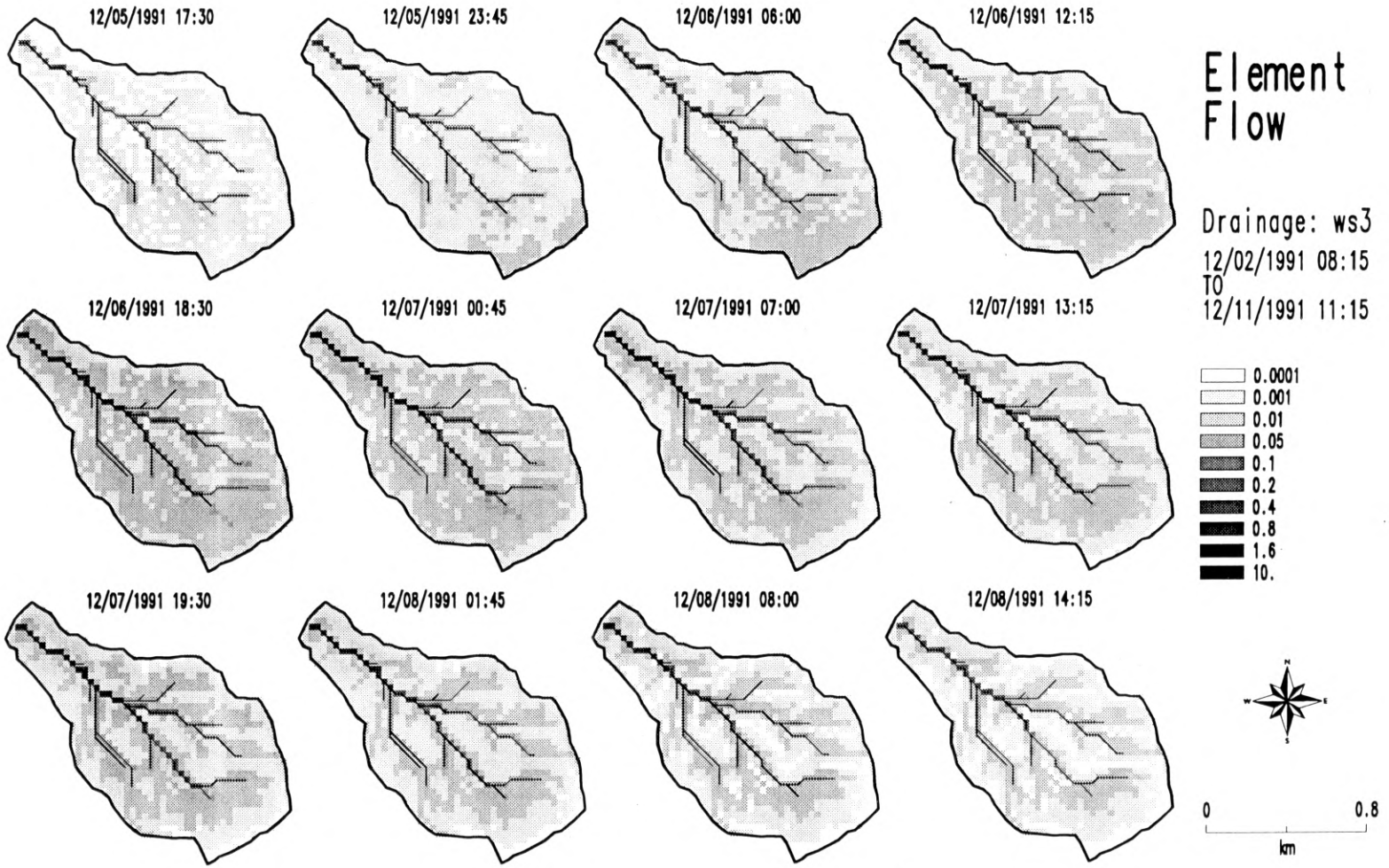


Figure 4.5 Spatial pattern of element outflow for watershed #3 during a 10 day simulation



Figure 4.6 Spatial pattern of factor of safety for watershed #1, #2 and #3 during a 10 day simulation

The calibrations start with values of maximum saturated conductivity calculated from the equations shown in the Appendix. These values are based on the soil texture (Brooks and Corey, 1964; Rawls and Brakensiek, 1989). Because of nonlinearities in these complex systems and heterogeneities in soils present in the watersheds, a complete calibration would be time consuming. Only simple increases or decreases of these parameter values were assessed, first by visual examination of hydrographs, and then by examination of quantitative measures. The final parameter set was based on the overall performance in comparison to observed hydrographs (Figure 4.3).

The overall performance as evaluated by the mean sum-of-square error and correlation analysis (Table 4.4). Generally, the calibrated parameter set is best for WS#2 with small errors in the total volume of runoff, peakflow size and time. Larger differences between simulated and observed hydrographs for WS#2 and WS#3 may be explained by factors other than inappropriate parameter values. Errors in input precipitation data, produced by local variations of storm, for example, may explain simulation discrepancies. Although these watersheds are close to each other geographically, orography may induce variation in precipitation input. The precipitation data we used is from the gage at WS#2 which may not represent the actual input for WS#1 and WS#3.

The simulated hydrographs rise slower and decay faster than observed hydrographs (Table 4.4). Observed flows also have higher rising slopes on an hourly scale (0.05-0.029 m^3/s hr for observed vs. 0.005-0.01 m^3/s hr for simulated) and smaller decay coefficients (1.005-1.0087 1/hr for observed vs. 1.004-1.0059 1/hr). This may be a model-inherent error from non-representation of unsaturated flow, which may dampen the decay rate of the watershed responses.

The Nov. 20, 1992 storm is a mixed rain and snow event that clearly shows in the watershed average snow depth calculation. None of the simulations performed well on this event (Figure 4.3). Yet the snow module performed well with the point simulation of Vanilla Leaf snow measurements. In CLAWS, a constant lapse rate is used to extrapolate the observed point temperature to distributed elements. Detailed examination of temperature at the HJ Andrews Experimental indicates that the lapse rates vary temporally and spatially with elevation, aspect, season and day-night pattern (Personal

Table 4.5 Simulation results for three watersheds during 12/01/91-01/22/92

Watershed	WS#1	WS#2	WS#3
Initial flow at the mouth (m^3/s)	0.066	0.038	0.059
Observed runoff/precipitation	0.714	0.658	0.736
Simulated runoff/precipitation	0.852	0.67	0.748
Mean sum of square error	0.002	<0.001	0.001
R Square of hydrographs	0.703	0.989	0.887
Observed peakflow time (hr)	135.5	140	135.75
Simulated peakflow time (hr)	148.25	139	140.25
Observed peakflow (m^3/s)	0.613	0.253	0.423
Simulated peakflow (m^3/s)	0.486	0.311	0.489
Simulated maximum snow water equivalent (cm)	3.7	5.9	5.1

communication, Lynn Rosentrater, University of Oregon, 1995). Thus a simplified constant lapse rate is clearly not the best choice for this region for fine-scale simulation.

Spatial patterns of soil moisture in WS#3 during the Dec. 1991 storm (Figure 4.4) clearly show the saturation extending from stream to hillslope. Headwater hollows are also readily saturated because of relatively higher convergence. The flows from each element are consistent with the soil moisture patterns, and show increasing flows along stream channels accompanying storm progression (Figure 4.5). This supports the variable source area concept of streamflow production from a distributed modeling perspective. The factor of safety, which represents the landslide potential of the three small watersheds (Figure 4.6), showed that midslope and headwater areas are more vulnerable to landslides.

The calibrated parameters were also validated with a longer data series of more than 45 days during Dec. 1, 1991 to Jan. 22, 1992 using streamflow observations from the three watersheds. Approximately 33 cm of precipitation was observed at the WS#2 gage for this period. The hydrographs (Figure 4.7, Figure 4.8 and Figure 4.9) show good correlations between observed and simulated, with mean square error less than 0.002 and correlations coefficients greater than 0.7. Close approximations were shown in the amounts of runoff, peakflow time and size (Table 4.5). The model results also show that snow in all three watersheds increased gradually during this simulation period (Figure 4.7, Figure 4.8 and Figure 4.9). Because of the elevation difference between watersheds, the

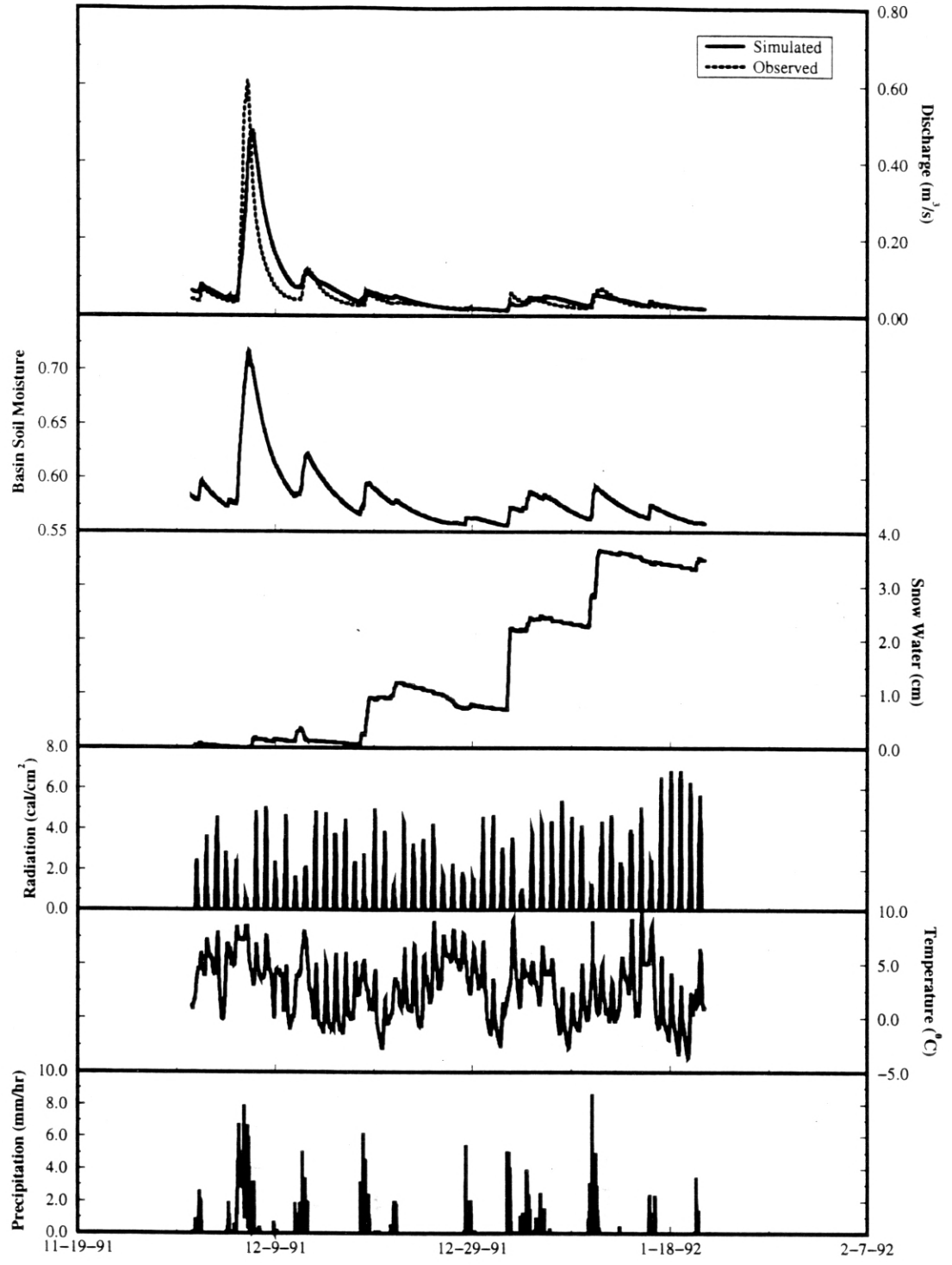


Figure 4.7 Simulation results for WS#1 between Dec. 1, 1991 and Jan. 22, 1992. Observed and simulated hydrographs, simulated basin soil moisture, simulated mean basin snow storage, solar radiation, temperature and precipitation are plotted from top down.

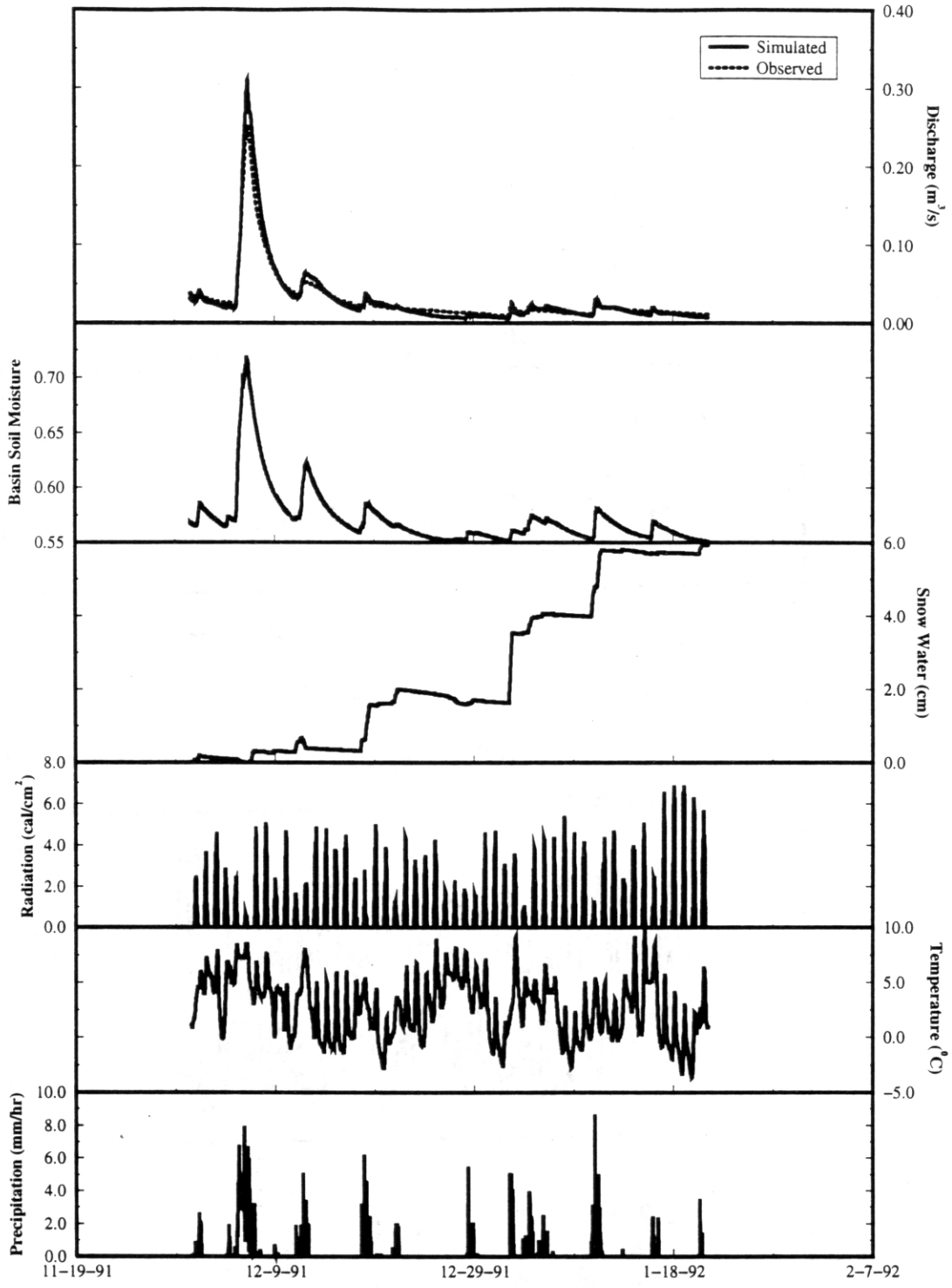


Figure 4.8 Simulation results for WS#2 between Dec. 1, 1991 and Jan. 22, 1992. Observed and simulated hydrographs, simulated basin soil moisture, simulated mean basin snow storage, solar radiation, temperature and precipitation are plotted from top down.

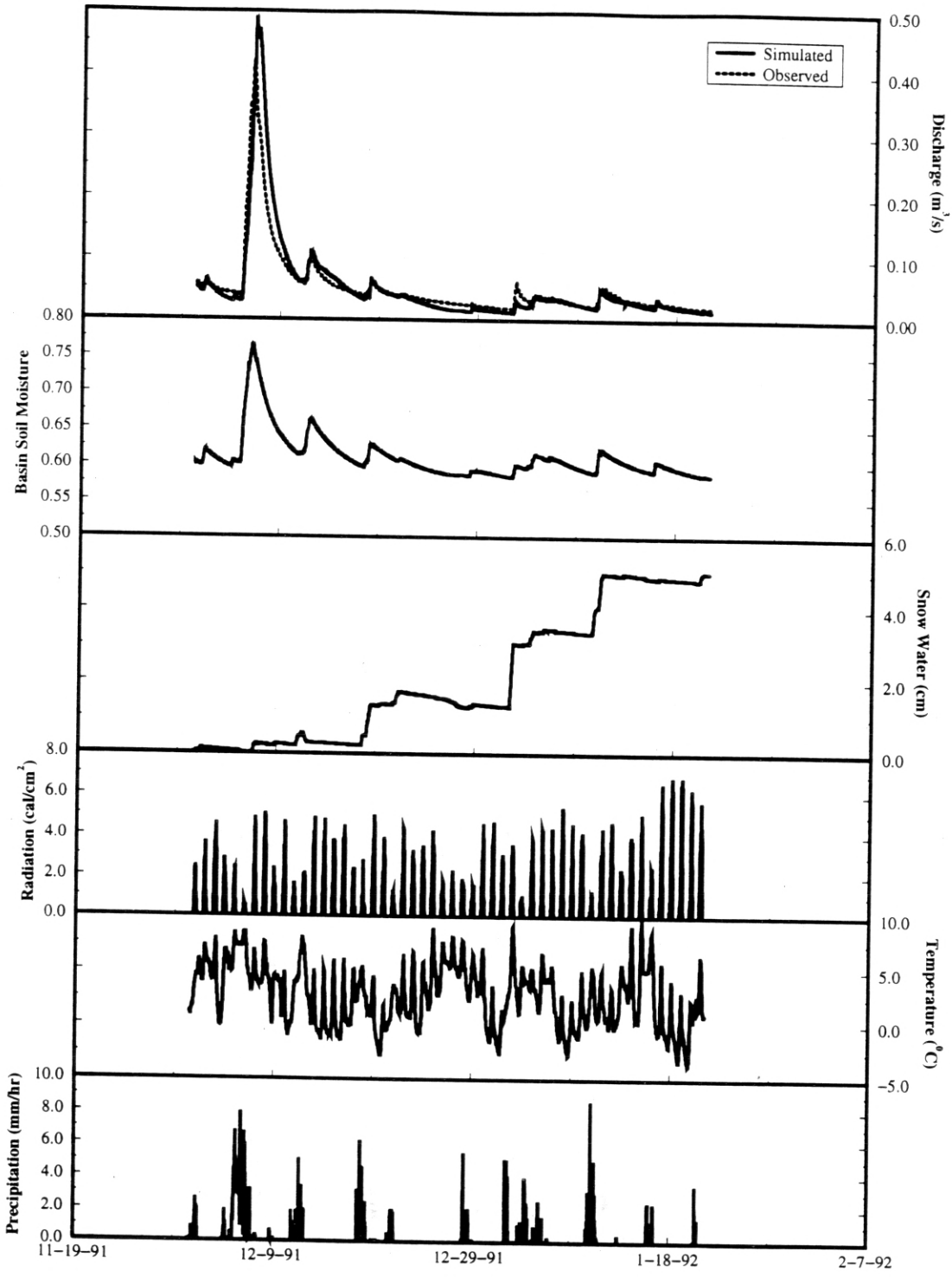


Figure 4.9 Simulation results for WS#3 between Dec. 1, 1991 and Jan. 22, 1992. Observed and simulated hydrographs, simulated basin soil moisture, simulated mean basin snow storage, solar radiation, temperature and precipitation are plotted from top down.

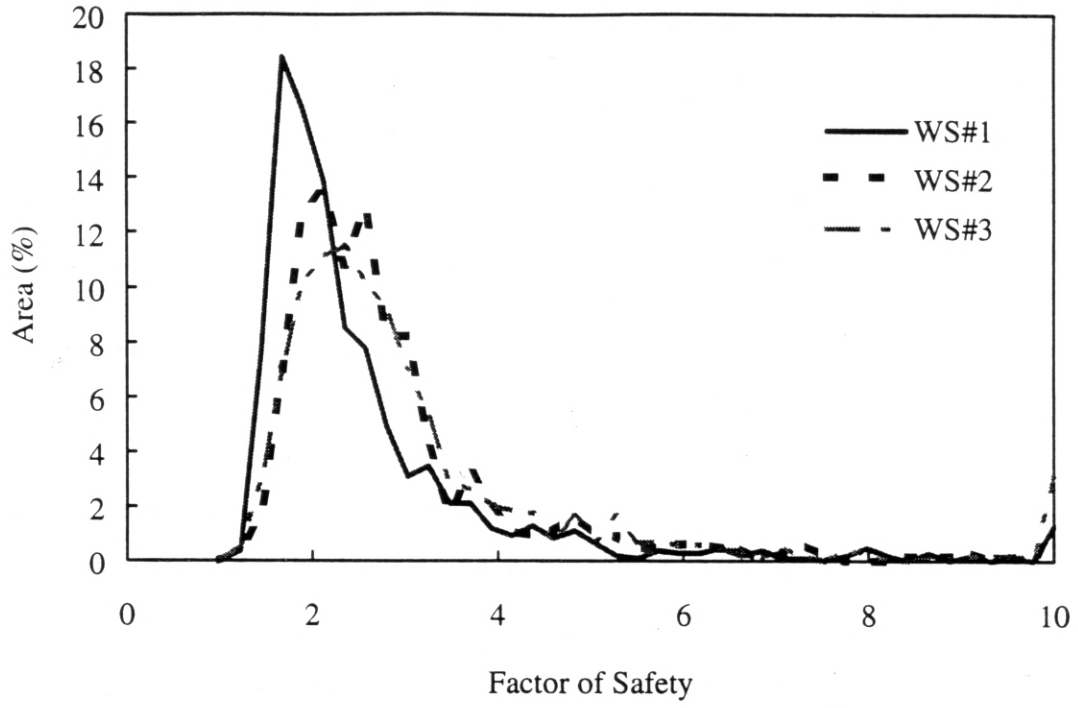


Figure 4.10 Frequency distribution of factor of safety for three watersheds during 12/1/91-1/22/92.

low elevation WS#1 had 3.5 cm of basin average water equivalent of snow compared to 5.9 and 5.1 cm at WS#2 and WS#3, respectively (Table 4.5). The calculated factor of safety based on limited equilibrium analysis shows that WS#1 had higher landslide potential during the one and a half month period, and that 50% of the area possesses a factor of safety of less than 2, while slide potential in WS#2 and WS#3 are 34% and 30%, respectively (Figure 4.10).

As should be noted, the calibration is based on limited storms in wet seasons to evaluate the ability to reproduce historic time series of observed streamflow. These storms are single-peak events. Two of the storms are dominant rain events (11/1/84 and 12/2/91) and one (11/20/92) is rain-and-snow event. Although a two month simulations (12/1/91-1/22/92) well depict the dynamics of an relatively dry period and some small rain-on-snow simulations based on the calibrated parameters, neither summer low flow days nor large rain-on-snow events are simulated. More thorough examination of different events that

span the range of expected model behavior, such as wet/dry antecedent conditions, snow/rain input, big/small and simple/complex hydrograph response is desirable. Also, detailed validation is needed to systematically test the transferability of CLAWS to different climatic and geographic regimes, based on the stationary and nonstationary conditions (Klemes, 1986).

4.7 Sensitivity Analyses

Since there are many sources of error in complex and nonlinear models, their accuracy can be unclear. Uncertainties in model parameters, in particular, may control the predictions of the model. Some of these uncertainties stem from spatial heterogeneity and measurement error associated with input data or parameter values (Beven and Binley, 1992; Hammond et al., 1992).

Models are often sensitive to factors we know the least about. This implies that model accuracy is limited. Coupled models, combining several processes, necessarily involve more parameters, which may result in over parameterization. Thus sensitivity analyses are an important step in understanding process relationships and model

Table 4.6 Parameters used in sensitivity analysis

Parameter Name	Unit	Uncertain Range	Default Value	Test Range
Maximum saturated conductivity	ms^{-1}		0.001	0.0001-0.01
Saturated profile coefficient	--		3	0.3-30
Deep groundwater conductivity	ms^{-1}		$4x10^{-8}$	$4x10^{-9}$-$4x10^{-7}$
Loss rate of deep groundwater storage	ms^{-1}		$4x10^{-8}$	$4x10^{-9}$-$4x10^{-7}$
Soil depth	m	Vary	1.2	0.1-12
Soil porosity	--	0.33-0.58*	0.49	0.37-0.61
Field capacity	--	0.018-0.46*	0.28	0.22-0.34
Maximum biomass	kPa	2-4**	3	0.3-30
Maximum root strength	kPa	0-20**	12.5	0.1-125
Soil cohesion	kPa	0-50**	2.5	0.25-25
Internal friction angle	^{o}	26-45**	38	26-50

Source: * Maidment, 1993 Handbook of Hydrology; ** Hammond et al., 1992;

performance.

The Generalized Likelihood Uncertainty Estimations (GLUE) technique (Beven and Binley, 1992) provides a better way to address the uncertainty in distributed models. GLUE explicitly recognizes the equivalence or near-equivalence of different parameter sets or model structures in the representation of hydrologic responses using a Monte Carlo procedure (Beven and Binley, 1992). Due to limited knowledge about stochastic distributions of parameters and correlations between parameters at the test site, in addition to extensive computational requirements, this type of algorithm is not implemented here.

In this study, eleven parameters (Table 4.6) were chosen to evaluate how the model performs as these terms were allowed to vary. This is accomplished by varying one parameter at a time with other parameters fixed for a calibrated parameter set. The change of parameter values is based on ratios or difference from values which we calibrated for events at a small watersheds as discussed before. Visual graphs and quantitative measures of the change of the hydrologic and geomorphic responses are examined to see the sensitivities of these parameters

WS#2 was chosen as the sensitivity analysis site and storm events between December 1, 1991 and December 11, 1991 were selected arbitrarily. The flow peak has a return period of 5 years for observed data.

4.7.1 Maximum saturated conductivity

The maximum saturated conductivity is defined while the soil profile is fully saturated. When maximum saturated conductivity is changing in a range of 0.1 to 10 times the standard value, the outlet hydrograph, soil moisture and stability change accordingly (Figure 4.11). Increasing saturated conductivity, precipitation and runoff ratios show that more water will flow out of the watershed, peakflow size increases and time advances, and the falling limb of the hydrograph decays faster. Stability is positively affected in that the factor of safety for the watershed increases, because the basin soil moisture is generally lower at higher saturated conductivity.

4.7.2 Saturated profile coefficient

The saturated conductivity of the soil is assumed to vary with soil depth based conceptually on an exponential distribution. The saturated profile coefficient describes the shape of the exponential profile. The coefficient influences the conductivity more when soil is at a low saturation level. Increasing this coefficient reduces conductivity of the lower soil profile, while decreasing the coefficient increases conductivity of the lower soil profile. So increasing the coefficient produces the same effect on watershed response as decreasing the saturated conductivity (Figure 4.12).

4.7.3 Deep groundwater conductivity

Deep groundwater conductivity is the rate deep groundwater moves to the next element. Since it is not measurable for a site, it can only be calibrated. When it changes from 0.1 to 10 times the standard value, more water will leak through the deep ground layer, decreasing the precipitation ratio and peakflow size. The peakflow time is constant because it is controlled by the precipitation and movement in the subsurface layer (Figure 4.13). Hydrographs will decay somewhat faster, when more water leaks into deep groundwater. Generally, this parameter is not a very sensitive contributor to major hydrologic and geomorphic changes.

4.7.4 Loss rate of deep groundwater storage

The rate at which deep groundwater moves out of the system is accounted for in our model by the loss rate of deep groundwater storage. Changes in this constant did not make much difference for the watershed response in the range of our calibrations (Figure 4.14). Apparently it is not a sensitive parameter in the model.

4.7.5 Soil depth

Soil is described here as the layer of apparent high saturated conductivity and not necessarily the total thickness of unconsolidated material. There is no reliable method to estimate the soil depth based on topographical information, although some progress has been reported in relating terrain analysis to soil depth (Dietrich et al., 1993). The mean thickness derived from an inventory compiled by forest soil scientists (SCS, 1964) was

used in the model and future work should incorporate soil depth interpolation methods (Dietrich et al., 1993). Decreasing soil depth will increase water yield from the watershed during the simulation time. Peakflow will be higher and advanced. The increased likelihood of saturated overland flow on shallow soils, results in high soil moistures and hydrographs that are very responsive to precipitation variation (Figure 4.15). Shallow soils also tend to be much more stable.

4.7.6 Soil porosity

Porosity affects soil moisture storage capacity and rate of movement in the subsurface. Since we do not simultaneously change saturated conductivity along with the change of porosity, the porosity mainly controls how much space is available for water and thus the saturated density of soils. Decreasing porosity results in increased soil moisture, increased water yield from the watershed, higher and advanced peakflows, and faster decay limbs of hydrographs (Figure 4.16). Decreasing porosity increases instability in our simulations, but not significantly.

4.7.7 Field capacity

Field capacity has been defined as the water content of the near surface soil profile at which drainage becomes negligible (e.g., Jury et al., 1991). It is important in CLAWS to define the storage of soil moisture after rainfall-event redistribution has ceased, although in reality this is hard to determine. Changing this parameter significantly influences the hydrologic response of the watershed, but has only minor ramifications for landslide potential (Figure 4.17).

4.7.8 Maximum biomass

Biomass depends on species, health, age and density of timber stands. It is not a sensitive parameter in the infinite slope model (Hammond et al., 1992). Sometimes the biomass surcharge will have a positive effect on stability for certain combinations of other parameters such as cohesion, friction angle and slope (Simons et al., 1978). Figure 4.18 shows that the stability is only increased slightly for the watershed with increasing biomass.

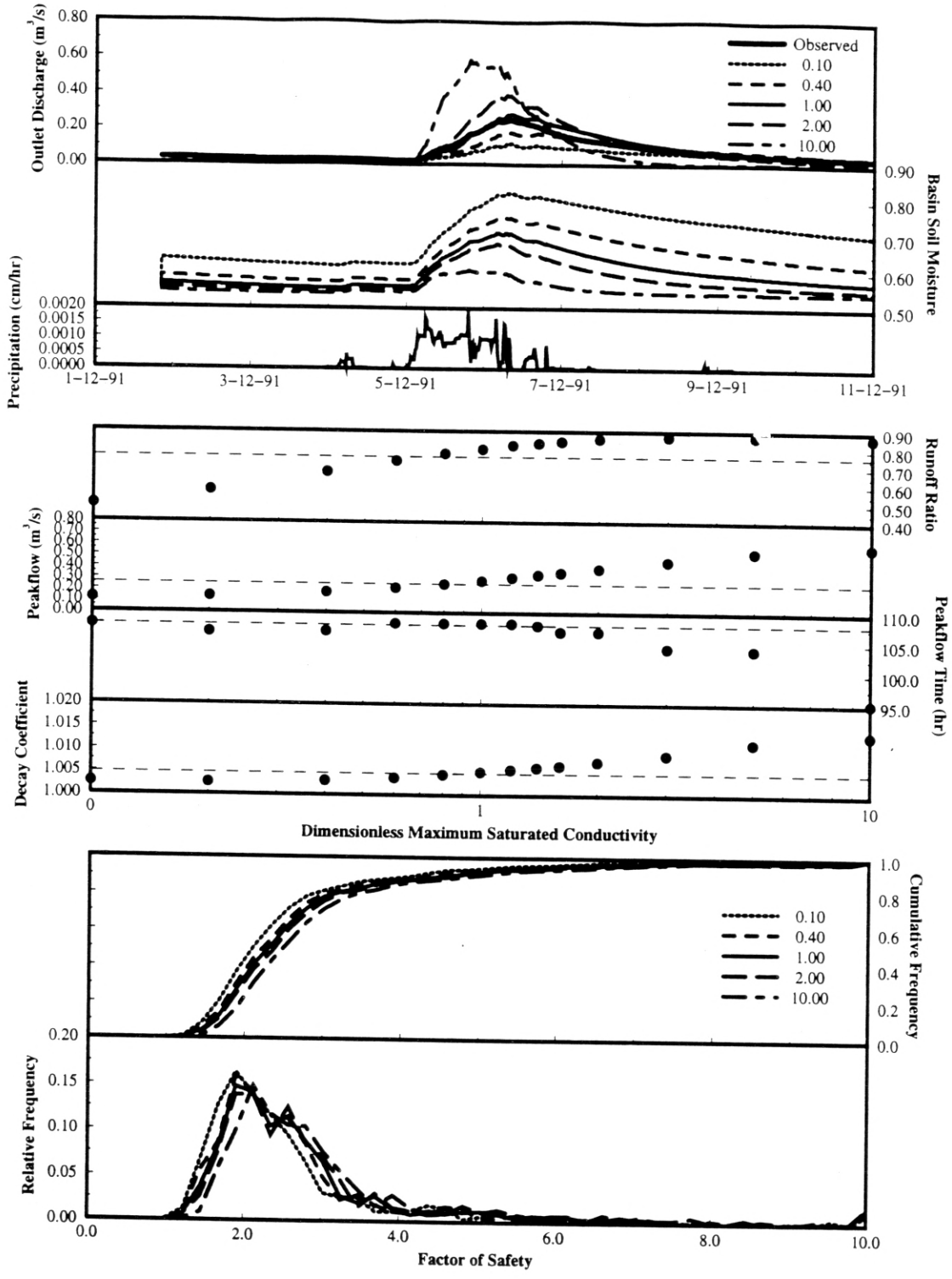


Figure 4.11 Sensitivity analyses of maximum saturated conductivity. This graph shows the hydrographs, basin soil moisture, input precipitation, characteristics of hydrograph including runoff/precipitation ratio, peakflow size and time, and decay coefficients, and, cumulative and relative frequency of factor of safety for the whole watershed.

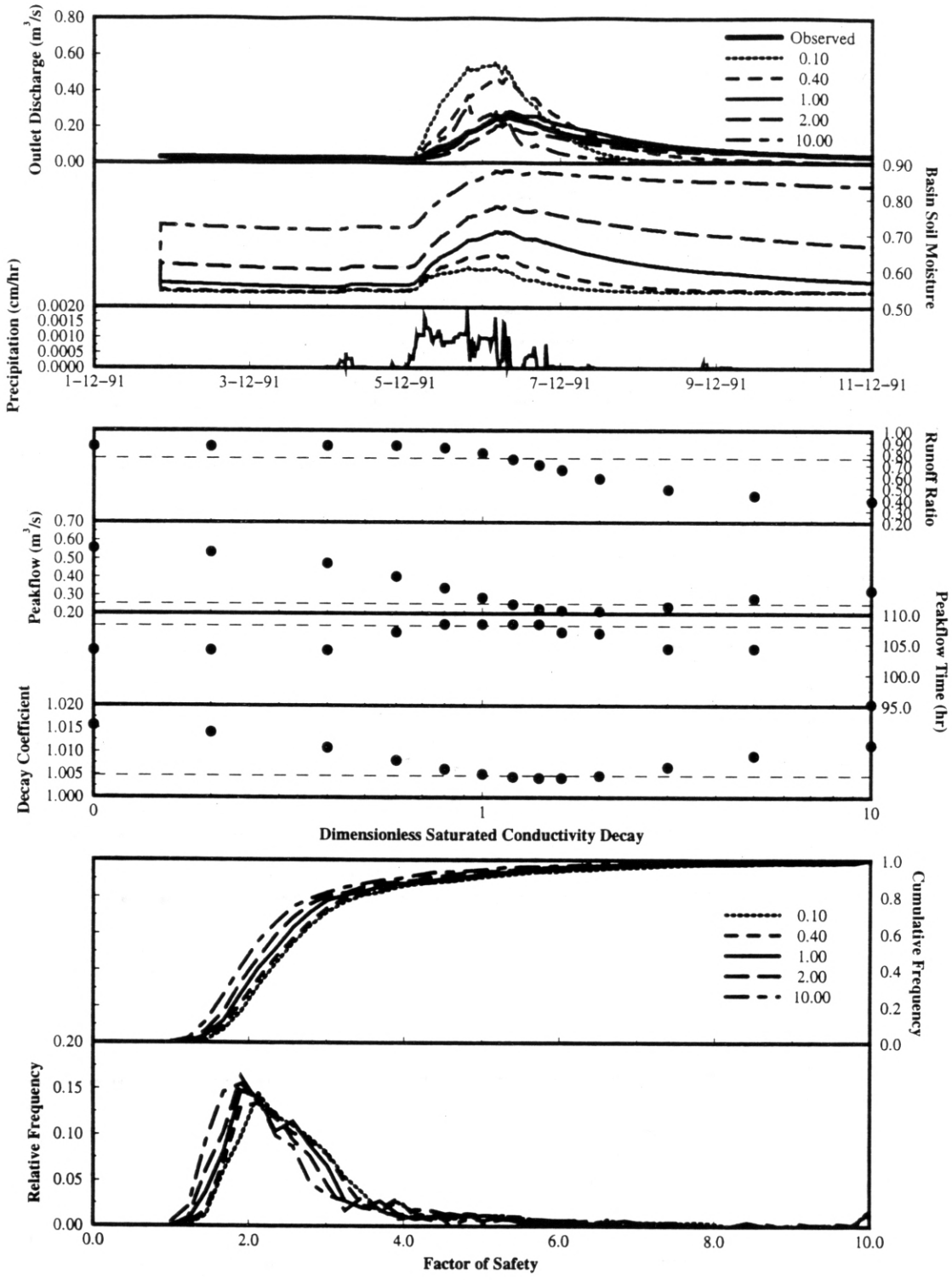


Figure 4.12 Sensitivity analyses of saturated profile coefficient. This graph shows the hydrographs, basin soil moisture, input precipitation, characteristics of hydrograph including runoff/precipitation ratio, peakflow size and time, and decay coefficients, and, cumulative and relative frequency of factor of safety for the whole watershed.

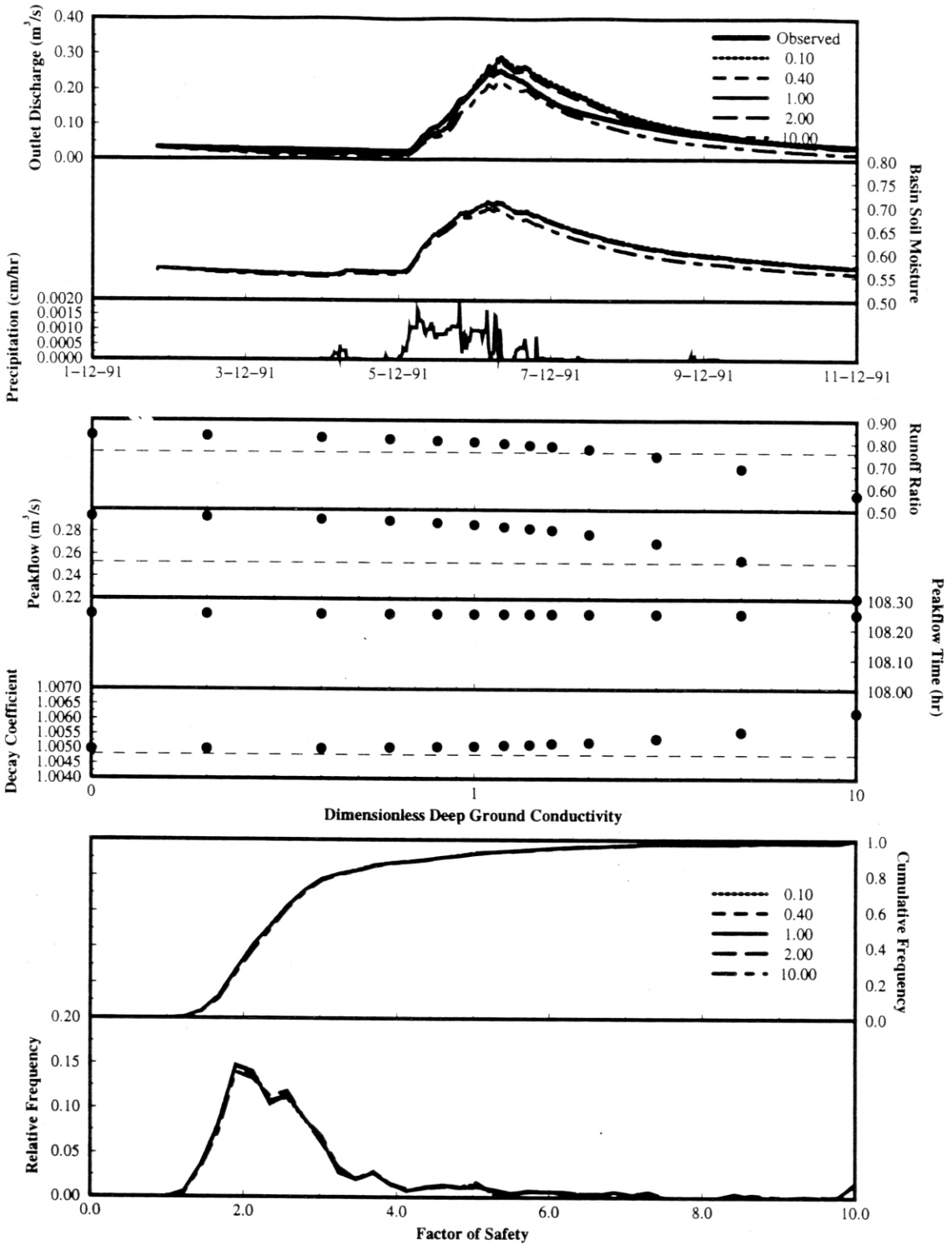


Figure 4.13 Sensitivity analyses of deep groundwater conductivity. This graph shows the hydrographs, basin soil moisture, input precipitation, characteristics of hydrograph including runoff/precipitation ratio, peakflow size and time, and decay coefficients, and, cumulative and relative frequency of factor of safety for the whole watershed.

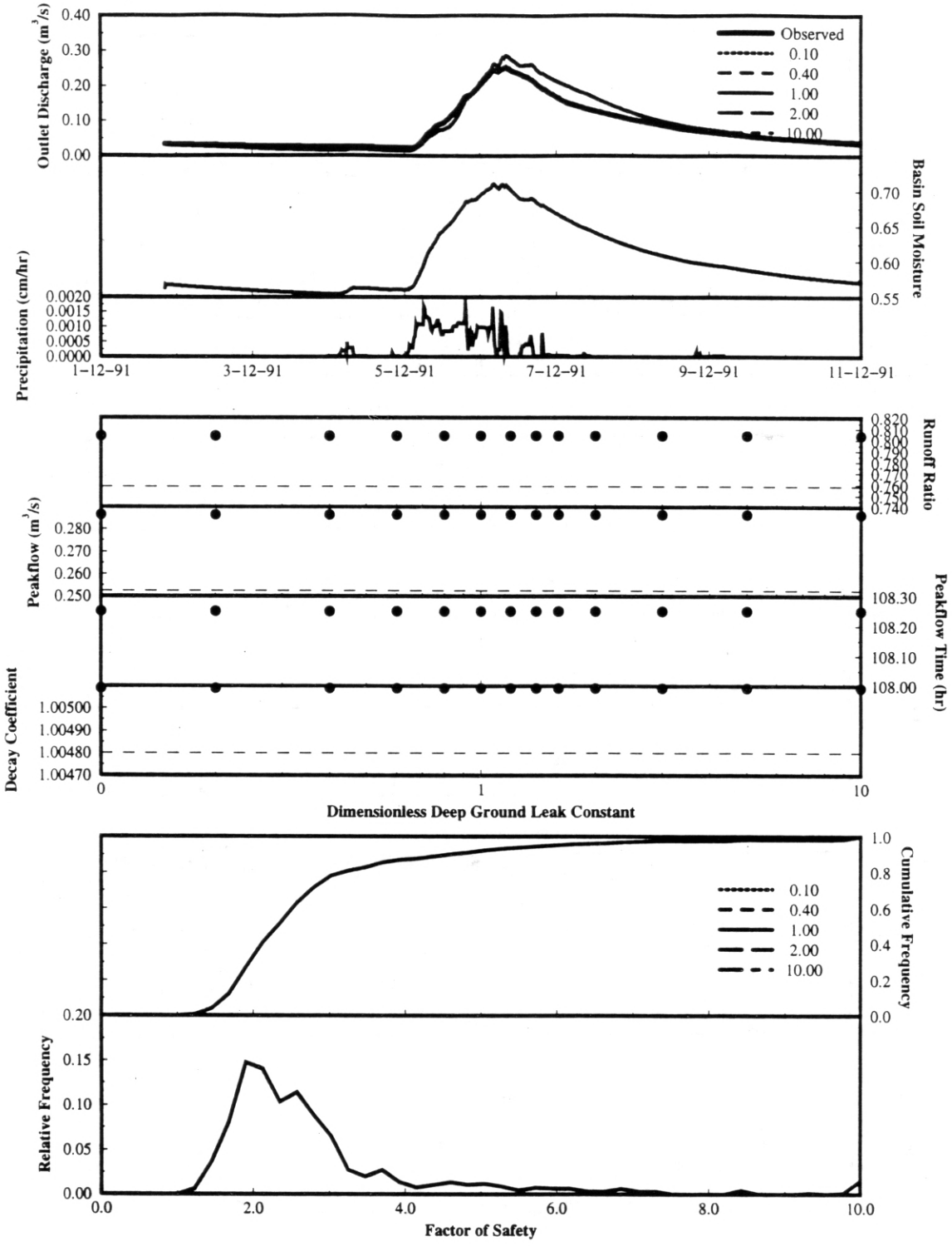


Figure 4.14 Sensitivity analyses of loss rate of deep groundwater storage. This graph shows the hydrographs, basin soil moisture, input precipitation, characteristics of hydrograph including runoff/precipitation ratio, peakflow size and time, and decay coefficients, and, cumulative and relative frequency of factor of safety for the whole watershed.

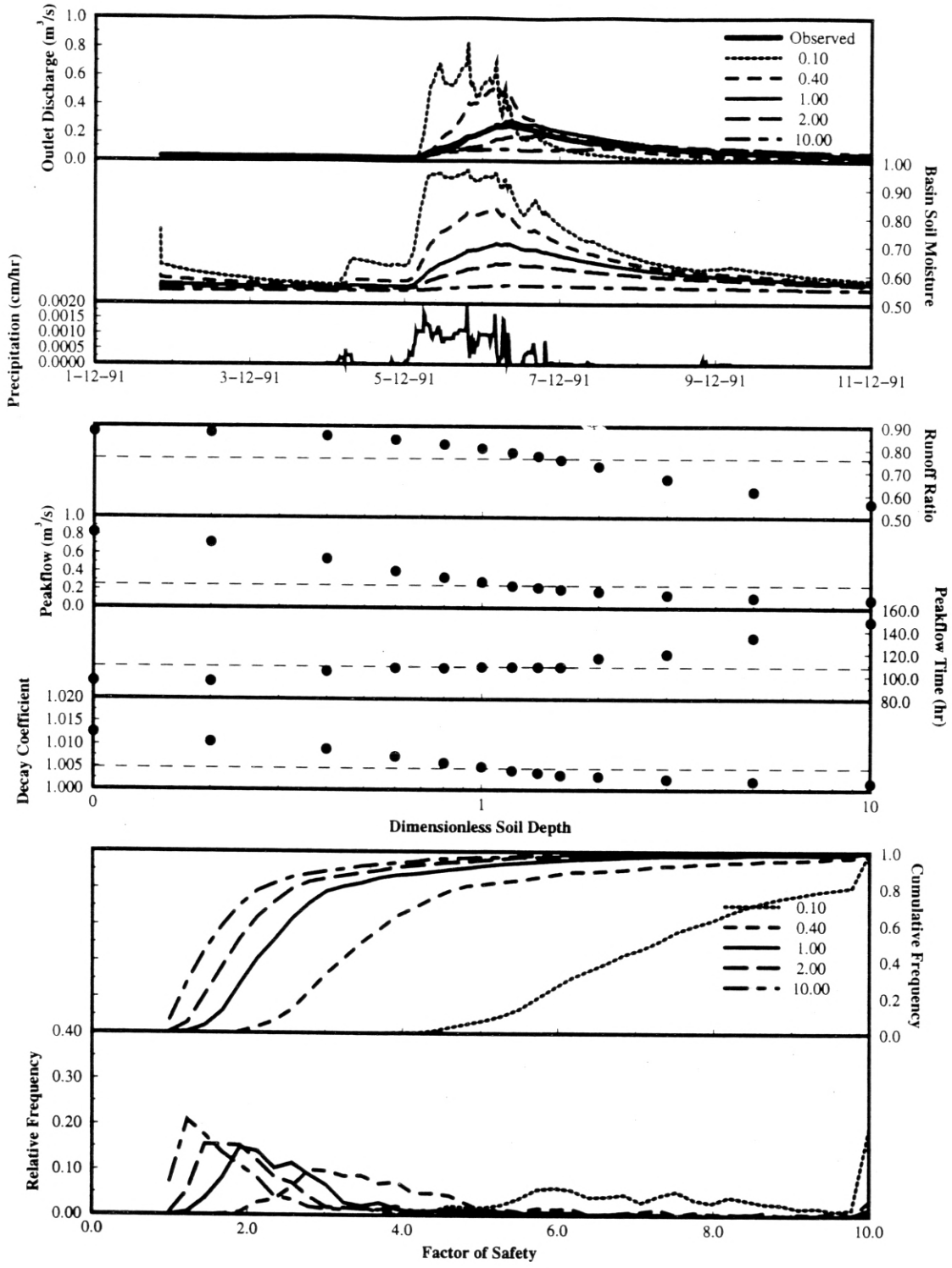


Figure 4.15 Sensitivity analyses of soil depth. This graph shows the hydrographs, basin soil moisture, input precipitation, characteristics of hydrograph including runoff/precipitation ratio, peakflow size and time, and decay coefficients, and, cumulative and relative frequency of factor of safety for the whole watershed.

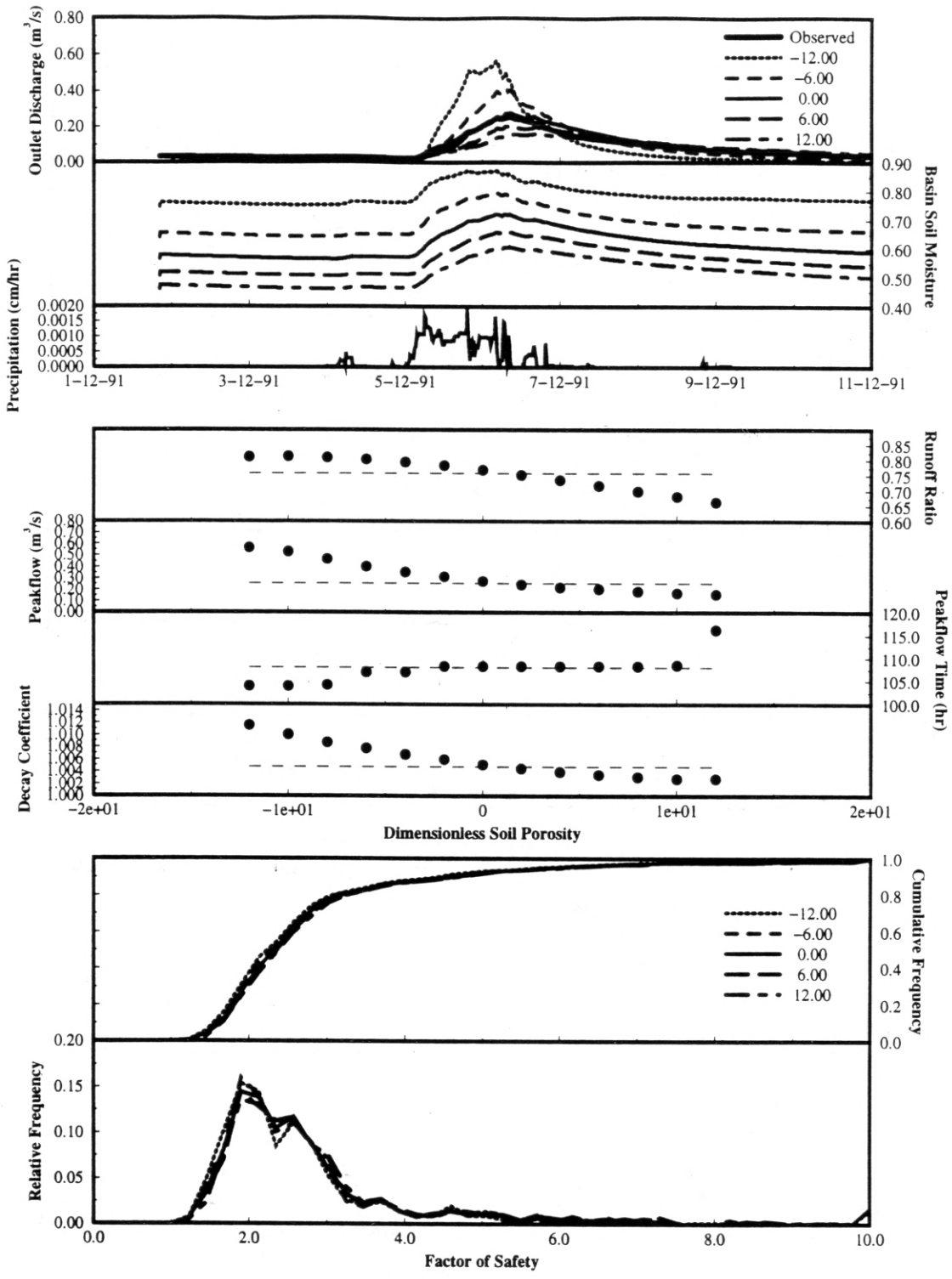


Figure 4.16 Sensitivity analyses of soil porosity. This graph shows the hydrographs, basin soil moisture, input precipitation, characteristics of hydrograph including runoff/precipitation ratio, peakflow size and time, and decay coefficients, and, cumulative and relative frequency of factor of safety for the whole watershed.

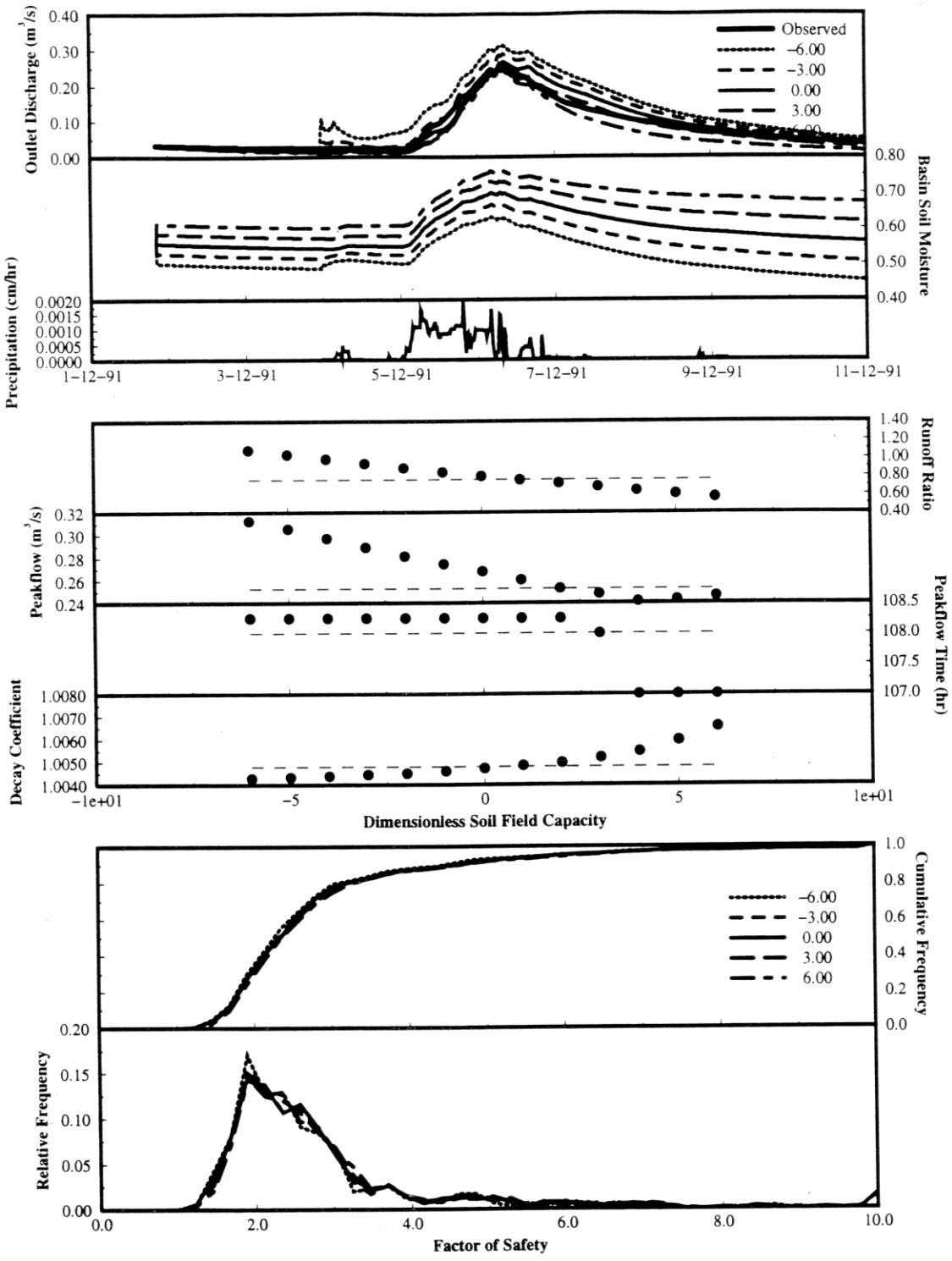


Figure 4.17 Sensitivity analyses of field capacity. This graph shows the hydrographs, basin soil moisture, input precipitation, characteristics of hydrograph including runoff/precipitation ratio, peakflow size and time, and decay coefficients, and, cumulative and relative frequency of factor of safety for the whole watershed.

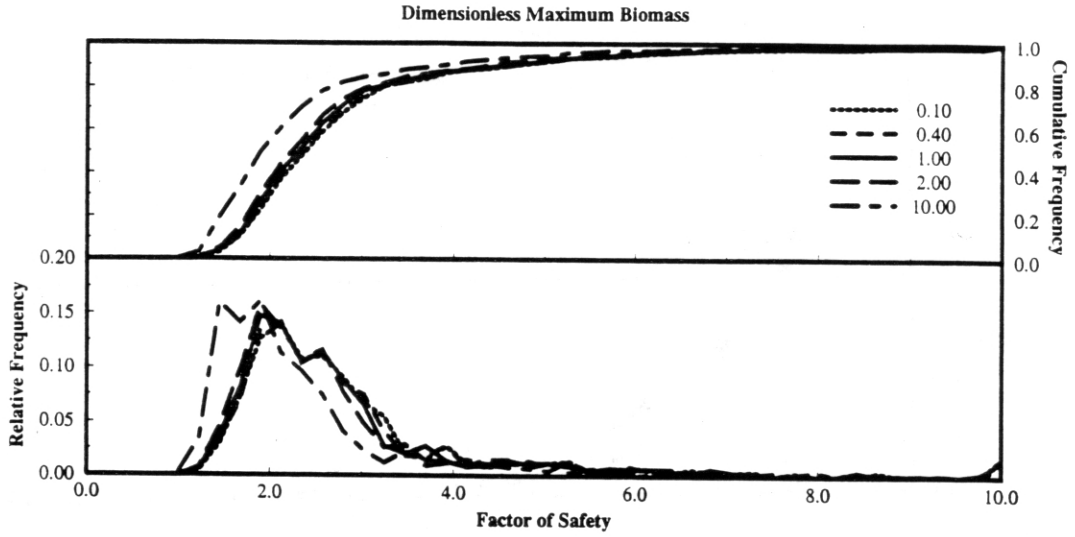


Figure 4.18 Sensitivity analyses of maximum biomass. This graph shows cumulative and relative frequency of factor of safety for the whole watershed.

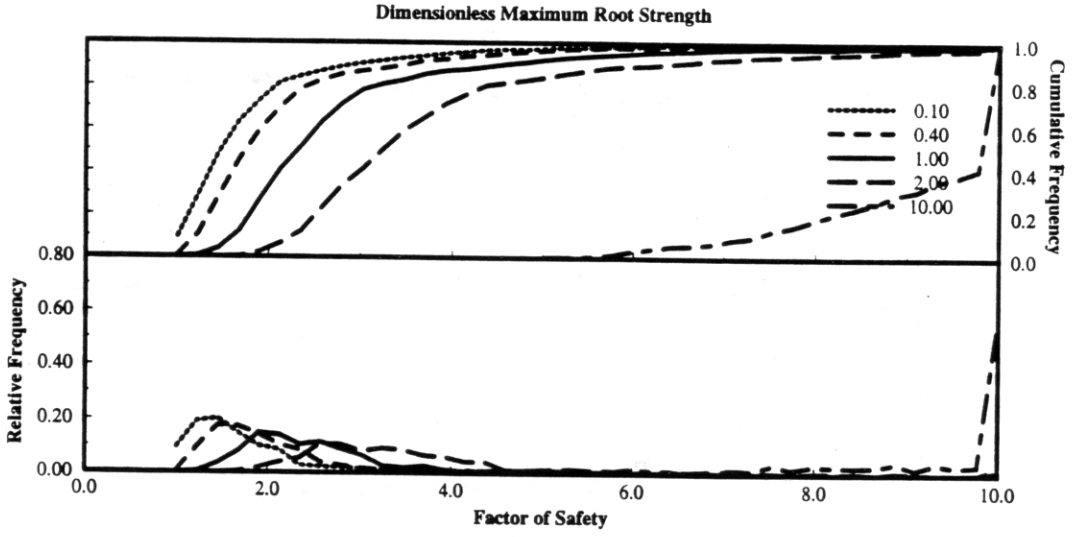


Figure 4.19 Sensitivity analyses of maximum root strength. This graph shows cumulative and relative frequency of factor of safety for the whole watershed.

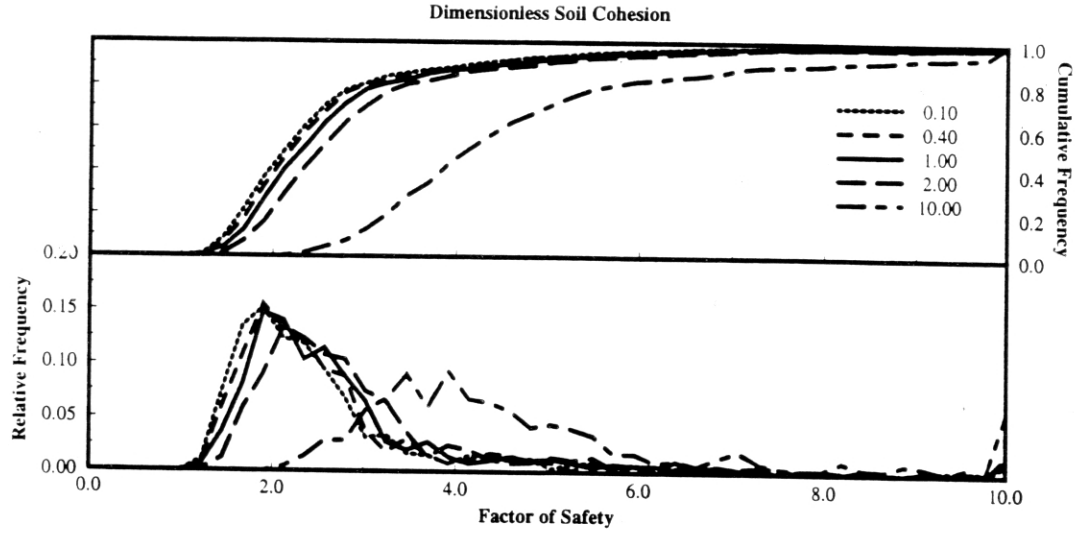


Figure 4.20 Sensitivity analyses of soil cohesion. This graph shows cumulative and relative frequency of factor of safety for the whole watershed.

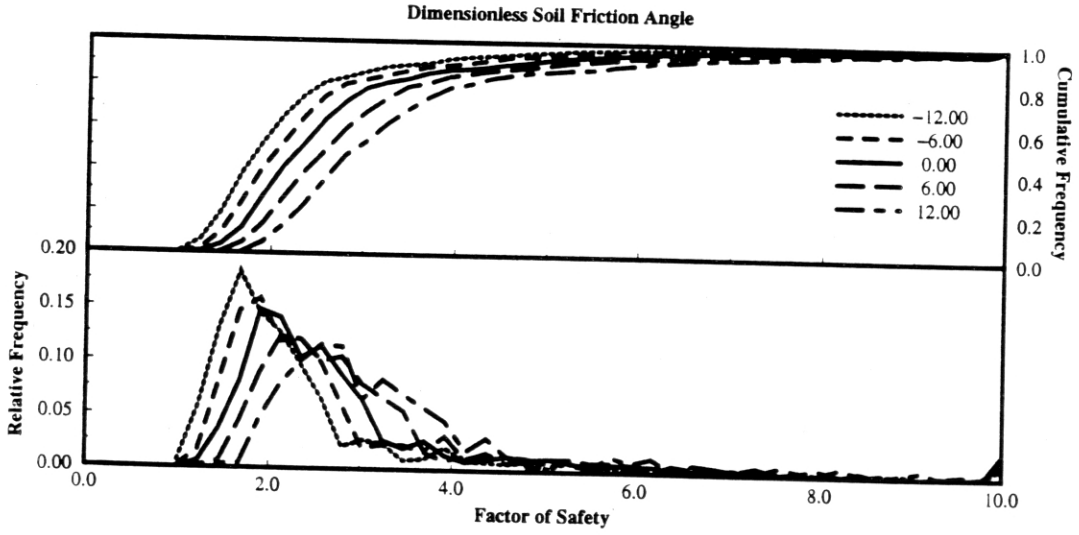


Figure 4.21 Sensitivity analyses of internal friction angle. This graph shows cumulative and relative frequency of factor of safety for the whole watershed.

4.7.9 Maximum root cohesion

Tree roots add shear strength to the soil mass in three ways (Hammond et al., 1992): by providing a laterally reinforcing surface layer that acts as a membrane to hold the underlying soil in place (O'Loughlin and Ziemer, 1982), by anchoring an unstable soil mantle to stable subsoils or rock where the roots penetrate a potential failure surface, and by acting as buttress piles and/or arch abutments to support the soil uphill from the trees (Gray and Megahan, 1981). Studies summarized by Hammond et al. (1992) show that the root strength varies between 0 to 20 kPa with a mode of about 5 kPa. Higher root strength will create greater stability (Figure 4.19).

4.7.10 Soil cohesion

Shear strength contributed by soil cohesion is different depending on the soil type and consolidation (Hammond et al., 1992). The stability influence of this parameter has about the same pattern as the root strength (Figure 4.20).

4.7.11 Internal friction angle

Frictional angle is influenced by soil texture, structure and composition. Decreasing soil frictional angle will increase the potential of instability (Figure 4.21).

4.7.12 Implications

The sensitivity analyses identified saturated conductivity, soil depth and porosity as significant in influencing watershed hydrologic response. Soil depth and cohesion, root strength, and internal friction angle were identified as the most significant factors affecting slope stability. In nature, many variables are correlated, so unilaterally varying one while holding others constant does not address true interdependencies, and techniques like GLUE (Beven and Binley, 1992) may be a better approach to sensitivity analysis.

The sensitivity analyses suggest several characteristics of watershed hydrologic response. First, they identify the different watershed behaviors under different watershed settings of soil and vegetation. For example, the hydrograph is dampened and the peak attenuated in a watershed with thick soils, compared to the response of a watershed with

thin soils. Second, since these sensitive parameters are very important in controlling watershed behavior, accurately measuring or estimating these parameters will help to understand the watershed response. At last more effort should be focused on these sensitive parameters in model calibration.

4.8 Conclusions

I have described the calibration, and sensitivity analyses of CLAWS, a coupled hydro-geomorphic model, using observations from three small watersheds in western Oregon. Simulated hydrographs showed acceptable agreement with recorded observations. Quantitative measures demonstrated that the simulation results from CLAWS described well the hydrograph characteristics, such as peak size and timing, and decay coefficient, with the overall consistency represented by high correlations and low mean square errors. Sensitivity analyses on 11 main parameters of soil and vegetation not only identified their significance in the model, but also represented different watershed behaviors under different watershed conditions.

The sparseness of observation networks in mountainous regions necessitates interpolation or extrapolation of driving input variables. This is a major limit to the model simulation results, as with other distributed models. Improving input data quality and developing sound algorithms for data distribution without increasing the number of parameters are areas where research should be focused.

Chapter 5

Hydrologic and Geomorphic Responses of Watersheds to Logging: Perspectives from CLAWS, a Physically-Based Spatially-Distributed Model

Jinfan Duan, Gordon E. Grant and Robert L. Beschta

In Preparation

5. HYDROLOGIC AND GEOMORPHIC RESPONSES OF WATERSHEDS TO LOGGING: PERSPECTIVES FROM CLAWS, A PHYSICALLY-BASED SPATIALLY-DISTRIBUTED MODEL

5.1 Abstract

A general framework and primary results from computer-based simulation of effects of forest cutting on watershed hydrologic and geomorphic responses are presented. Storm events and antecedent conditions are first simulated randomly from observed parameters. For each simulated event, a series of post-harvesting years ranging from one to 100 in vegetation and root properties is assumed and input to a physically-based, spatially-distributed model (CLAWS). The model then simulates watershed responses to specific events following cutting. Results from about 1500 of these simulated events are consistent with long-term observations at HJ Andrews Experimental Forest in western Oregon. Hydrologic responses, such as annual water yield, soil moisture, and flow peaks, have the greatest change in the first years after cutting. By contrast, landslide potential, controlled by root strength change, peaks about 10-15 years after cutting. About 40 years are needed for a watershed to recover to pre-cutting levels of streamflow, soil moisture and landslide susceptibility. Changes in hydrologic responses also vary with season and storm intensity. Summer has the highest relative changes and lowest absolute changes because it is the dry season. Small storms are more sensitive to forest cutting than large storms in terms of relative changes. Success of this research shows that distributed modeling can enhance traditional paired-watershed studies with long-term observations.

5.2 Introduction

Landuse activities that alter the type and extent of vegetation cover on a watershed may change its hydrologic and geomorphic responses (Brown and Beschta, 1985). The potential for forest harvesting to alter watershed processes has caused much concern among

scientists, land managers and the public. This area of research is becoming more important as forested watersheds become more intensively managed and attempts are made to minimize possible adverse impacts on ecosystems and biological diversity.

Precipitation drives hydrologic processes in watersheds. Modifications to precipitation by logging are often neglected. However, in some instances, precipitation in the form of fog-drip or snow can be significantly affected by harvesting. Studies in Bull Run Municipal Watershed, where fog is common, showed that forested areas receive 387 mm more precipitation than clearcut areas during a 40 week sample period (Harr, 1982). The rate of snow accumulation and melt may also change following harvest because of altered wind and other conditions that differ between clearcuts and forested areas (Harr, 1981).

Vegetation affects the proportion of precipitation that evaporates or is transpired, and consequently the amount available for soil moisture storage, groundwater recharge and dry weather stream flow. The proportionate contribution of precipitation to streamflow varies by the manner in which interception and evapotranspiration are influenced by type, development, rooting depth, and health of vegetation. Some logging activities compact the soil, reduce infiltration rate, increase bulk density, and convert soil macropores to micropores, blocking downward percolation. Road systems alter drainage patterns and intercept subsurface flows (Wemple, 1994).

The paired-watershed method is often used to evaluate effects of timber harvesting on streamflow. Watersheds with similar soils, vegetative cover, geology, topography, and size, are selected to test the effects of harvesting using controls and treatments (Hewlett, 1967; Brooks et al., 1991). Few efforts at finer scale modeling account for spatial and temporal heterogeneity of the landscape and vegetation in watersheds. Recently, physically-based spatially-distributed models have been developed. Here we present simulated effects of clearcutting within small watersheds on hydrologic and geomorphic responses and patterns using CLAWS (Coupled Landscape and Water System), a coupled hydrologic and geomorphic model with vegetation dynamics.

5.3 Methodology

The general procedure to model effects of harvesting practices on watershed responses is based on random simulation of precipitation events and initial conditions from observed parameters of precipitation and baseflow records. Then for each simulated event, a series of post cutting years ranging from one to one hundred is assumed and is input to a physically-based, spatially-distributed model (CLAWS) to simulate the watershed responses to the specific event in the century following cutting.

The components required for the investigation can be described as follows, following Beven (1987) and Eagleson (1972):

- A distributed precipitation-runoff model to simulate watershed responses. CLAWS, a coupled hydrologic-geomorphic model is used here.
- A precipitation model to simulate the duration, intensity, profile of

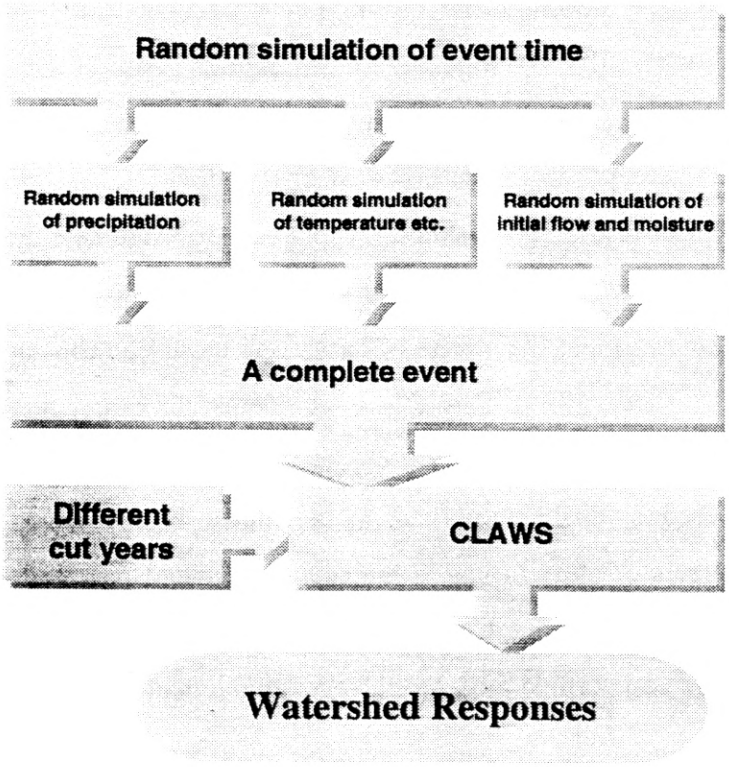


Figure 5.1 General procedure of Monte Carlo simulation of clearcutting on watershed responses

precipitation events, and time (month) of each event.

- A model to simulate other meteorological input data the runoff production model needs, such as temperature and solar radiation. I simplified this step by searching an inventory of more than 20 years of observation for these inputs at fine resolution according to an extra-module of detailed time simulation.
- An initial condition model to simulate the initial streamflow and soil moisture at the start of the event.

Each component is described briefly in the following sections. Readers should note that in our treatment, harvest was assumed clearcut with 100% removal of vegetation, and road effects and initial snowpack are not simulated. WS#1, WS#2, WS#3, three small watersheds at HJ Andrews Experimental Forest, western Oregon were used as simulation watersheds. These three watersheds have been studied for the effects of forest harvesting on streamflow for more than four decades (Rothacher 1964; Harr 1983; Grant and Wolff 1991; Jones and Grant, 1996). WS#1 was clearcut from 1962 to 1966. On WS#3, roads covering 2.64 km (6% of the drainage) were completed in 1959, and three discontinuous clearcuts composing 25% of the watershed area were logged in 1962-1963. WS#2 served as a control without any treatment.

5.3.1 Model of watershed responses

Watershed responses are simulated with a physically-based, spatially-distributed hydrologic and geomorphic model, CLAWS. Interception is modeled as a linear function of leaf area index through the storage capacity. Total evapotranspiration from each element uses the Penman-Monteith (Monteith, 1965) equation and is subdivided into three components: evaporation from bare soil and non-canopy substrate, evaporation from canopy, and transpiration from canopy. Subsurface water movement is based on Dupuit's (1863) assumption of slope-parallel saturated flow through a limited depth of soil over a relative impermeable layer of parent material or bedrock. Overland flow is assumed to occur only when the ground is saturated. Some exchange between deep groundwater and subsurface layer is incorporated. Intercell water movement is modeled with the kinematic

Table 5.1 Observed monthly precipitation characteristics for HJ Andrews Experimental Forest, western Oregon.

Month	Probability of Storms	Mean Intensity (mm/hour)	Mean Duration (hour)	Mean Interval (day)
Jan	0.104	1.34	43.37	4.56
Feb	0.113	1.31	32.19	4.58
March	0.129	1.25	26.34	4.2
April	0.092	1.2	26.24	4.93
May	0.081	1.27	18.83	5.43
June	0.034	1.29	21.09	11.46
July	0.012	1.16	13.06	15.38
Aug	0.031	1.28	16.08	17.44
Sept	0.046	1.34	25.33	16.43
Oct	0.085	1.34	29.65	9.08
Nov	0.153	1.41	36.15	3.77
Dec	0.121	1.38	38.01	4.74

continuity equation, and a combined subsurface and overland flow equation is solved to route water from one element to another.

In CLAWS, landslide occurrence is simulated with an infinite-slope model using the hydrologic simulation results. Given any instance of slope instability, the possible runout path or debris flow is simulated using the local slope, channel geometry and a mass decay function. Sediment transport out of the watershed by streamflow is based on a rating curve to discharge.

5.3.2 Precipitation model

Precipitation storms were defined as periods with a mean precipitation intensity greater than 1 mm h^{-1}, separated by at least 12 hours with precipitation less than 1 mmh^{-1} (Beven, 1987). Precipitation processes are simulated from four components of storm time (month), storm volumes, durations and intra-storm intensity profile. The month of a precipitation event is simulated with a monthly precipitation probability (Table 5.1). Storm volume, duration and internal profile are treated as independent random variables (Beven, 1987). An exponential distribution is used for precipitation mean intensity I_m and duration D_p as

$$f(I_m) = \frac{e^{-I_m/\lambda_P}}{\lambda_P} \tag{5.1}$$

$$f(D_P) = \frac{e^{-D_P/\lambda_D}}{\lambda_D} \tag{5.2}$$

where f(.) denotes a probability density function and, λ_P, λ_D are mean storm intensity and mean storm duration, respectively, based on the simulated month.

Precipitation analyses of meteorological gage #2, which has the longest history of observation at HJ Andrews Experimental Forest, show that over a 36-year period (water years 1958 to 1993), about 1097 storms fit the above criteria (Figure 5.2). Periods between November and April are more likely to have precipitation events with larger intensities, longer durations and short recurrence intervals (Table 5.1).

Beven (1987) has shown that mean intensity alone did not represent flow characteristics well and that within-storm variation of precipitation intensity is needed. The mean intensity profile of HJA storms has been calculated (Figure 5.2c) without differentiating monthly variation and by adding a random component with normal distribution to the mean profile for each simulated storm.

5.3.3 Model for other meteorological variables

It is desirable to simulate other meteorological data, such as solar radiation, temperature, wind speed and relative humidity, that are inputs to CLAWS. Accurate simulation of those variables requires extensive work, especially the fine resolution simulation of temperature and humidity. To provide these input data, I used a fine resolution inventory of actual observation data. From the simulated month of the occurrence, the start date and time of the event is also randomly simulated, assuming events are uniformly distributed between the year 1973 and 1993 when we have detailed observations of temperature, solar radiation, wind speed and humidity in the nearby Primet gage. To account for the storm-event distribution for different months, the start month of the simulated storm is adjusted based on results from the above precipitation model. Then the date and time simulated is used to get other meteorological variables such as temperature, wind speed, humidity and solar radiation from our observed inventory with

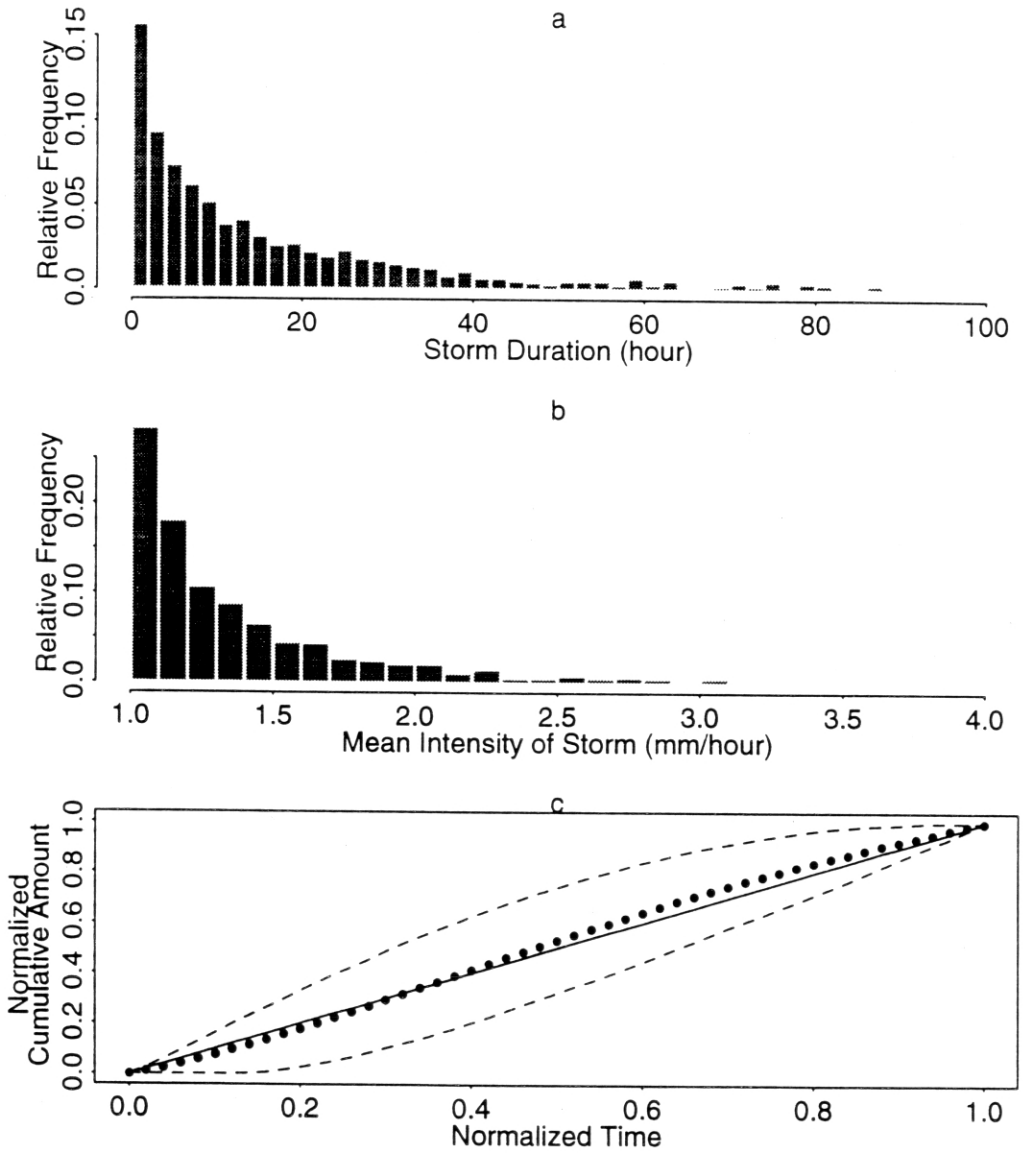


Figure 5.2 Storm characteristics at gage #2, HJ Andrews Experimental Forest: (a) storm intensity; (b) storm duration; (c) intra-storm distribution, dotted line is the intensity distribution; dash lines are the deviation; and the solid line is the uniform line.

Table 5.2 Parameters for initial baseflow (m^3/s) at WS#1, WS#2, WS#3. Note parameters have been logarithmic transformed with base ten.

Month	WS#1		WS#2		WS#3	
	Mean	Deviation	Mean	Deviation	Mean	Deviation
Jan	-1.345	0.347	-1.32	0.347	-1.337	0.3
Feb	-1.332	0.323	-1.292	0.345	-1.316	0.299
March	-1.302	0.3	-1.306	0.279	-1.316	0.243
April	-1.483	0.333	-1.455	0.3	-1.45	0.249
May	-1.722	0.318	-1.675	0.286	-1.641	0.228
June	-2.078	0.358	-1.989	0.309	-1.901	0.245
July	-2.5	0.259	-2.325	0.2	-2.172	0.16
Aug	-2.775	0.346	-2.561	0.241	-2.349	0.196
Sept	-2.705	0.364	-2.642	0.354	-2.346	0.214
Oct	-2.374	0.455	-2.511	0.507	-2.187	0.305
Nov	-1.697	0.518	-1.799	0.579	-1.69	0.432
Dec	-1.37	0.383	-1.36	0.423	-1.353	0.349

fine-resolution data over 25 years. A major problem with this approach is the correlation between precipitation and other variables. We argue that for our purpose, this approach is the best available when detailed simulation methods are intractable.

5.3.4 Initialization model

The initial discharges of each watershed were simulated using a monthly lognormal distribution. Table 5.2. shows the parameters of different months for the three watersheds. Winter and spring have higher baseflows and summer has low baseflows based on 36 years of observation in these watersheds (Figure 5.3). These baseflow values result from a computer program for streamflow analysis (Duan et al., in preparation). So, the initial discharge before the storm is simulated with a lognormal distribution according to the previously simulated month.

Given an initial discharge, a nonlinear equation is used to describe the initial basin mean of soil moisture storage and the initial discharge based on the soil moisture and runoff relationship from CLAWS (Figure 5.4):

$$\theta_i = a + b\log Q_i + c(\log Q_i)^2 + d(\log Q_i)^3 \qquad (5.3)$$

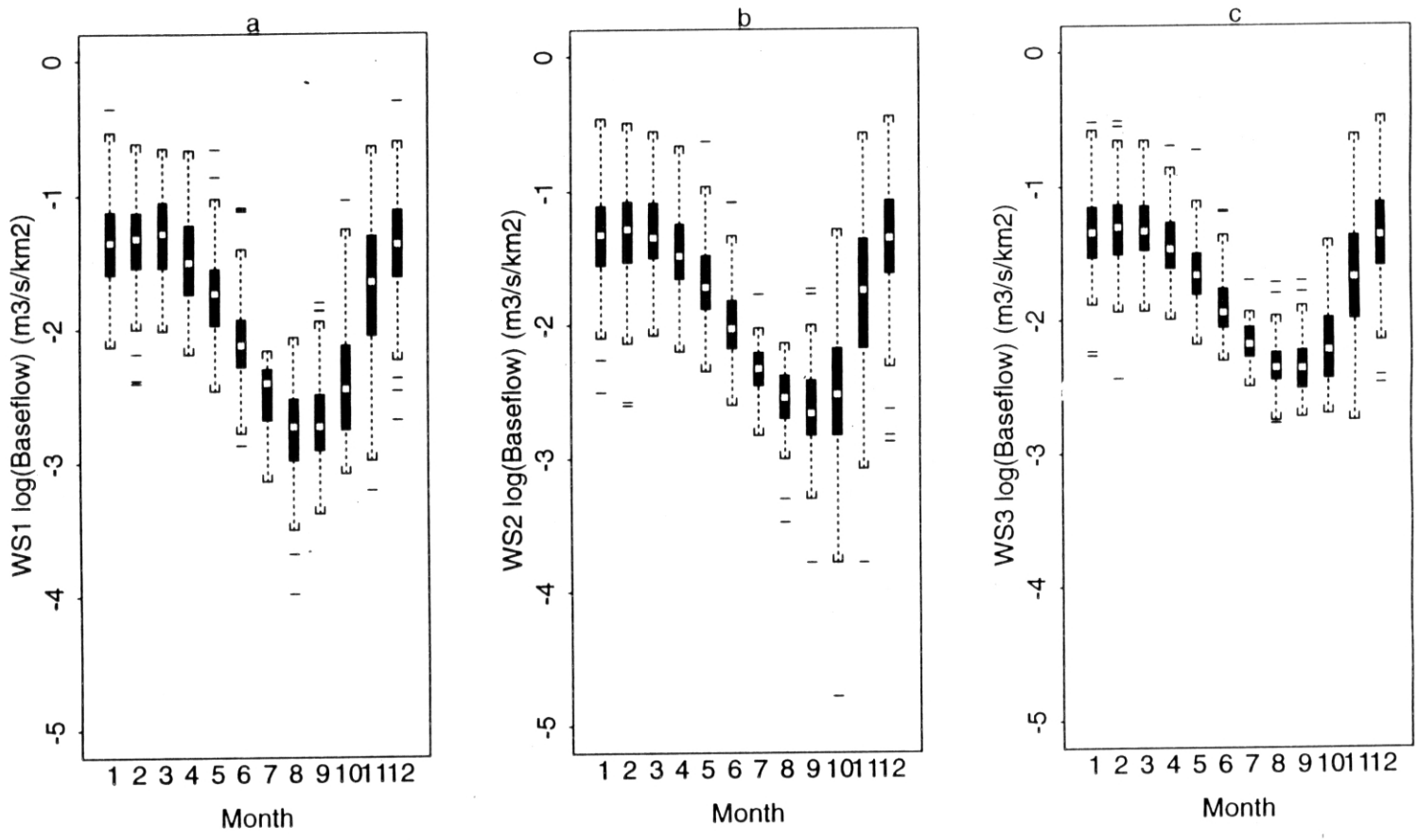
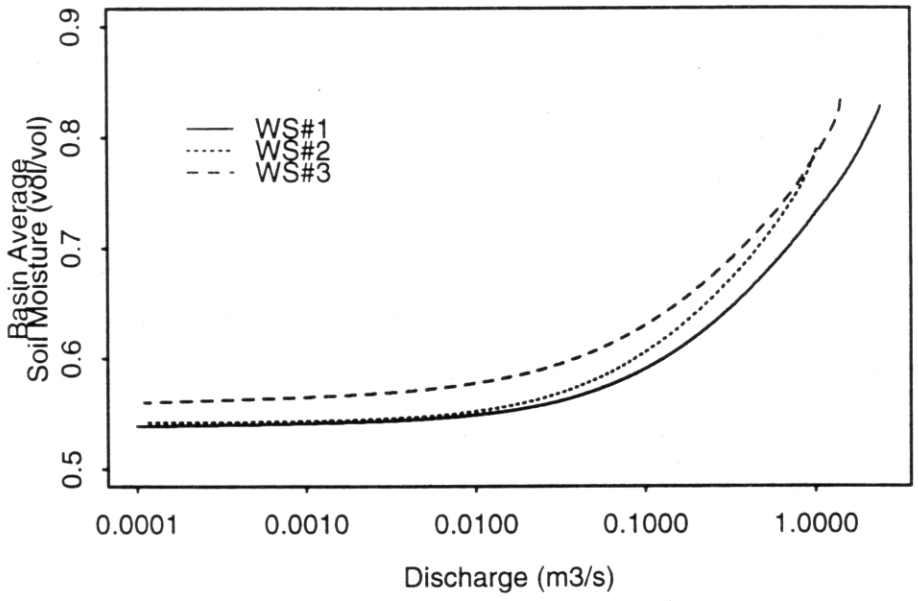


Figure 5.3 Observed baseflow distributions in different months for three small watersheds, WS#1, WS#2 and WS#3. Data are generated from 36 years of observation (1958-1993). Note that the discharge values are unit discharge and plotted with logarithm transformation.

Figure 5.4 Relationship between outlet discharge and basin average of soil moisture for three small watersheds, WS#1, WS#2 and WS#3, simulated from CLAWS.



where Q_i is the initial outlet discharge and θ_i mean soil moisture; a, b, c and d are fitted parameters (Table 5.3). This means soil moisture θ_i is distributed to the whole watershed according to the topographical convergence index (TCI) (Beven and Kirkby, 1979)

$$TCI = \ln(\frac{A}{\tan \beta}) \tag{5.4}$$

where A is the contributing area (drainage area) of each element. For any element, the

Table 5.3 Parameters for discharge-soil moisture relationships of three watersheds

Watershed	a	b	c	d
WS#1	0.72511	0.08288	0.01245	0.00062
WS#2	0.76198	0.09885	0.01523	0.00080
WS#3	0.76924	0.08410	0.01170	0.00055

initial soil moisture θ is

$$\theta = \frac{TCI}{\overline{TCI}}\theta_i \qquad (5.5)$$

which relates the local TCI of element with the mean watershed TCI.

5.4 Simulation Results

There are 1500 storm events simulated that account for about 50 years of storms. A series of 1, 5, 10, 15, 20, 25, 30, 35, 40, 45, 50, 75, and 100 years after cutting were run for each of the simulated events. The effects of storm volume, peakflow size, decay coefficient of the hydrographs, maximum basin average soil moisture and landslide potential were examined to look at the annual trajectory, monthly variations and storm variations of watershed response to cutting.

To quantify watershed responses after cutting, the simulated results were compared with the 100-year forest conditions which we arbitrarily define as reference stands. For most hydrologic and geomorphic responses, 100-year forests showed behavior similar to several hundred year old growth. Hereafter the watershed responses of forest with age over 100 years are called responses of old growth.

5.4.1 Runoff amount

Total streamflow runoff in units of depth of water over the watershed were summed for all simulated storms. Figure 5.5a shows that streamflow amount decays from a 33% increase in the first year after cutting compared with the old growth reference state. As expected, this increase shows strong seasonal and storm variations. This can be described using storm responses for the first year after cutting, the other years after cutting are the same pattern but in an attenuated way. During the first year after cutting summer storms had the largest relative increase (maximum in July of 400%), while storms in winter and spring had less dramatic effects (Figure 5.5b). Clearly evapotranspiration in the growing season is strongly influenced by presence of vegetation. Owing to the distribution of storm (Table 5.1) and related runoff production (Figure 5.5c), most runoff

occurs in the wet season between November and April in HJ Andrews. Hence the largest increases in runoff amount following harvest are in spring and fall. This is consistent with the observation of largest runoff increase by seasons (Rothacher, 1970; Hicks et al., 1991). This simulation also suggests that seasonal runoff changes as a function of potential evapotranspiration amount, precipitation amounts, and soil moisture.

Increase of runoff also varies between storms represented by sizes of peakflows in the old growth condition. Greatest increases are associated with smallest storms and large storms show less influence of cutting (Figure 5.6). This is consistent with the conceptual model that for small storms, much or even all of the precipitation is intercepted and evapotranspired if vegetation is present, which makes a great difference in relative runoff production. By contrast, for large storms, the percentages intercepted and evapotranspired are relatively unimportant.

5.4.2 Peakflow

After cutting, peakflows increase the most in the first year and decline with vegetation regrowth (Figure 5.7a). After 40 years of recovery, peakflow increase is undetectable. Monthly patterns show that the increase of flow peaks are largest in the dry season when evapotranspiration and interception have the most significant influence (Figure 5.7b).

Peakflow changes also show considerable variation with storm size and flow discharges (Figure 5.7c). Large storms are relatively less influenced than small storms. For low flow days, flow peaks increase the largest, especially when the flow is extremely low in summer days; this increase can be 1000 times greater than that of old growth. For large peakflows the increases are less than ten percent.

For all the Monte Carlo simulated storms, a series of extreme peakflows were extracted. The partial duration series selected based on the equivalent years of streamflows (which is 50) were used to estimate changes the flood frequency using the Weibull plotting position (Figure 5.8). For flood with return periods less than 5 years, the increases are obvious between old growth and first year after cutting, but the general pattern becomes more ambiguous for peakflows with lower recurrence.

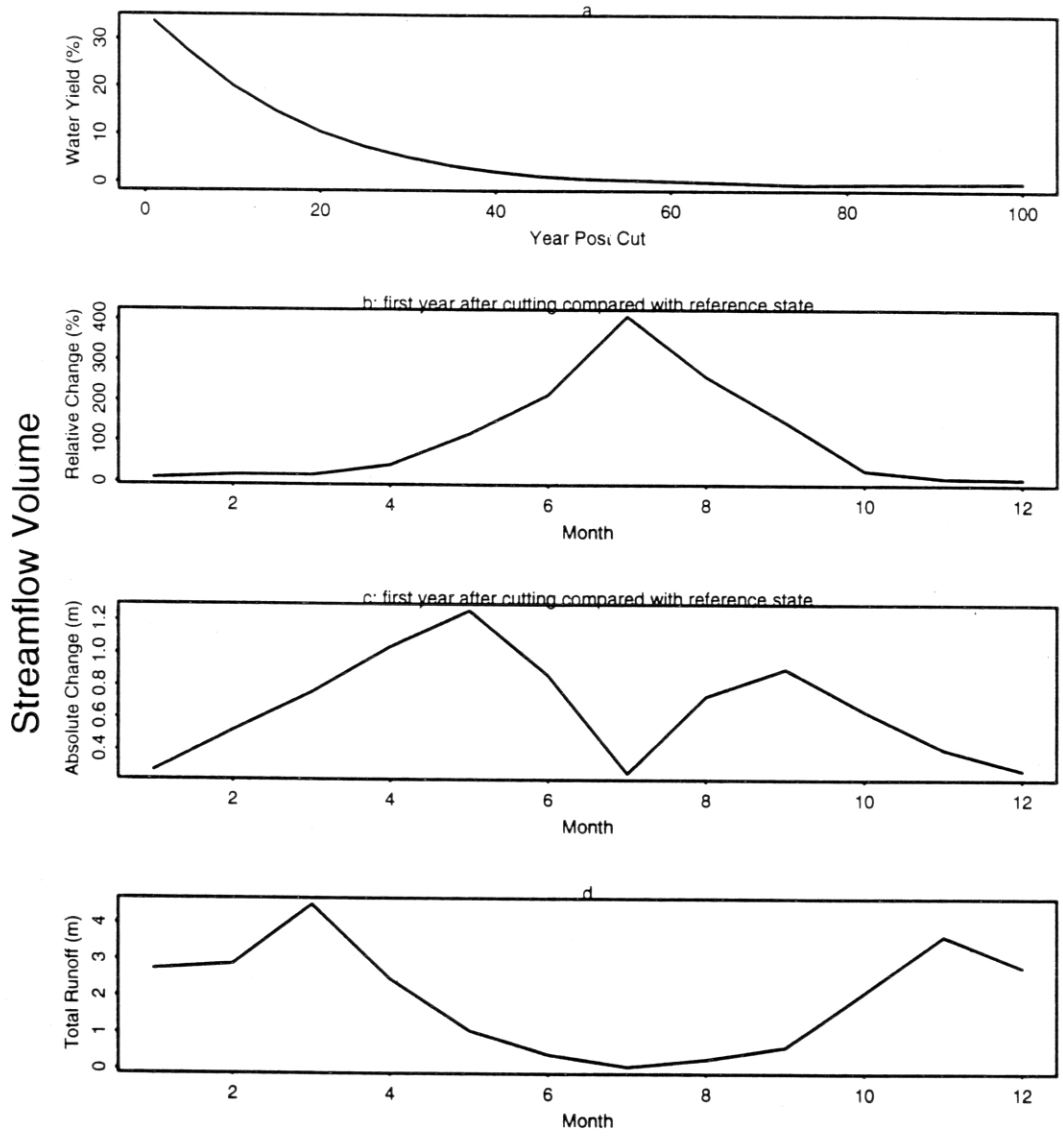


Figure 5.5 Streamflow volume changes post cutting for WS#1. (a). annual pattern of relative increase for water yield; (b) relative increase in first year after cutting; (c) absolute increase in first year after cutting; (d) runoff distribution for different months, in absolute value.

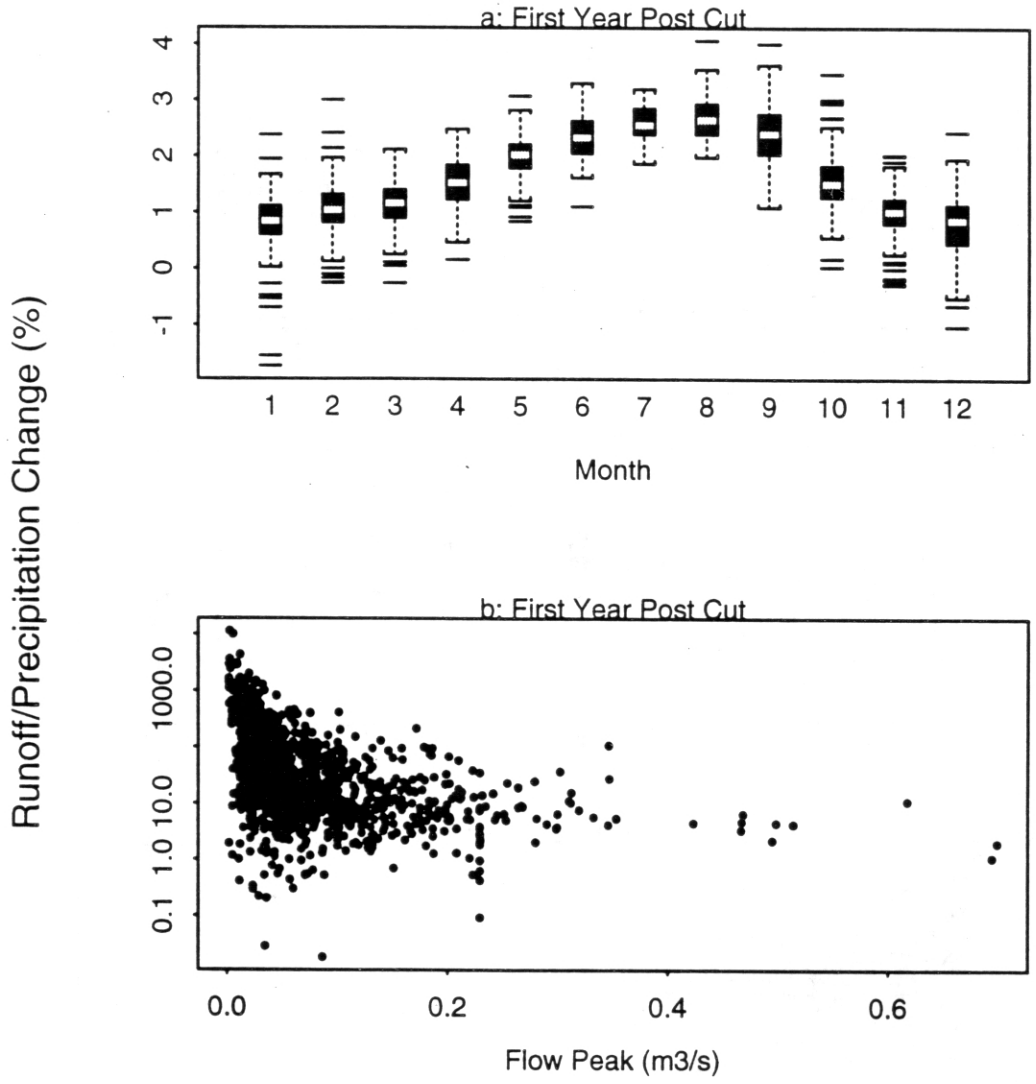


Figure 5.6 Monthly and storm variation of runoff/precipitation ratio after cutting. (a) monthly variations with logarithm transformation on changes in first year after cutting; (b) storm variation in first year after cutting.

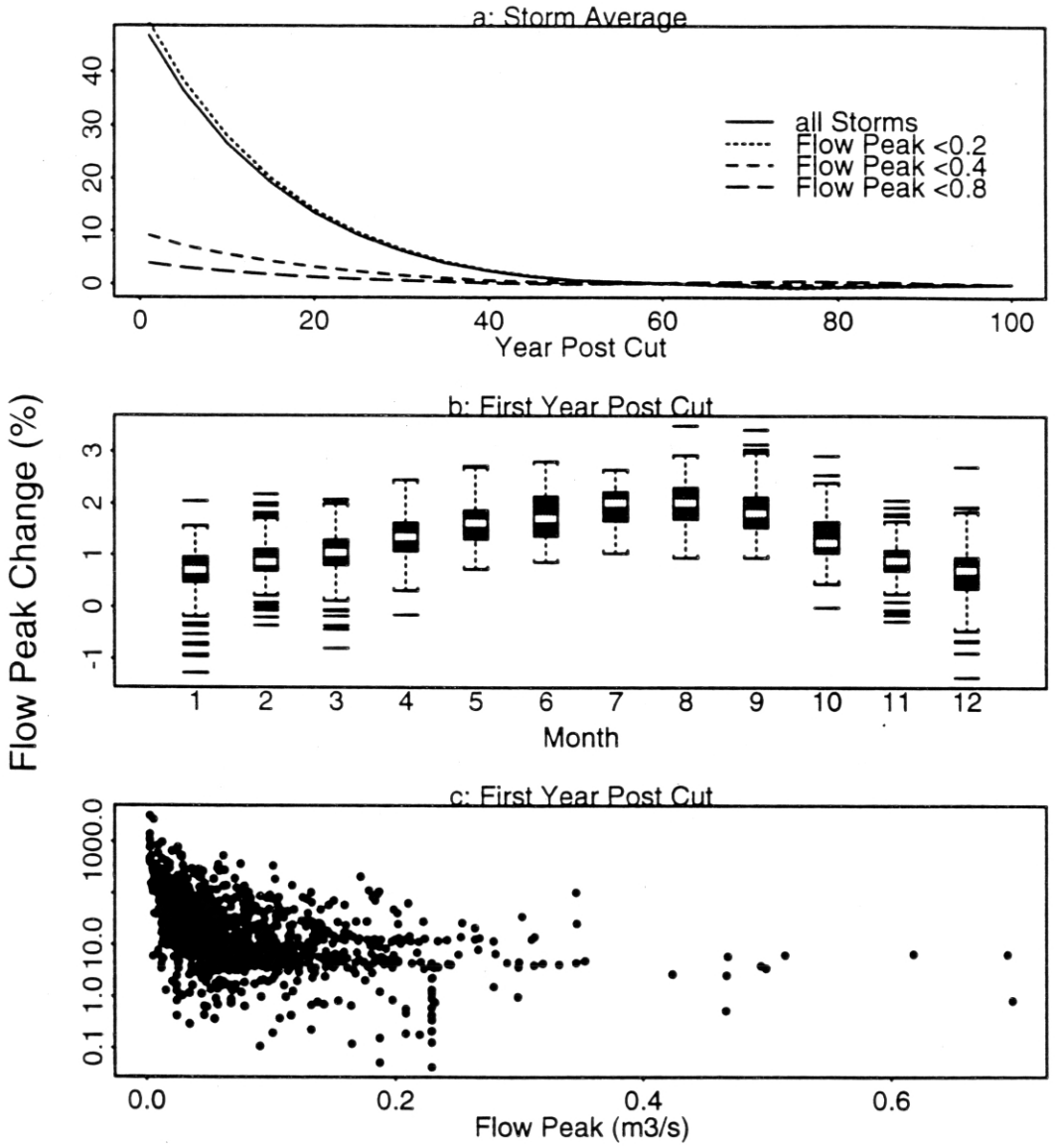
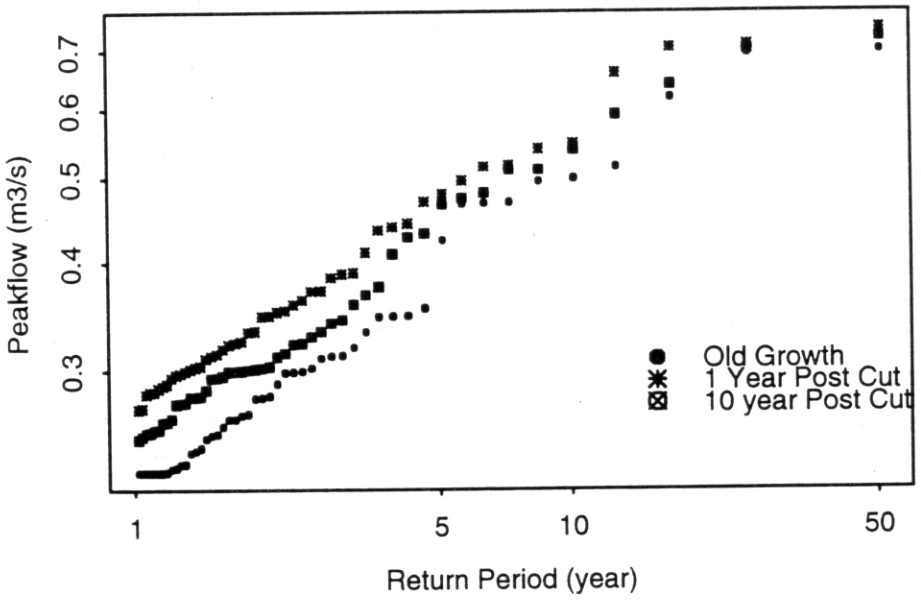


Figure 5.7 Flow peak changes post cutting. (a) storm average using different categories; (b) monthly variation in first year after cutting with logarithm transformation on changes; (c) storm variations.

Figure 5.8 Peakflows postcutting. Peaks are generated using the 50 largest events under the old growth vegetation condition in the simulation and plotted based on Weibull plotting position.



5.4.3 Soil moisture

In the simulation we only recorded the maximum basin average soil moisture during each Monte Carlo simulation. The end soil moisture is not recorded but we think that the large difference between old growth and forest cutting may be more pronounced than what we show here.

Soil moisture is highest in the first year after cutting, although this increase is not very significant and only about 2% (Figure 5.9a). Monthly variation shows that spring and fall have the greatest change and summer events are more stable (Figure 5.9b). Small storms will produce larger variations, but the changes during large storms are relatively small and insignificant (Figure 5.9c).

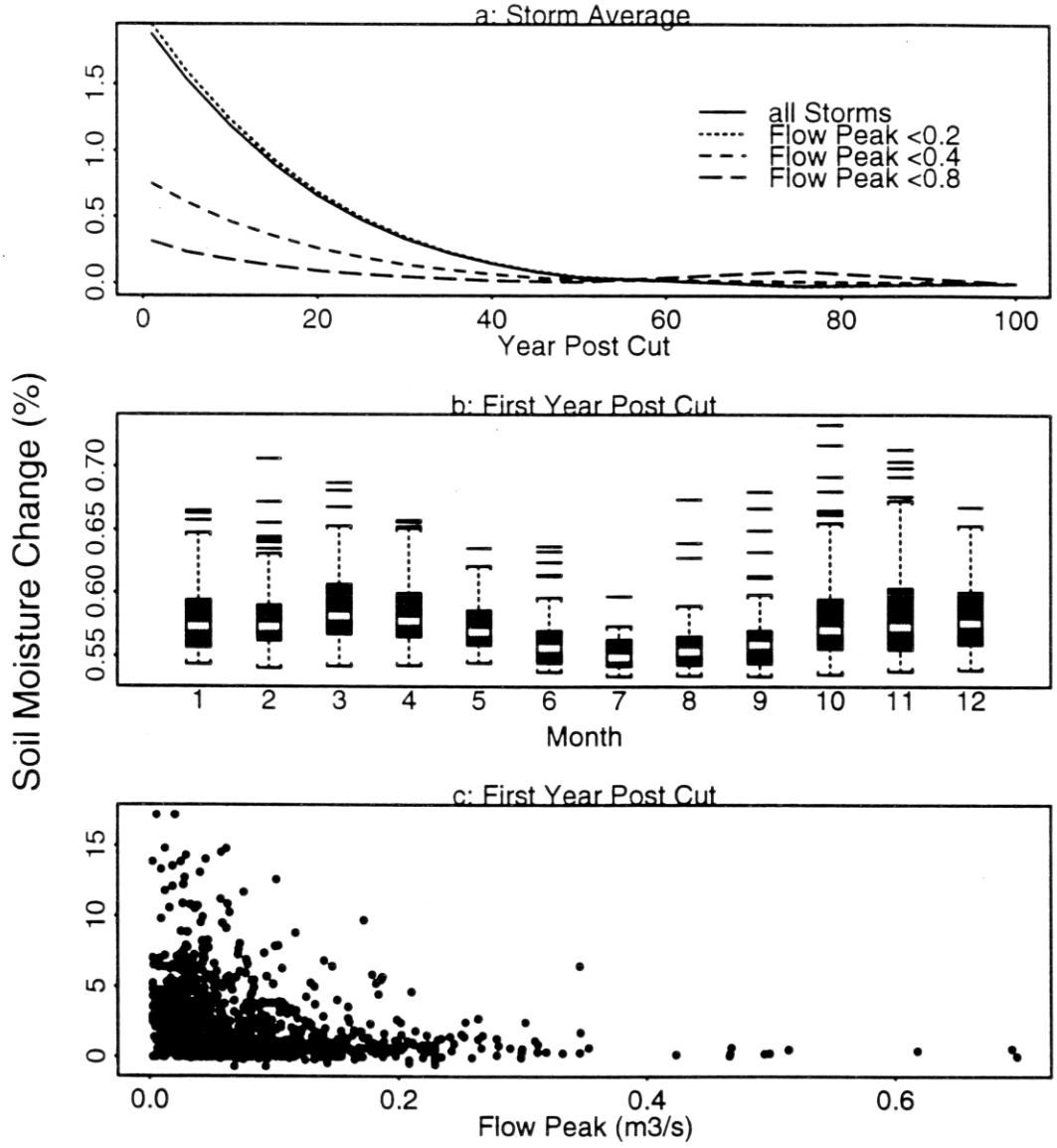


Figure 5.9 Soil moisture changes after cutting. (a) storm average using different categories; (b) monthly variation in first year after cutting with logarithm transformation on changes; (c) storm variations.

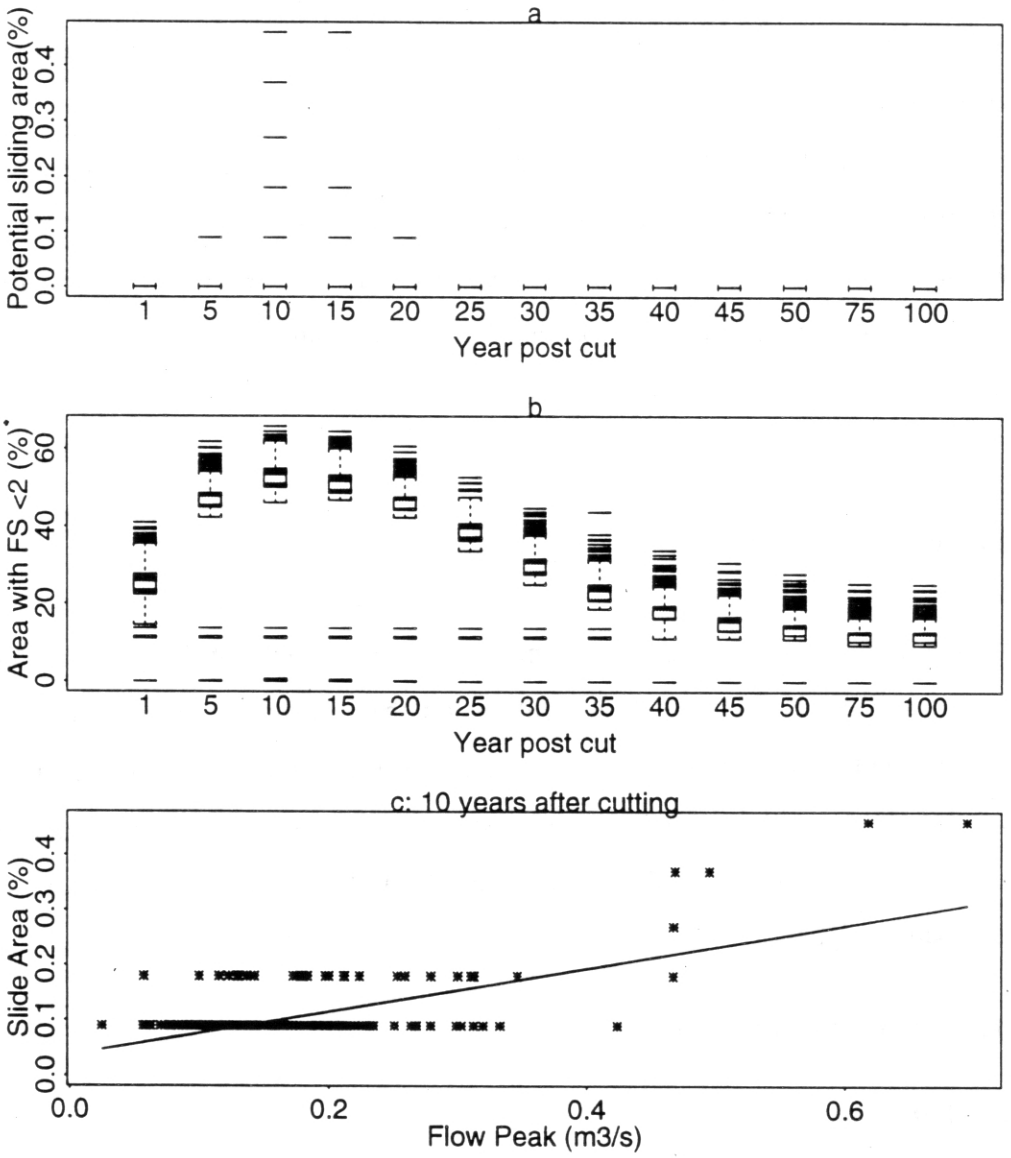


Figure 5.10 Changes in the factor of safety (FS) after cutting. (a) potential slide areas and year post cutting; (b) areas with FS less than 2 and year post cutting; (c) potential slide areas and peakflows.

5.4.4 Landslide potential

Landslide potential after cutting is closely connected with vegetation dynamics, especially the decay and regrowth of root strength. In the simulations of about 50 years of precipitation events, only the several largest storms trigger landslides (Figure 5.10a). Landslides occur 5 to 20 years after cutting with 10 to 15 years post cutting having the highest slide potential.

The legacies of cutting on stability last far longer than 20 years as shown in Figure 5.10b. Examination of the percentage of areas where factors of safety are less than two show that about 40 years are needed for the whole cutting area to recover. The stability analyses also show storm variation. As expected, large storms are more dangerous than small storms (Figure 5.10c).

5.5 Discussion

Physically-based, spatially-distributed models, such as CLAWS, give us an opportunity to examine the effects of forest cutting on the hydrologic and geomorphic response of watersheds simultaneously over a wider range of climatic conditions. Most of the findings are consistent with long-term observations, and give more detailed insight into watershed responses which are difficult to discriminate from field observations due to the variability in observed signals.

5.5.1 Comparison with observation

5.5.1.1 Runoff amounts

Water yield increases after cutting because of reduced interception and evapotranspiration (Hewlett, 1967; Bosch and Hewlett, 1982; Stednick, 1996). The amount of increase depends on factors such as watershed area cut, percent area of soil disturbed, annual precipitation and time after cutting (Harr, 1983). As Hibbert (1967) reported, the increase in stream flow is proportional to the amount of cover removed. Partial cutting is less effective than clearcutting at augmenting streamflow. This was clear

from observations in the WS#1 and WS#2 studies (Rothacher, 1970, 1971). WS#1, the clearcut watershed increased 38 cm (34%) in annual average after logging, compared to an 18 cm increase at WS#3, a 25% patchcut watershed with 6% roads. Watershed studies in this region show that the increase is about 36-54 cm after 100-percent clearcut and 10-30 cm after partial cut (Harr, 1983).

Local site conditions influence streamflow responses to the removal of vegetation. Streamflow increases in watersheds with soil and topographic conditions favorable for tree growth are smaller and diminish faster than those in other watersheds. Water yields in the Pacific Northwest are typically short-lived because of conditions that support rapid regrowth of forest and other vegetation. In general, there is a decrease in annual water yield after an initial increase, since vegetation growth gradually offsets logging effects (Hicks et al., 1991).

An important exception to the pattern of increased flows after logging was observed in the Fox Creek watershed study within Portland's Bull Run municipal watershed (Harr, 1980), where a small decrease in annual water yield was noted. Harr (1980) pointed out that the fog drip decreased and caused a decrease in precipitation.

For WS#1, the logging activities spanned five years from 1962 to 1966 because of operational problems. Initial water yield in 1965, when 90% of the area had been clearcut, increased about 60% (Harr, 1983). This observation is larger than the simulation result of only 33% increase. This is because we use 1500 storms which account for about 50 years of events, so the larger sample size of simulation can be viewed more as an average rather than a specific yearly increase. Large sample sizes reduced the variation and should be closer to the population statistics. A linear model using actual observations showed that about 27 years are required for yield increases to disappear (Harr, 1983), which differs from the simulation projection of about 40 years. This may also be resulted from the variations caused by sample size as well.

Seasonality is one of the factors influencing water yield. Monte Carlo simulations clearly agreed with observations. The greatest portion of observed yield increases occurred during the wet October-March season for WS#1 (Rothacher, 1971; Harr et al.,

1979). Although relative increases during low flow summer periods were substantial initially, absolute summer increases were small (Harr, 1983).

5.5.1.2 Peakflows

There has been continuing speculation about the influence of timber harvesting activities on peakflows Difficulties in data analyses based on paired-watershed studies have made such studies inconclusive. The change in size of peak flows after logging can be explained in terms of what portion and to what degree the forest hydrologic system was altered by logging activities. The most common cause of increased size of peak flows has been wetter, hydrologically more responsive soils after timber cutting. Rothacher (1971, 1973) reported fall increases of peakflows up to 200% at WS#1 in first year after cutting but no significant increase in the large winter peaks, and suggested that normal logging activity may not sufficiently compact the soil to reduce the infiltration capacity below the rate of precipitation. Because of high infiltration rates and relatively low precipitation intensities in the Pacific Northwest, there may be no large-scale shift from subsurface to surface flow. Harr et al. (1976) reported that no consistent change in time to peak was found in three partially clearcut watersheds in the Alsea Study. The Alsea Study also showed that large winter peaks after logging are related to soil compaction, with the more area compacted the greater magnitude of peak flows.

The Caspar Creek Study (Wright et al., 1990) reported that storm hydrographs were shifted forward in time by logging, but their shapes were unchanged. Another important aspect revealed by this study is the influence of larger events. They concluded that logging or forest road construction that causes <16% are of ground disturbances is unlikely to change a watershed's streamflow regime adversely in a rain-dominated hydrologic environment. As pointed out by Wright et al. (1990), other studies in this region (Harr et al., 1975, 1979) suggested that increases in large winter peakflows were the result of incomplete data for high flows either during the calibration period or after treatment. The lack of data, not the hydrologic changes, were responsible for the "observed" increase in peak flows.

Results from the random simulation show that cutting effects on extreme events are relatively small -- less than 10%. Considering the gage error of about 10% for stream flow measurements, it is difficult to assess the effects of logging on peakflow because of limited data for extreme events needed to confer statistical significance.

5.5.1.3 Soil moisture

Logging temporarily reduces vegetation cover, thus decreasing interception and evapotranspiration and increasing soil moisture levels (Bethlahmy, 1963). Burning further increases moisture retention by suppressing plant survival and regrowth (Gaweda, 1983). Twenty years of observation at WS#3 between 1960 to 1980 of soil moisture in the upper 120 cm of soil in clearcuts were compared with that in the forested control (Adams et al., 1991). The initial year showed that clearcut areas averaged more than 10 cm greater soil moisture than in forested control. But this increase only lasted for three years; thereafter, in 1967, clearcut areas had deficits of 2 cm of moisture over the control area. The deficits, caused by rapid plant regrowth after the light slash burn, persisted in the upper 30 cm of soil through the rest of the study (Adams et al., 1991).

In our model simulation, soil moisture change is storm-based and does not account for cumulative effects in terms of seasonal trends. So the soil moisture change is less dramatic than that observed in field studies. Also the vegetation dynamic modeling is not entirely effective in simulating the potentially rapid growth of vegetation at the early stage.

5.5.1.4 Landslides

Timber harvesting has clearly accelerated the number and frequency of landslides in the Pacific Northwest (e.g., Swanson and Dyrness, 1975; Gresswell et al., 1979). Most mass movements are associated with road construction (Dyrness, 1967; Megahan and Kidd, 1972; Swanson and Dyrness, 1975), which was not modeled. The model suggests that landslide potential is highest in 10-15 years after cutting. This is consistent with the observed summary for the three small watersheds (Grant and Wolff, 1991). Observations also show that most of the landslides in the western Cascade Mountain Ranges occurred in 1964 during a storm of about 50-100 year return interval. Although this random simulation demonstrated a trend of susceptibility, the actual occurrence may be quite

different from this trend because it is also strongly affected by low frequency precipitation events.

It should be noted that the hydrologic changes after cutting do not play an important role in the shallow landsliding, but root strength dynamics are the main control. Large storms are usually more significant geomorphically in shaping the landscape, but they are not significantly influenced by cutting, as previously discussed. Losses from evapotranspiration and interception for large storms are not dramatically changed after cutting. Soil moisture changes for large storms are also less dramatic. Landslide potential is inversely related to the root strength development.

5.5.2 Limitations

This research explored the hydrologic and geomorphic responses of watersheds with computationally intensive simulation of large sets of storm events. Although this work gives interesting perspectives of forest harvesting on watershed responses, there are certain limitations in interpreting the random simulations.

First, this research included only small watersheds of about 100 hectares in size. Because of spatial scale effects and channel routing influences, the streamflow responses of large scale watersheds (e.g., over 100 km^2) can not be generalized from this result.

Second, extreme events at HJA are mostly rain-on-snow related (Harr, 1981). The accumulated snowpack provides an effective additional water source augmenting the incoming warm rainfall. Rain-on-snow events play an important role in shaping the watershed responses at HJA. Because actual data to define the snow depth before an storm events are lacking, we did not simulate the initial snow depth, hence rain-on-snow events were not simulated.

Third, this research examined only the effect of clearcutting the whole watersheds. In most recent cases, the harvesting management regimes use partial cutting although different landscape patterns may be used (e.g., aggregated vs. dispersed, Franklin and Forman, 1987). This work also ignored the influence of roads, although road networks provide additional drainages to stream flow and are often the slide prone areas in steep watersheds (Wemple, 1994).

5.6 Conclusions

Using random simulations of precipitation events and initial conditions, watershed responses after cutting are simulated using CLAWS. Major findings include:

1. The general hydrologic and geomorphic patterns after cutting are controlled by regrowth of vegetation. Streamflow and soil moisture peak in the initial year and then decay in a nonlinear trend. Landslide potentials are controlled by root strength, the maximum susceptibility occurs about 10-15 years after cutting when the root strength is minimal.

2. Monthly variations of hydrologic responses, such as peakflow, soil moisture, and runoff production show that summer has the greatest absolute change, but the specific dry summer conditions of the test site cause the relative change in summer to be insignificant. Spring and fall have the most significant changes in watershed hydrologic responses.

3. Watershed responses are also controlled by storm size and antecedent conditions. Small storms tend to have greater relative changes than large storms. However, most geomorphic work occurs during large peakflow events.

4. Simulation of effects of forest harvesting on streamflows and landslides show reasonable agreement with long-term observations. therrefore it is appropriate touse this type of model to complement and build on traditional experimental studies. Distributed models can be used to check the response of different types of treatment. Large sets of simulations can also provide statistical rigor for analyses of results. They also give us the chance to examine effects of low frequency events that do not occur in actual records. Success of this research shows that distributed modeling provides an alternative to traditional paired watershed studies that may require many years of data collection to produce results.

6. GENERAL SUMMARY

Interest in effects of forest management and other disturbances on watershed processes has prompted the development of models that are sensitive to landuse changes. Models are needed to allow researchers and resource managers to investigate the effects of alternative cutting patterns on stream flows and geomorphic processes in watersheds and thereby provide tools for planning harvest activities across landscapes. This research involves the construction, validation and application of CLAWS (Coupled Landscape and Water System) a physically based, spatially distributed hydrologic-geomorphic model coupled with vegetation-dynamics. Results were compared to long-term observation data from three small watersheds at H. J. Andrews Experimental Forest, western Oregon.

6.1 Key Achievements

The CLAWS model incorporates important hydrologic-geomorphic processes operating at the watershed level. Spatial variability of topography, soil, vegetation, and climate drive a hydrology module that calculates the water budget at given time steps with a user-specified spatial resolution. Hydrologic processes modeled include snow hydrology, interception, evapotranspiration, infiltration, subsurface flow, deep ground water exchange, overland flow and channel flow. Hydrology drives hillslope and channel geomorphic processes including probability of mass movements (landslides, debris flows) and fluvial sediment transport. Both the hydrologic and geomorphic modules are linked to forest growth simulation so that effects of changing forest stand structure in response to clear cutting or other disturbances through time can be examined.

I also present a single layer, energy and mass balance model for snow accumulation and melt. Incoming precipitation is separated into rainfall and snow based on a two point linear scheme. A single layer snowpack is simulated using the energy and mass exchange between atmosphere and subsurface soil using a finite difference numerical

scheme. This energy and mass balance procedure is used for each element or hydrologic response unit in a distributed watershed subdivided into facets. Water is assumed to flow out of the snowpack and into the subsurface soil layer when the maximum liquid water holding capacity of the snowpack is exceeded. This algorithm was tested using temporal observations and then incorporated into CLAWS.

A physically-based, spatially-distributed model, no matter how complex, is associated with uncertainties and errors from many sources. Calibration and testing of physically based models are not straightforward tasks because of the large number of model parameters involved and the computational requirements of making multiple simulations. In this study, the sensitivities and uncertainties of watershed hydrologic and geomorphic responses to selected soil and vegetation parameters were investigated. Simulated hydrographs showed acceptable agreement with recorded observations. Quantitative measures demonstrated that simulation results from CLAWS described the hydrographic characteristics such as peak size, timing, and decay coefficient well, with the overall consistency represented by high correlations and low mean square errors. Sensitivity analyses on eleven soil and vegetation parameters not only identified their significance in the model, but also represented different watershed behavior under different watershed conditions. Simulations using measured and estimated parameter values provide a reasonable representation of basin hydrologic and geomorphic responses.

Because time and expertise required for data preparation and model parameter estimations, and post-run spatial analysis and data visualization can be prohibitive, a Geographic Information System has been dynamically linked with CLAWS. This expedites both the pre-run terrain analysis based on Digital Elevation Model data and other spatial layers of soil and vegetation characteristics, and the post-run spatial data visualization, which includes elemental flow, soil moisture distribution, factor of safety, debris flow path and snow distribution output at any point during the simulation. The input and output are based on GIS readable files and accompanying ARC Macro Language (AMLs).

CLAWS was further extended by Monte Carlo simulations of storm events and antecedent conditions to investigate the effects of forest cutting on watershed hydrologic and geomorphic responses. Hydrologic responses such as annual water yield, soil

moisture, and flow peaks exhibit the greatest change in the first year after cutting. Landslide potential, controlled by changes in root strength, peaks about 10-15 years after cutting. About forty years are needed for watersheds to recover to their pre-cutting status in terms of streamflow, soil moisture and landslide susceptibility. Changes in hydrologic response also vary with season and storm intensity. Summer has the highest relative changes and lowest absolute changes because it is the dry season. Small storms are more sensitive than large storms in terms of relative changes. Success of this research also shows that distributed modeling can complement traditional paired-watershed studies

6.2 Lessons

CLAWS provides not only the advantages and disadvantages possessed by other physically-based, spatially-distributed hydrologic models, but also a unique opportunity to examine hydrologic and geomorphic responses of watersheds with forest dynamics.

The coupling between forest dynamics, hydrologic and geomorphic processes provide us with a tool to investigate watershed responses over a range of climatic conditions in a cost-effective way. It also lets us check storm events of a variety of antecedent conditions with different forest management options. These give us clear and detailed quantatitive information about the effects of forest management on watershed response, while signals from observed paired-watershed studies are often hard to determine because of variation and noise from various aspects, such as climate. The uniqueness of this coupling also lets us discriminate the importance of different processes in triggering shallow landslides, such as those associated with changes in root strength as the main control rather than hydrologic factors. This cannot be achieved through non-coupled setups.

Any model is only a simplification of a complex natural system. Uncertainties and predictabilities can be influenced by many factors including input data quality, poorly known boundary conditions and unknown spatial heterogeneity effects, and imperfect

process approximation by the model equations (Stephenson and Freeze, 1974, Binley et al., 1991). There is also the problem of over parameterization. As stated by Beven (1993):

> "These arguments for the invalidation of current physically-based distributed models suggests that belief in the predictions of such models is an act of faith, resting insecurely on scientific principles. Because of differences in measurement and element scales of parameter values and variables, it is unlikely that the modelling process can be redeemed satisfactorily by calibration. Thus such predictions should be treated as prophecy."

The sparseness of observation networks in mountainous regions necessitates interpolation or extrapolation of driving input variables. These estimates may limit to model simulation accuracy. Also there is the inherent problem of quality of input data, as with other distributed models. Improving input data quality and developing sound algorithms to interpolate point data over larger regions are major areas in which research should be focused. This has been demonstrated in the precipitation and temperature-related calculations.

Computational efficiency is another issue that should be considered in a spatially-distributed, physically-based modeling approach. Smaller pixel size and more accurate numerical solutions of non-linear differential equations increase computation. Computer resources currently constrain spatial resolution, but this limitation will undoubtedly diminish in the future.

6.3 Future Research

Continued research will focus on improving the model and expanding its application to some fundamental landuse questions. Application of the present model or any later enhanced version to different geographic regions also needs to be examined.

6.3.1 Model improvements

These improvements to CLAWS are either more realistic approximations of process or implementations of the new processes. Of course, comparisons of performances are needed to evaluate model prediction.

Erosion and sedimentation: There is no sheet erosion and sediment modules except the shallow landslide and debris flow simulations. Physically based erosion mechanisms will be implemented later.

Road effects: Road effects to watershed responses have been the important aspects in forest land use. This might be improved in the near future.

6.3.2 Application to landuse and climate change

This model will also be used in management simulation to find the critical cut area of watersheds. When cutting area exceeds this percentage, it produces significant changes in hydrologic and geomorphic responses. When cutting area is below this critical value, changes in watershed responses may be negligible.

Watershed responses from different vegetation patterns such as riparian buffers, cut options (partial vs. clearcut) and rotations can also be examined with this model. Global change effects, examined in connection with General Circulation Models (GCMs), will also be an important direction.

BIBLIOGRAPHY

Abbott, M. B., J. C.Bathurst, J. A.Cunge, and others. 1986. An introduction to the European Hydrological System - SYSTEM HYDROLOGIQUE EUROPEAN, "SHE", 1: history and philosophy of a physically-based, distributed modeling system. *Journal of Hydrology* 87:45-59.

Adams, P. W., A. L.Flint, and R. L.Fredriksen. 1991. Long-term patterns in soil moisture and revegetation after a clearcut of a Douglas-fir forest in Oregon. *Forest Ecology and Management* 41:249-263.

Anderson, E. A. 1968. Development and testing of snow pack energy. *Water Resources Research* 4(1):19-37.

Anderson, E. A. 1976. A point energy and mass balance model of a snow cover. *NOAA Tech. Rep.* NWS 19. Silver Spring. MD.

Aston, A. R. 1979. Rainfall interception by eight small trees. *Journal of Hydrology* 42:383-396.

Band, L. E., and E. F. Wood. 1988. Distributed Hydrologic Simulation. *Applied Mathematics and Computation* 27:23-37.

Bathurst, J. C. 1986 Physically-based distributed modelling of an upland catchment using the System Hydrologique Europeen. *Journal of Hydrology* 87:79-102.

Beasley, D. B., L. F. Huggins, and E. J. Monke. 1980. ANSWERS: a model for watershed planning. *Transaction of the ASAE.*

Benda, L. 1985 Delineation of channels susceptible to debris flows and debris floods. In *International Symposium on Erosion, Debris Flow and Disaster Prevention.*

Benda, L. 1990. The influence of debris flows on channels and valley floors in the Oregon Coast range, USA. *Earth Surface Processes and Landform* 15:457-466.

Berris, S. N., and R. D. Harr. 1987. Comparative snow accumulation and melt during rainfall in forested and clear-cut plots in the western Cascades of Oregon. *Water Resources Research* 23(1):135-142.

Bethlahmy, N. 1963. Soil moisture variation as affected by vegetation and depth of sampling. Soil Sci. 95:211-213.

Beven, K. 1981. Kinematic subsurface stormflow. *Water Resources Research* 17(5):1419-1424.

Beven, K. 1982. On subsurface stormflow: predictions with simple kinematic theory for saturate and unsaturated flows. *Water Resources Research* 18(6):1627-1633.

Beven, K. 1987. Towards the use of cathcment geomorphology in flood frequency predictions. *Earth Surface Processes and Landforms* 12:69-82.

Beven, K. 1989. Changing ideas in hydrology - the case of physically-based models. *Journal of Hydrolgy* 105:157-172.

Beven, K. 1993. Prophecy, reality and uncertainty in distributed hydrological modelling. *Advance in Water Resource* 16:41-51.

Beven, K. and A. Binley. 1992. the future of distributed models: model calibration and uncertainty prediction. *Hydro. Proc.* 6:279-298.

Beven, K. and P. Germann. 1982. Macropores and water flow in soils. *Water Resources Research* 18(5):1311-1325.

Beven, K. J., and M. J. Kirkby. 1979 A physically base, variable contributing area model of basin hydrology. *Hydrological Sciences* 24:43-69.

Binley, A. M., K. J. Beven, A. Calver, and others. 1991. Changing Responses in Hydrology: Assessing the uncertainty in Physically Based Model Prediction. *Water Resource Research* 27(6):1253-1261.

Bosch, J. M. and J. D. Hewlett. 1982. A review of catchment experiments to determine the effects of vegetation changes on water yield and evapotranspiration. *Journal of Hydrology* 55:3-23.

Box, G. E. P., and G. M. Jenkins. 1970. *Time Series Analysis Forecasting and Control.* San Francisco: Holden Day.

Brakensiek, D. L. 1967. Kinematic flood routing. *Trans. ASAE* 10:340-343.

Bras, R. L. 1990. *Hydrology: an introduction to hydrologic sciences.* Addison-Wesley Publishing Company, Inc.

Brooks, K. N., P. F. Ffolliott, H. M. Gregersen, and J. L. Thames. 1991. *Hydrology and the management of watersheds.* Iowa State University Press.

Brooks, R. H., and A. T. Corey. 1964. *Hydraulic properties of porous media.* Colorado State University Hydrol. Paper 3:27.

Brown, G. W., and R. L. Beschta. 1985. The art of managing water. *Forestry* 83(10):604-615

Burrough, E. R., Jr. 1984. A landslide hazard rating for portions of the Oregon Coast Range. In *Symposium on effects of Forest Land Use on Erosion and Slope Stability*, May 7-11, 1984, Honolulu. ed. O'Loughlin, C.L., and A. J. Pearce.

Cannon, S. H., and W. Z. Savage. 1988. A mass-change model for the estimation of debris-flow runout. *Journal of Geology* 96:221-227.

Chow, V. T. 1959. *Open channel hydraulics*. New York: McGraw-Hill, Inc.

Chow, V. T., D. R. Maidment, and L. W. Mays. 1988. *Applied hydrology*. New York: McGraw-Hill, Inc.

Clarke, R. T. 1973 A review of some mathematical models used in hydrology, with observations on their calibration and use. *Journal of Hydrology* 19:1-20.

Collins, E. H. 1934. Relationship of degree-days above freezing to runoff, Eos *Trans. AGU* 15:624-629.

Dickinson, R. E. 1984. Modelling evapotranspiration for three-dimensional global climate models. *In Climate Processes and Climate Sensitivity, Geophys. Monogr. Ser., AGU, v. 29*, ed. Hansen, J. E., and T. Takahashi, 58-72.

Dickinson, R. E., A. Henderson-Sellers, C. Rosenzweig, and others. 1991. Evapotranspiration models with canopy resistance for use in climate models, a review. *Agricultural and Forest Meteorology* 54:373-388.

Dietrich, W.E., R. Reiss, M. Hsu, and D. Montgomery. 1995. A process-based model for colluvial soil depth and shallow lansliding using digital elevation data. *Hydrological Processes* 9:383-400.

Donald, J. R., E. D. Soulis, N. Kouwen, and others. 1995. A land cover-based snow cover representation for distributed hydrologic models. *Water Resource Research* 31(9):995-1009.

Dooge, J. C. I. 1965. Analysis of linear system by means of laguerre functions. *J. SIAM Control*, Ser A 2(3).

Duan, J., and G. E. Grant. 1996a. Comment on "A distributed hydrology-vegetation model for complex terrain" by Mark S. Wigmosta, Lance W. Vail, and Dennis P. Lettenmaier. *Water Resource Research* 32(1):211-212.

Duan, J., and G. E. Grant. 1996b. Integrated GIS and hydrologic-geomorphic modeling for watershed study. *Transaction of GIS* (submitted).

Dupuit, J. 1863. *Etudes theoriques et practiques sur le mouvement des eaux dans les canaux d'ecouverts et a travers les terrains permeables*. 2nd ed. Paris: Dunod.

Dyrness, C. T. 1967. Mass soil movements in the HJ Andrews Experimental Forest. *USDA For. Serv. Res. Pap.* PNW-42. Portland, OR: Pac. Northwest For. and Range Exp. Stn.. p.12

Dyrness, C. T. 1967b. Surface soil conditions following skyline logging. *USDA For. Serv. Res. Pap.* PNW-55. Portland, OR: Pac. Northwest For. and Range Exp. Stn.

Eagleson, P. S. 1970. *Dynamic hydrology*. New York: McGraw-Hill.

Frank, E. C., and R. Lee. 1966. Potential solar beam irradiation on slopes: tables for 30° to 50° latitude. *USDA Forest Service, Rocky Mt. Forest Range Exp. Stn. Rep.* RM-18:116.

Franklin, J. F . and R. T. T. Forman. 1987. Creating landscape patterns by forest cutting: ecological consequences and principles. *Landscape Ecology* 1:5-18

Gaweda, F. M. 1983. *First-year effects of broadcast burning on soil infiltration and wettability in southwest Oregon*. M.S. thesis. Oregon State University, Corvallis, OR.

Gorgens, A. H. M. 1983 *Conceptual modeling of the rainfall-runoff process in semi-arid catchments. Report 1/83.* South Africa: Hydro. Res. Unit, Dept. of Geography, Rhodes University.

Grant, G. E., and A. L. Wolff. 1991. Lont-term patterns of sediment transport after timber harvest, western Cascade Mountains, Oregon, USA. *Proceedings of the Vienna Symposium* 203:31-40.

Gray, D. H., and W. F. Megahan. 1981. Forest vegetation removal and slope stability in the Idaho Batholith. *Intermountain Forest and Range Experiment Station Res. Pap*. INT-271:23. Ogden, UT: USDA Forest Service.

Grayson, R. B., I. D. Moore, and T. A. Mcmahon. 1992a. Physically based hydrological modeling 1. A terrain-based model for investigative purposes. *Water Resource Research* 28(10):2639-2658.

Grayson, R. B., I. D. Moore, and T. A. Mcmahon. 1992b. Physically based hydrologica modeling 2. is the concept realistic? *Water Resource Research* 28(10):2659-2666.

Green, I. R. A., and D. Stephenson. 1986. Criteria for comparison of single event models. *Hydrological Science* 31(1)

Green, W. H., and G. A. Ampt. 1911. Studies on soil physics: 1. flow of air and water through soils. J. Agric. Sci 4:1-24.

Gresswell, S., D. Heller, and D. N. Swanston. 1979. Mass movement response to forest management in the central Oregon Coast Ranges. *Resource Bulletin* PNW-84.

Hammond, C. D., D. Hall, S. Miller, and P. Swetik. 1992. Level I stability analysis (LISA) documentation for version 2.0. *General Tech. Rep.* INT-285:190. Ogden, UT: USDA Forest Service, Intermountain Research Station.

Hancock, N. H., P. J. Sellers, and J. M. Crowther. 1983. Evaporation from a partial wet canopy. *Geophysicae* 1:139-146.

Harr, R. D. 1976. Forest practices and streamflow in western oregon. *USDA Forest Service Gen. Tech. Report* PNW-49:17. Portland, OR: Pacific Northwest Forest and Range Experiment Station, USDA Forest Service.

Harr, R. D. 1979. Effects of timber harvest on streamflow in the rain-dominated portion of the Pacific Northwest. *USDA, FSL report.*

Harr, R. D. 1980. Streamflow After Patch Logging in Small Drainage Within the Bull Run Municipal Watershed. Oregon. *USDA Forest Service Gen. Tech. Report* PNW-268:16. Portland OR: Pacific Northwest Forest and Range Experiment Station, USDA Forest Service.

Harr, R. D. 1981 Some characteristics and consequences of snowmelt during rainfall in western Oregon. *Journal of Hydrology* 53:277-304.

Harr, R. D. 1982. Fog drip in the Bull Run Municipal watershed, Oregon. *Water Resources Bulletin* 18(5):785-789.

Harr, R. D. 1983. Potential for augmenting water yield through forest practices in western washington and western Oregon. *Water Resources Bulletin* 19(3):383-393.

Harr, R. D., W. C. Harperm, J. T. Krygier, and R. S. Hsieh. 1975. Changes in Storm Hydrographs After Road Building and Clearcutting in the Oregon Coast Range. *Water Resources Research* 11(3):436-444.

Harr, R. D., R. L. Fredricksen, and J. Rothacher. 1979. Changes in Streamflow Following Timber Harvest in Southwestern Oregon. *USDA Forest Service Gen. Tech. Report* PNW-249:22. Portland OR: Pacific Northwest Forest and Range Experiment Station, USDA Forest Service.

Herwitz, S. R. 1985. Interception storage capacities of tropical rainforest canopy trees. *Journal of Hydrology* 77:237-252.

Hewlett, A. B. 1967. Forest treatment effects on water yield. In *Forest Hydrology*, ed. Sopper, W. E., and H. W. Lull,527-43. Oxford:Pergamon Press.

Hewlett, J. D., and R. Doss. 1984. Forest, floods, and erosion. a watershed experiment in the Southeastern Piedmont . 30(2): 424-434

Hibbert, A. R. 1967. Forest treatment effects on water yield. *In International symposium on Forest Hydrology*, ed. Sopper, W. E., and H.W. Lull, 526-43. New York: Pergamon.

Hicks, B. J., R. L. Beschta, and R. D. Harr. 1991. Long-term changes in streamflow following logging in western Oregon and associated fisheries implications. *Water Resource Bulletin* 27:217-226.

Hungr, O., G. C. Morgan, and R. Kellerhals. 1984. Quantitative of debris torrent hazard for design of remedial measures. *Can. Geotech. J.* 21:663-677.

Iverson, R. M., and J. J. Major. 1986. Groundwater seepage vectors and the potential for hillslope failure and debris flow mobilization. *Water Resources Research* 22(11):1543-1548.

Iverson, R. M., and J. J. Major. 1987. Rainfall, ground-water flow, and seasonal movement at Minor Creek landslide, northwestern Califoria: Physical interpretation of empirical relations. *Geotechnological Society of America Bulletin* 99:579-594.

Jarvis, P. G. 1976 The interpretation of the variations in leaf water potential and stomatal conductance found in canopies in the field. *Philosophical transactions of the Royal Society, London B.* 273:593-610.

Johnson, A. M. 1970. *Physical processes in geology.* San Francisco: Freeman, Cooper & Company.

Jones, J. A. and G. E. Grant. 1996. Long-term stormflow responses to clearcutting and roads in small and large basins, western Cascades, Oregon. *Water Resources Research.* 32(4):959-974.

Jones, N. L., S. G. Wright, and D. R. Maidment. 1990. Watershed Delineation with Triangle-based Terrain Models. *Journal of Hydraulic Engineering* 116(10):1232-1251.

Jury, W. A., W. R. Gardner, and W. H. Gardner. 1991. *Soil Physics.* New York: John Wiley & Sons, Inc.

Kelly, R. J. 1987. *Mathematical models of mutil-phase snowmelt.* Ph.D thesis. University of East Anglia.

Kibler, D. F., and D. A. Woolhiser. 1970. The kinematic cascade as a hydrologic model. *Hydro. Pap.* 39:27. Fort Collins: Colorado State University.

Klemes, V. 1986. Operational testing of hydrological simulation models. *Hydrological Science.* 31:13-24.

Kustas, W. P., and A. Rango. 1994 A simple energy budget algorithm for the snowmelt runoff model. *Water Resources Research* 30(5):1515-1527.

Laramie R. L., and J. C. Schaake, Jr. 1972. Simulation of the continuous snowmelt process. *Ralph M. Parsons Laboratory Tech. Report* No. 143. Cambridge, Mass.: MIT Department of Civil Engineering.

Leavesley, G. H. 1989. Problems of snowmelt runoff modelling for a variety of physiographic and climatic conditions. *Hydrological Sciences* 34(6):617-634.

Leavesley, G. H. 1994. Modeling the effects of climate change on water resources - a review. *Climatic Change* 28:159-177

Leavesley, G. H., R. W. Lichty, B. M. Troutman, and L. G. Saindon. 1983. Precipitation-runoff modeling system: user's manual. *USGS Water Resources Investigation* 83-4238:207.

Liang, X., D. P. Lettenmaier, E. F. Wood, and others. 1994. A simple hydrologically based model of land surface water and energy fluxes for general circulation models. *Journal of Geophysical Research* 99(D7):14,415-14,428.

Linsley, R. K. 1982. Rainfall-runoff models: an overview. In *Rainfall-runoff relationship*, ed. V. P. Singh, 582. Littleton, Colorado: Water Resource Publications.

Louis, J. 1979. A parametric model of vetical eddy fluxes in the atmosphere. *Boundary Layer Meteorol.* 17:187-202.

Maidment, D. R. (ed) 1992. *Handbook of Hydrology.* New York: McGraw-Hill, Inc.

Means, J. E., and T. E. Sabin. 1989. Height growth and site index curves for Douglas-fir in the Siuslaw National Forest, Oregon. *WLAF* 4(4):136-142.

Megahan, W.F., and W. J. Kidd. 1972. Effects of logging and logging roads on erosion and sediment deposition from steep terrain. *Journal of Forestry* 70:136-141.

Monteith, J. L. 1965. Evaporation and environment. *Symp. Soc. Expl. Biol.* 19:205-234.

Monteith, J. L., and M. H. Unsworth. 1990. *Priciples of environmental physics.* 2nd ed. New York: Routledge, Chapman and Hall, New York.

Montgomery, D.R., G. E. Grant, and K. Sullivan. 1995. Watershed analysis as a framework for implementing ecosystem management. *Water Resources Bulletin* 31(3):369-386.

Moore, I. D., G. J. Burch, and D. H. Mackenzie. 1988. Topographic effects on the distribution of surface soil water and the location of ephereral gullies. *Transaction of ASAE* 31(4):1098-1107.

Moore, I. D., and R. B. Grayson. 1991. Terrain Based Catchment partitioning and runoff prediction using vector elevation data. *Water Resource Research* 27(6):1177-1191.

Moore, I. D., R. B. Grayson, and A. R. Ladson. 1991. Digital terrain modeling: A review of hydrological, geomorphological and biological applications. *Hydrological Processes* 5(1):3-30 .

Morris, E. M. 1991. Physics-based models of snow. *In Recent Advances in the Modeling of Hydrologic Systems*, ed. Bowles, D. S., and P. E. O'Connell, 85-112. Netherlands: Kluwer Academic Publisher.

Mulvaney, T. J. 1851. On the use of self-registering rain and flood gages in making observations of the relations of rainfall and flood discharges in a given catchement. *Proceedings of the institution of Civil Engineers of Ireland* 4:18-31.

Nash, J.E. 1958. The form of the instantaneous Unit Hydrograph. *Intl. Assoc. Sci. Hydrol.* 45:114-121.

O'Connell, P. E. 1991. A historical perspective. In *Recent Advances in the Modeling of Hydrologic Systems*, ed. Bowles, D. S., and P. E. O'Connell, 667. Netherlands: Kluwer Academic Publisher.

O'Donnell, T. 1960. Instantaneous Unit Hydrograph. *Intl. Assoc. Sci. Hydrol.* 151:546-557.

O'Loughlin, C. L., and R. R. Ziemer. 1982, The importantce of root strength and deterioration rates upon edaphic stability in steepland forests. In *Carbon uptake and allocation in subalpine ecosystems as a key to management: Proceedings of an IUFRO workshop,70-80. Augest, 1982*. Corvallis, OR: Forest Research Laboratory, Oregon State University.

O'Loughlin, E. M. 1986. Prediction of surface saturation zones in natural catchments by topographic analysis. *Water Resource Research* 22(5):794-804.

Osborn, H. B., L. J. Lane, C. W. Richardson, and M. P. Molnau. 1982. Precipitation. In *Hydrologic modeling os small watersheds*, ed. Hann, C. T., H. P. Johnson, and D. L. Brakensiek,81-120.

Perreault, P. 1674. *De l'Origine des Fontaines, Paris.*

Rawls, W. J., and D. L. Brakensiek. 1989. Estimation of soil water retention and hydraulic properties. In *Unsaturated Flow in Hydrologic Modeling: Theory and Practice*, ed. H.J. Morel-seytoux, 275-300. Kluwer Academic Publishers.

Regional Interagency Executive Committee (RIEC). 1995. *Ecosystem analysis at the watershed scale: Federal guid for watershed analysis (Version 2.2).* Portland, Oregon.

Richards, F. J. 1959. A flexible growth function for empirical use. *Journal of Experimental Biology* 10:290-300.

Rodriguez-Iturbe, I., and J. B. Valdes. 1979. The geomorphologic structure of Hydrologic Response. *Water Resource Research* 15(6):1409-1420.

Rothacher, J. 1964. Streamflow from small watersheds on the western slope of the Cascade Range of Oregon. *Water Resources Bulletin* 1(1):125-134.

Rothacher, J. 1970. Increase in water yield following clear-cut logging in the Pacific Northwest. *Water Resources Research* 6(2):653-658.

Rothacher, J. 1971. Regimes of streamflow and their modification by logging. In *Forest Land Uses and Stream Environment*, ed. Krygier, J.T., and J.D. Hall, 40-45. Corvallis, OR: Continuing Education Publication.

Rothacher, J. 1973. Does harvest in west slope Douglas-fir increase peak flow in small forest Streams? *USDA Forest Service Gen. Tech. Report* PNW-163:13.Portland OR: Pacific Northwest Forest and Range Experiment Station, USDA Forest Service.

Rothacher, J., C. T. Dyrness., and R. L. Fredriksen. 1967. Hydrologic and related characteristics of three small watersheds in the Oregon Cascades. *USDA Forest Service Res. Pap.*. Portland, OR:Pacific Northwest Forest and Range Experiment Station, USDA Forest Service.

Sellers, P. J., Y. Mintz, Y. C. Sud, and A. Dalcher. 1986. A simple biosphere model (SiB) for use within general circulation models. *J Atmos. Sci* 43(6):505-531.

Sherman, L.K. 1932. streamflow from rainfall by Unit-Graph method. *Eng. News record* 108:501-505.

Sherrod, D. R., and J. G. Smith. 1989. preliminary map of upper Eocen to Holocene volcanic and related rocks of the Cascade Range, Oregon. *USGS open-file rept. 89-14.* Menlo Park, California.

Shuttleworth, W. J., and J. S. Wallace. 1985. Evaporation from sparse crops -an energy combination theory. *Quart. J.R. Met. Soc* 111:839-855.

Sidle, R. C. 1987. A dynamic model of slope stability in zero-order basins: Erosion and Sedimentation in the Pacific Rim. *Proceedings of the Corvallis Symposium* 165:101-110.

Sidle, R. C. 1991. A Conceptual Model of Changes in Root Cohesion in Response to Vegetation Management. *J of Environment Quality* 20: 43-52.

Sidle, R. C. 1992. A theoretical model of the effects of timber harvesting on slope satability. *Water Resource Research* 28(7):1897-1910.

Simons, D. B., R. M. Li, and T. J. Ward. 1978. Mapping of potential landslide areas in terms of slope stability. Contract No. 16-712.01-CA, Colorado State University, Fort Collins, CO. Flagstaff, AZ: USDA Forest Service, Rocky Mountain Forest and Range Experiment Station. (Draft final report). p73.

Sloan, P. G., and I. D. Moore. 1984. Modeling subsurface stormflow on steeply sloping forested watersheds. *Water Resources Research* 20(12):1815-1822.

Soil Conservation Service (SCS). 1965. *TR-20 project formulation hydrology*. USDA, SCS central Technical Center, Portland, Oregon.

Stednick, J. D. 1996. Monitoring the effects of timber harvest on annual water yield. *Journal of Hydrology* 176:70.

Stephenson, G. R., and R. A. Freeze. 1974. Mathematical simulation of subsurface flow contributions to snowmelt runoff, Renolds Creek watershed, Idaho. *Water Resource Research* 10:284-294.

Stork, P., D. P. Lettenmaier, B. A. Connelly, and T. W. Cundy. 1995. *Implications of forest practices on downstream flooding, phase II final report*. University of Washington.

Swanson, F. J. 1979. Geomorphology and Ecosystems. *Proceedings 40th Annual Biology Colloquium*.159-170.

Swanson, F. J., L. E. Benda, S. H. Duncan, and others. 1986. Mass failures and other processes of sediment production in Pacific Northwest forest landscapes. *Proc. of a symposium*. 9-38.

Swanson, F. J., and C. T. Dyrness. 1975. Impact of clearcutting and road construction on soil erosion by landslides in the western Cascade Range, Oregon. *Geology* 3(7):393-396.

Swanson, F. J. and M. E. James. 1975. Geology and geomorphology of the HJ Andrews Experimental Forest, western Cascades, Oregon, *USDA Forest Serv. Res. Pap.* PNW-163. Portland, OR: Pacific NW Res. Stn.

Swanston, D. N. 1974. Slope stability problems associated with timber harvesting in mountainous regions of the western United States. *USDA Northwest For. Range Exp. Stn.*, Portland, Oregon, Forest Service, Gen. Tech. Rep. PNW-21:14.

Swanston, D. N. 1976. *Erosion processes and control methods in North America: `16th IUFRO World Congress Proceedings*. 251-275.

Swift, L. W. Jr. 1976. Algorithm for solar radiation on mountain slopes. *Water Resource Research* 12(1):108-112.

Takasao, T., and M. Shiiba. 1988. Incorporation of the effect of concentration of flow into the kenematic wave equations and its application to runoff system lumping. *J. Hydrology* 102:301-322.

Tetens, O. 1930. Uber einige meteorologische begriffe. *Z. Geophys*. 6:203-204.

Thompson, E. S. 1976. Computation of solar radiation from sky cover. *Water Resource Research* 12(5):859-865.

U.S. Army Corps of Engineers. 1956. *Snow hydrology, Portland, Oregon, USA*. pp 437.

Wemple, B. C. 1994. *Hydrologic integration of forest roads with stream networks in two basins, Western Cascades, Oregon*. M.S. thesis. Oregon State University, Corvallis, p 85.

Whitehead, D., and F. M. Kelliher. 1991. Modeling the water balance of a small Pinus radiata catchment. *Tree Physiology* 9:17-33.

Wigmosta, M. S., L. W. Vail, and D. P. Lettenmaier. 1994. A distributed hydrology-vegetation model for complex terrain. *Water Resource Research* 30(6):1665-1679.

Wood, E. F., M. Sivapalan, and K. Beven. 1990. Similarity and scale in catchment storm response. *Reviews of Geophysics* 28(1):1-18.

Wood, E. F., M. Sivapalan, K. Beven, and others. 1988. Effects of Spatial Variability and Scale with implication to Hydrologic Modeling. *Journal of Hydrology* 102:29-47.

World Meteorological Organization (WMO). 1974. *Guide to hydrological practices*. 3rd ed. WMO no. 168. Geneva.

World Meteorological Organization (WMO). 1975. Intercomparison of conceptual models used in operational hydrological forecasting. *Operational Hydrology Report* no. 7. WMO. Geneva.

Wright, K. A. 1990. Logging effects on streamflow: storm runoff at Caspar Creek in Northwestern California. *Water Resource Research* 26(7):1657-1667.

Wu, W. 1993. *Distributed slope stability analysis in steep, forested basins*. Ph.D dissertation. Utah State University, Logan, Utah. p.135.

Young, R. A., C. A. Onstad, D. D. Bosch, and others. 1989. AGNPS; A nonpoint-source pollution model for evaluating agricultural watersheds. *Journal of Soil and Water Conservation* ?:168-173.

Zinke, P. J. 1967. Forest interception studies in the United States. In *Forest Hydrology*, ed. Sopper, W.E., and H.W. Lull, 137-60. Oxford: Pergamon Press, Oxford.